2017

Assessment of Varying Model Representations in CFD Simulations

Caitlin R. Gerdes
South Dakota State University

ASSESSMENT OF VARYING MODEL REPRESENTATIONS IN CFD SIMULATIONS

BY

CAITLIN R. GERDES

A thesis submitted in partial fulfillment of the requirement for the

Master of Science

Major in Mechanical Engineering

South Dakota State University

2017

ASSESSMENT OF VARYING MODEL REPRESENTATIONS IN CFD SIMULATIONS

This thesis is approved as a creditable and independent investigation by a candidate for the Master of Science in Mechanical Engineering degree and is acceptable for meeting the thesis requirements for this degree. Acceptance of this thesis does not imply that the conclusions reached by the candidate are necessarily the conclusions of the major department.

Stephen Gent, Ph.D. Date
Thesis Advisor

Kurt Bassett, Ph.D., P.E. Date
Head, Department of Mechanical Engineering

Kinchel Doerner, Ph.D. Date
Dean, Graduate School

ACKNOWLEDGEMENTS

This material is based upon work supported by the National Science Foundation Graduate Research Fellowship Program under Grant No. 1356106 and Grant No. 1417537. Any opinions, findings, and conclusions or recommendations expressed in this material are those of the author(s) and do not necessarily reflect the views of the National Science Foundation.

I would personally like to thank several people for their support throughout my undergraduate and graduate school career. I would first like to thank God for all of the blessings and strength He has bestowed upon me. My faith has been a central part of my being through all stages of life, and I could not have completed this work without it.

I would like to express my gratitude to Dr. Stephen Gent for his guidance and encouragement in my years as both an undergraduate and graduate student at South Dakota State University. He has taught me so much throughout the years both in and out of the classroom. I could not ask for a better advisor.

Thank you to my mother, father, sister, and brother for their constant love and guidance. They have always been there to support me and encourage me to be my best. I could not have done any of this without them. Thank you as well to my wonderful husband, Joshua. The joy he has brought to my daily life is indescribable. I would also like to thank him for taking care of our beautiful son, Tobias, while I worked to complete this thesis. I know we both had some long days, but we would not trade it for the world.

I would also like to thank my thesis committee for their input and time in helping me to complete this work. Thank you to Dr. Gregory Michna for his support throughout

my college career and for his challenging courses that pushed me to be a better student and engineer. Thank you also to Michael Twedt for being such a great undergraduate advisor and supportive member of this committee. Thank you to Cristina Lammers for her help and time in this committee as well.

Lastly, I would like to thank the National Science Foundation for funding my graduate research and coursework. I am greatly honored to have been a Graduate Research Fellow.

TABLE OF CONTENTS

NOMENCLATURE

A_s	surface area of the particle (m^2)
c	speed of sound (m/s)
c_p	specific heat of the particle (J/kg-K)
D_p	particle diameter (m)
f_x	x-component of body force per unit mass acting on the fluid (N/kg)
f_y	y-component of body force per unit mass acting on the fluid (N/kg)
f_z	z-component of body force per unit mass acting on the fluid (N/kg)
g	gravitational acceleration (m/s^2)
g	gravitational vector (m/s^2)
G_b	turbulent production due to buoyancy (Pa/s)
G_k	turbulent production (Pa/s)
h	heat transfer coefficient (W/m^2-K)
m_p	mass of the particle (kg)
m_{pr}	rate of mass transfer to the particle (kg/s)
Nu_p	particle Nusselt number (dimensionless)
p	pressure (Pa)
Pr	Prandtl number of the continuous phase (dimensionless)
Q_t	rate of convective heat transfer (W)
Q_{rad}	rate of radiative heat transfer (W)
Q_s	rate of heat transfer from other sources (W)
R_p	particle Reynolds number (dimensionless)
S	modulus of the mean strain tensor (s^{-1})

t	time (s)
T	temperature of continuous phase
T_p	temperature of the particle (K)
u	x-component of velocity (m/s)
u_b	velocity component perpendicular to **g** (m/s)
v	y-component of velocity (m/s)
v_b	velocity component parallel to **g** (m/s)
V	fluid velocity (m/s)
$\vec{V}$	velocity vector field in Cartesian space (m/s)
w	z-component of velocity (m/s)
W	rotation rate tensor (s^{-1})
β	coefficient of thermal expansion (K^{-1})
ρ	density of the continuous phase (kg/m^3)
σ_t	turbulent Prandtl number (dimensionless)
$\nabla \cdot \vec{V}$	divergence of the velocity (m/s)
∇T	temperature gradient vector (K/m)
μ	dynamic viscosity (Pa·s)
μ_t	turbulent viscosity (Pa·s)
Υ_M	dilatation dissipation (m^2/s^3)

LIST OF FIGURES

LIST OF TABLES

ABSTRACT

ASSESSMENT OF VARYING MODEL REPRESENTATIONS IN CFD SIMULATIONS

CAITLIN GERDES

2017

This thesis investigates the effects of varying model refinement and representation of computational fluid dynamics (CFD) simulations in two case studies. Product and process realization in engineering design requires substantial resources (time and money) in order to test novel designs for effectiveness. In recent decades, engineering has been relying more heavily on simulation-based analysis in the design process with computer models to help reduce the demands for real-life testing. The first case study analyzed in this thesis is a photobioreactor, which is used to grow microalgae for biofuel and require a balance of nutrients, light, and mixing for growth. The second case study analyzed is a laboratory scale grain dryer used to assess and quantify the drying mechanics of corn. The air flow in the system is analyzed to look at both the velocity and temperature stratification of the packed bed of corn within the drying chamber. The model refinement techniques used in these systems involved refining the computational grid and increasing the complexity of the simulated systems. A recommended model was obtained with successful iterations of the simulations. This model could then be used to describe and predict the system behavior. Through the use of modeling and simulation with CFD, the design process can be simplified.

Chapter 1: Introduction

The field of engineering largely involves the area of design. In fact, it has been said that the essence of engineering is design [1]. From brainstorming new ideas for a product to determining the safety factor needed for a bridge being constructed, engineers need to be able to make sound design decisions based on multiple design requirements, financial constraints, and available data. These design decisions can be accomplished by following the proper design process and analysis of the system in question.

The process of engineering design has changed significantly throughout the years. In the early 1900s, it involved mainly the creation of prototypes and the use of physical experiments for system optimization. This made many designs limited by available time and money. A better system was needed in order to efficiently test new ideas. Analytical calculations were a way to improve this process, but they could take months to complete [2, 3, 4]. However, as technology became more advanced, these calculations could be done more quickly. With the advent of the space program, analyses could be done computationally. The more complicated equations were integrated into computer coding, making theoretical analysis more efficient.

Today, modeling and simulation software exists that can almost completely take the design process from start to finish. An example of this is product lifecycle management (PLM) software. PLM takes a design from the initial idea through model creation and simulation to manufacturing [5]. Each step of the design process can be communicated and coordinated easily between collaborators. In industry, it helps to get information to the right

people at the right time [5]. Using this type of software to streamline design has the potential to save companies valuable time and money in product development.

Even though the execution of the design process has changed greatly, the same principles are in place for the development of a new design. A chart showing the recognized steps for creating a new design is shown in Figure 1 [1, 6, 7]. Engineers have used and enriched this process over the years in order to make the best design decisions for a given situation.

1.1 Engineering Design Process

The basics of science and engineering are built on careful experimentation and analysis of the world. Each new finding is a step towards a new discovery, proving a theory, or developing a different basis for how the world is viewed. Sometimes this research and experimentation takes place on a small level, such as a laboratory exercise in a physics course, to gain a better understanding of the principles being learned. Other times the experiment is being watched around the world, such as when a new probe is sent to explore the surface of Mars.

In all of these situations, including research done every single day around the world, costs are associated with the project. Financial costs are the first that come to mind, as funding is essential to most projects. However, another great expense is the use of time. For example, a rugged design may need to be subject to intense conditions for extensive amounts of time before valid data may be obtained. Other experiments may require long stretches of time for analysis just to prove their lifespan. Methods that reduce this time requirement for system analysis then become desirable.

The engineering design process is a method used to help in creating new models, testing designs, and determining a recommended system. There are many variations on this process, but it generally follows the same format. A chart of the design process is shown in Figure 1. This chart is based on several different sources [1, 6, 7] and gives an idea of the steps taken when developing a new design or testing an existing one.

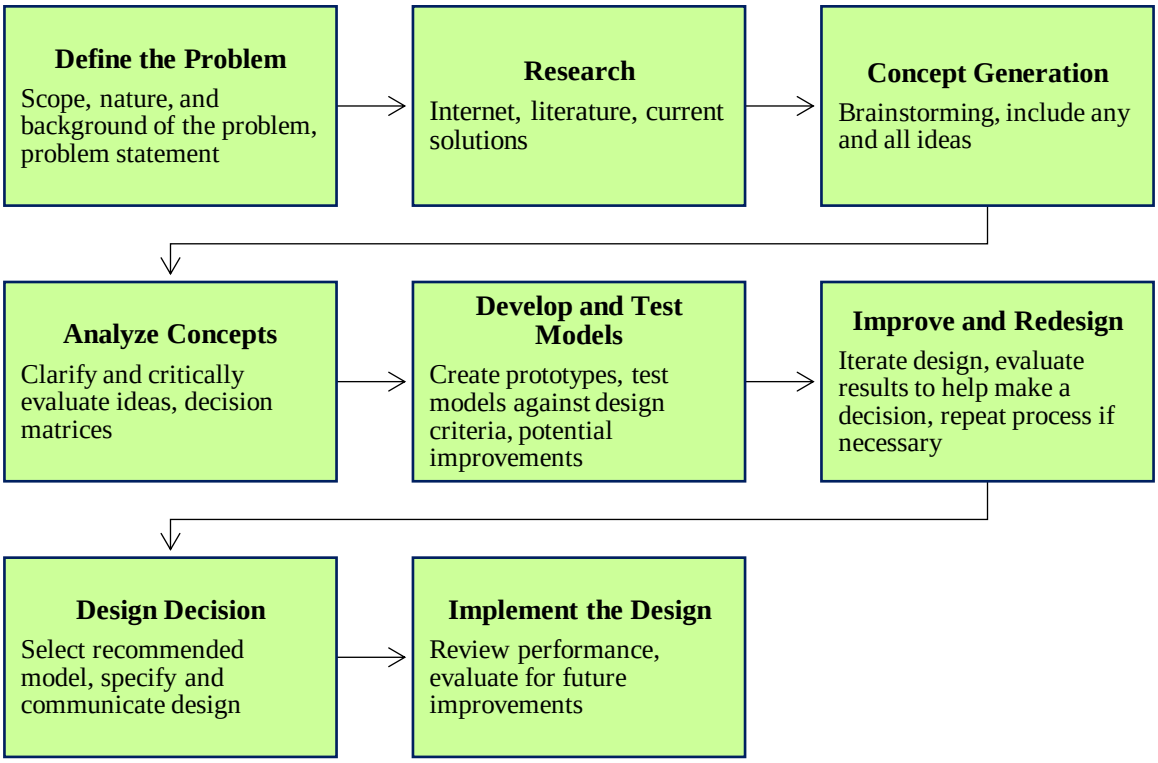

Figure 1: Engineering Design Process Chart [1, 6, 7]

For most design projects, time and money are limited resources. In order to move forward with analysis, engineers need to evaluate how to efficiently gain the knowledge necessary for design decisions. Computational resources can be used to help solve this common constraint of time and money. Whether it be detailed calculations or a simple design, computers are a valuable resource not to be overlooked.

Analysis costs can be greatly reduced through the use of computational software. Many programs exist for engineers in order to both design and test new products and systems, from computer-aided design (CAD) software to computational fluid dynamics (CFD). These software programs can be used to visualize a design idea through the use of modeling and simulation. This gives the engineer the ability to test and modify different designs without the need for expensive prototypes. With proper formulation, these computer models can demonstrate both the system geometry and setup and any interactions that may occur.

In order to properly build these models, however, a closer look needs to be taken at the decision making process along the way. One must ask, “Does the model follow the experimental setup to the degree that the results found are valid?”, “To what degree does the model need to be matching the real-life system to be a suitable representation of the situation?” among other questions. Once a proper representation of the system is obtained, the analysis tools also need to be chosen carefully. An example of this is the refinement of the computational grid used for analysis. A coarse grid will require less computer resources, but may not give very precise results. Too fine of a grid will almost always give excellent results, but the computational time is greatly increased, cutting into resources that may not even be necessary for the given simulation.

1.2 Computational Modeling in Engineering Design

Many best practices are in place in the field of engineering. A best practice, according to Rossi, et al. [8] is a practice that allows greater effectiveness than any other method. In the area of design this includes designing to given codes and standards. With

configuration design, this also involves specifying the function of the design, and considering safety, simplicity, and environmental impact [1]. A design engineer can implement these practices by comparing his designs to current available technology, strive for a simple yet effective system, and using computational resources for development and testing. The engineer must also use a plan for new product development, as suggested by Rossi, et al. [8]. This helps to streamline the process.

For computer modeling, a plan of action may involve brainstorming new ideas, researching current designs, experimenting with different model designs, and simulating ideas. The effectiveness can further be increased when working with others to help maximize creativity and design potential. Multiple ideas can be tested, and the best solutions will be moved forward [8]. With this method, the goal is that the majority of time and research will be spent on the most promising designs. The strength of the new system depends greatly on effective planning, collaboration, and efficient use of resources.

One way to effectively prepare a new design in the field of engineering is to initially perform basic calculations. These calculations give an idea of what to expect for system output. This will also signal which results may indicate that a problem exists with the experimental setup. Another advantage of preliminary calculations is that they may save time if they show the prospective design is a poor choice. Evaluating the model before its creation saves time when determining the boundary conditions and initial setup for the model in the simulation. After a few experimental tests with the computer, the results can be compared with the initial calculations, giving the engineer an idea if their simulation is performing the way it should, or if a large error exists somewhere. By having these calculations, the design engineer will also have a good idea of what assumptions should be

made about the model when simulated. Overall, making these calculations is good research practice in general as it helps the engineer understand the capabilities of the software he/she is using.

Computational modeling has the potential to compete with experimental research if the simulation that is being used is a good representation of the actual system. However, one should use caution not to solely rely on the computer results. A discrepancy in an experiment may mean that the engineer has made a mistake, not necessarily that the computational model and real life study do no match. Constant verification with both the experiment and the simulation can help prevent potential issues.

Overall, experimental and computational or theoretical studies are intended to complement each other. Should one have issues, the other may explain the discrepancy. The engineer should take great caution not to rely on one method too heavily or the results may come out biased or incorrect.

1.2.1 Model Refinement

In order to develop a model that is a good representation of the system being analyzed, the process of refinement may be used. With refinement, a computational model will better match the actual system, giving better results. The level of imprecision in the model will also decrease. This is demonstrated visually in Figure 2. However, increased model refinement also means increased computational resources and time required for analysis. Therefore, a good stopping point is necessary in the refinement process in order to efficiently test design ideas.

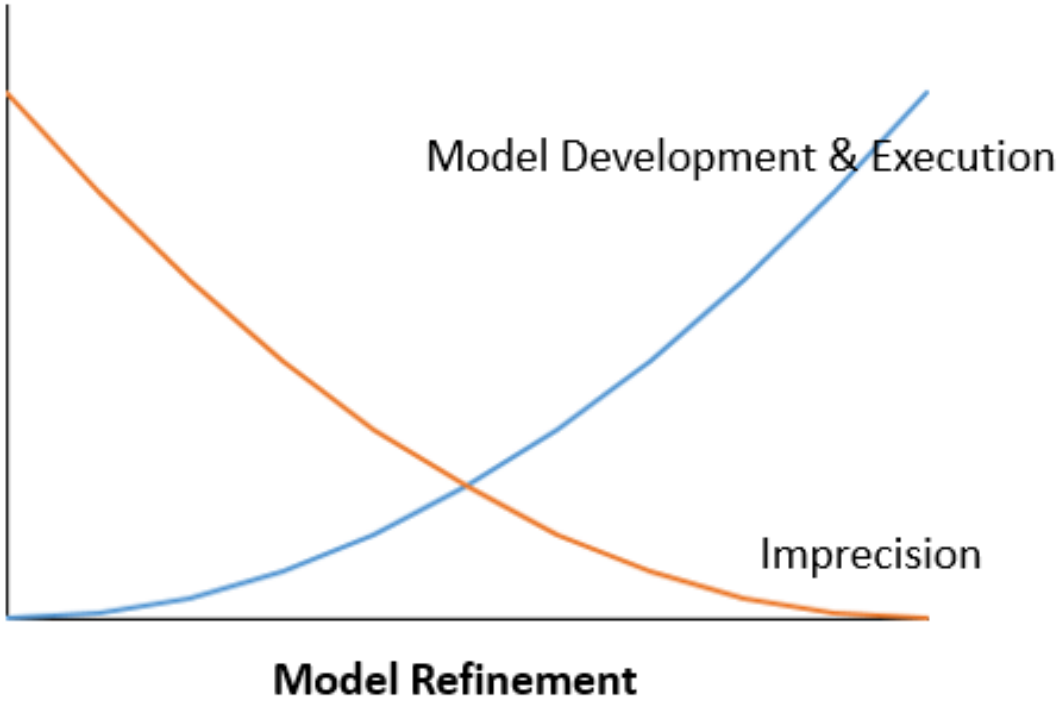

Figure 2: Model Refinement Graph

According to Panchal, et al. [9], the process of refining a simulation involves adding more information to the system so that the model better represents the actual behavior of the system. Model refinement can be accomplished several different ways. The first method involves refining the computational grid used for finite element analysis so that there are more data analysis points. A second method involves adding more features to the simulation so that it can replicate real life experimentation. An example of this would be to add curvature to fan blades versus only using flat blades for analysis. Simulations may not always need this level of detail if the design engineer desires only to obtain an idea of the expected outcome of the system. Determining what information is of value and what

information only serves to complicate the system is a necessary skill when evaluating these systems.

1.3 Computational Fluid Dynamics in Design

Engineers around the world are using CFD in their experiments today, as it gives a breadth of research options and can save time and money. CFD is the software tool used for analysis in this thesis. In order to use this software correctly, though, the problem of creating an accurate model exists. An excellent quote from Wendt [10] describes this idea: "The results of CFD are only as valid as the physical models incorporated in the governing equations and boundary conditions, and therefore are subject to error…"

Wendt's conclusion about validation of computational results reiterates the fact that experimental and computational studies are necessary checks for one another. When using CFD software, the engineer needs to have the simulation accurately represent the actual physical system setup. This can be accomplished in several different ways, such as a detailed CAD model or a very refined grid system.

In order to select a proper model for use with CFD, careful analysis is required. The user should determine whether or not the problem they are considering can be setup accurately in the CFD software they are using. Engineers should also consider if the use of CFD simulation software will actually aid in the analysis of their system. In some cases, it could just add an extra step to the design process that is not necessary. Another concern should be whether or not the problem being studied can be simplified successfully for use with CFD. A system with too many different interactions may need to be broken down into smaller parts in order to be successfully represented. All of these considerations involve

classifying the problem being analyzed, and studying the benefits and challenges facing CFD software, as discussed in Chapter 2.

The following sections discuss the two different systems chosen for this research. Analysis of these projects will help to demonstrate the validity of CFD modeling for use with making decisions about different design questions.

1.4 Applying Computational Fluid Dynamics to Design Problems

Although not every project may be helped through the use of CFD, the software's capabilities make it a strong force in the world of research. Numerous studies have been conducted that use CFD to enhance and illustrate results and give a new perspective on previously studied experiments or new designs.

Examples of projects that could benefit from the use of CFD include those in which the engineer may need further information, but has the inability to acquire this information due to complicated experimental geometry or limits with testing equipment and time. Some examples include the design of spacecraft or deep sea submarines. Other projects that may benefit are analyses where the heat and mass transfer or fluid flow needs to be measured. Using CFD can help engineers find good recommendations for project geometry, fluid flow rates, temperature boundaries, and countless other conditions. Often, these parameters are difficult or expensive to change and measure in actual experiments.

This research involves the study of a photobioreactor system and a laboratory scale grain dryer. These two projects study different problems that can be simulated using the CFD software, including multiphase flow and porous boundaries, respectively. Both of

these conditions require intensive calculations and complicated boundary conditions that may not be straightforward when analyzing either experimentally or theoretically.

1.4.1 Photobioreactors

First, a photobioreactor (PBR) was analyzed through the modeling and simulation process of CFD. Photobioreactors are tanks containing multiphase mixtures where light, oxygen, carbon dioxide bubbles, and nutrients are used to grow algae. An example of a PBR is shown in Figure 3. This algae can then be used in the production of biofuels. In order to photosynthesize, the microalgae need proper light penetration in the fluid. One way to increase light is through the use of light guides, which go through the middle of the tank and have light shone through them so more light is available to the algae in the inner portion of the PBR. Previous research has been done on similar PBR systems with light only being applied to the sides of the tank. The results from these studies showed the typical flow patterns with a multiphase mixture in a PBR tank. By adding structural members that penetrate the flow regime, new velocity and temperature profiles can be obtained to guide the engineer towards the recommended placement of light guides to maximize light without disrupting the bubble flow and mixing occurring.

The analysis process for the photobioreactor system involves starting with a simplified tank and adding light guides and increasing the grid refinement with each simulation. These results will be compare to similar research done both computationally and experimentally.

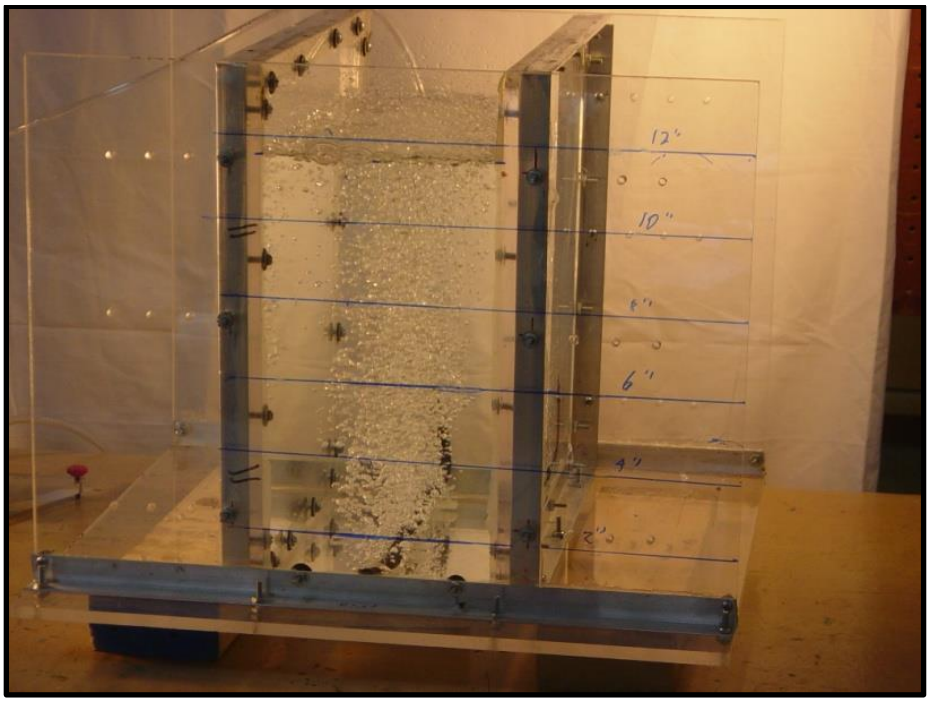

Figure 3: Photobioreactor Tank with Water

The analysis of the PBR systems includes a study of the bubble flow patterns within the tank, the heat transfer, and the fluid dynamics. These characteristics are studied at several different volumetric flow rates in CFD. With successful iterations, the goal is to significantly reduce or even eliminate the need to test the reactor in real life for the many different setups of each new design.

1.4.2 Grain Drying

Grain drying is an essential step for the proper storage and sale of the crop yield for the year. It is also the process that costs the most energy for the farmer. Harvesting and storing grain has its own concerns. Should the grain not be sufficiently dried after being harvested, mold and rot will diminish its value. If the grain is dried at too high of a

temperature, this could also reduce the seed yield and waste energy in the form of heat. Finding a recommended balance of drying temperature and time to dry can help solve these problems.

While performed on a large scale in most applications, grain drying can also be studied on a small scale. The improvements found can then be applied to full-scale commercial dryers. The mini-grain dryer system analyzed in this research is shown in Figure 4. The grain tested in the analysis was corn kernels. The corn needing to be dried was kept in a chamber next to an air duct. This chamber was considered porous in nature as the corn is a packed bed, with small spaces for air to penetrate. The system was first tested as a simple fan and drying duct. More features were added to the simulation with successful iterations. The tradeoff between more system information and a greater computational cost is also highlighted. A recommended system setup is then evaluated based on the information from the different models.

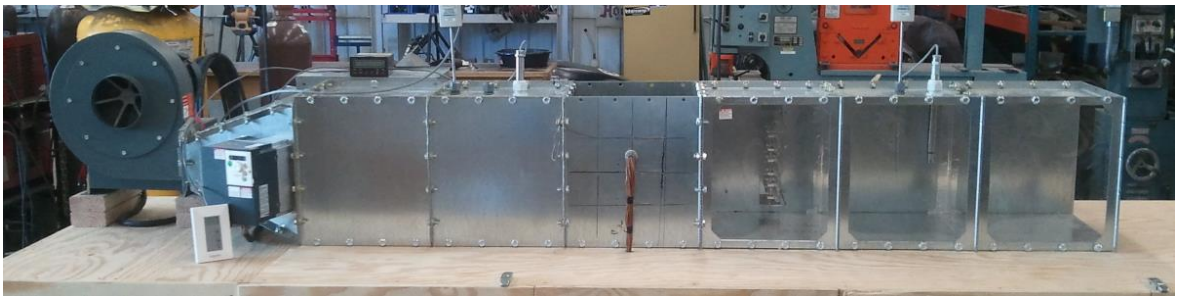

Figure 4: Laboratory Scale Grain Dryer

The grain drying simulation demonstrates how a large system can be assembled into a continuous flow model with both a rotating fan and a porous region. With each of the parts of the dryer interacting to make one model, the simulation can be used to simplify

the changing and testing of different parameters and seeing how each change affects the entire system. This in turn makes it easier for the engineer to know what to change when performing different experiments with the dryer. Some varying parameters include inlet air velocity and the temperature used for heating the air that reaches the porous corn chamber.

1.5 Motivation and Objectives

The goals in researching both the photobioreactor and the grain dryer are twofold. First, they allow a better understanding of each system and the working characteristics involved with each system. In addition, they exhibit two different problems that demonstrate the utility of CFD when trying to solve different engineering problems through the process of model refinement. The more computational resources are properly understood and executed, the greater the ability for more problems with intense calculations can be solved.

Computational fluid dynamics is growing to be an integral part of most scientific and engineering research. This thesis will discuss the importance of CFD for refining a model by showing its different abilities and how it can help to reduce costs and simplify the process of experimentation.

Both the photobioreactor and grain dryer simulations deal with complicated design problems. The PBR simulation analyzes a multiphase mixture. Through the use of CFD, different PBR setups can be tested easily. The grain dryer simulation studies the air flow occurring in the drying duct as well as a porous boundary with the packed bed of corn. Turbulence is present in both systems. As with every CFD simulation, these two systems

require an accurate representation of the actual setup, with proper boundary and physics conditions.

1.7 Organization of Thesis

The organization of this thesis is as follows: Chapter 2 gives insight into the past and current research involving computational fluid dynamics. The challenges and benefits of computational fluid dynamics are discussed. Chapter 2 also talks about the process of model refinement and different case studies that have been performed in relation to this aspect of modeling and simulation. This design process analysis is applied to CFD simulations.

Chapter 3 discusses the methodology associated with computational fluid dynamics. First, the methods for setting up simulations are studied in detail. Then, the relevant governing equations of CFD are described, including those used for the specific systems being analyzed. The proper representation of models is also discussed.

Chapter 4 looks more in depth into the first case study, that of photobioreactors. The history of research with PBRs and similar past studies performed at South Dakota State University are discussed. The initial modeling and setup of the PBR simulations is reviewed with relation to the design process analysis and model refinement. Relevant results for the specific research project are also analyzed.

Chapter 5 focuses on the second case study involving the modeling and simulation of the laboratory scale grain dryer. Once again, the different aspects of setting up the CFD model and running the simulation are discussed. The model refinement methods applied to

these simulations are discussed. The results of the grain dryer simulations are then analyzed and compared to experimental findings with the experimental setup.

Lastly, Chapter 6 is a discussion of the results and conclusions of the two case studies, and their greater impact on demonstrating the usefulness of CFD. An analysis of the resources required for each system analysis and the steps to refining each model are analyzed. Chapter 6 also looks at potential future work relating to this subject.

Chapter 2: Review of Related Literature

In this chapter, CFD and model refinement techniques are described. A brief background is given on the history of computational fluid dynamics and its capabilities as well as the available CFD software. Design process analysis is also discussed as it relates to using models in research.

2.1 Computational Fluid Dynamics

Computational fluid dynamics, or CFD, is, according to Wendt [10], "…the art of replacing the governing partial differential equations of fluid flow with *numbers*, and advancing these numbers in space and/or time to obtain a final numerical description of the complete flow field of interest." CFD is a practice which gives engineers the ability to test design problems involving fluid flow, including both internal and external flow [11]. This software can simulate designs involving solids, liquids, gases, and multiphase mixtures. CFD would not be available were it not for the study of fluids and heat transfer, and the associated equations. Its usefulness stems from its ability to take complex and time-consuming calculations and execute them at thousands of steps in time to give the user an answer to his/her specific fluids problem. Since it is built on the governing equations of fluid dynamics, CFD will always be reliant on basic fluid principles and laws.

2.1.1 Historical Overview of Computational Fluid Dynamics

Although the study of fluid flow has been carried out for several centuries, the creation of CFD started mainly in the 20th century. It began with the development of different equations applicable to CFD. Prandtl's work on the boundary layer theory and the

development of the Prandtl number was done in the early 1900s [2]. Other contributors around this time include Theodore von Karman, Geoffrey Ingram Taylor, Andrey Nikolaevich Kolmogrorov, and George Keith Batchelor. Their contributions were, respectively, the von Karman vortex street, the Taylor microscale and a statistical theory of turbulence, Kolmogorov scales and the universal energy spectrum for turbulence, and help with the theory of homogeneous turbulence [2].

Lewis Fry Richardson is named by several authors as the source of the earliest CFD calculations [2, 3, 4]. Richardson used a grid system and finite difference approximations to attempt to calculate weather for a single eight-hour period. His work on this took six weeks in real time and ended up being a failure. After this attempt, Richardson described a "forecast-factory" that would require a stadium full of 64,000 people, each with a mechanical calculator, to each perform part of the flow calculation. In the center, there would be a leader that would communicate the forecast. This resembles a very rough version of CFD, but is a step in the right direction. In 1933, the first calculation of flow past a cylinder was completed by Thom in England. Twenty years later (1953), in Japan, Kawaguti calculated a similar solution for flow across a cylinder. His work took 18 months of 20 hour weeks with a mechanical desk calculator [2, 3]. Around this same time, Kopal, in 1947, also compiled tables that numerically solved the supersonic flow over cones [10]. Kopal did this work on one of the early digital computers at the Massachusetts Institute of Technology. All of these calculations took place before high speed calculators were available, making these accomplishments even more impressive.

New developments for CFD arrived in the 1960s, the prime time for NASA and the space program. NASA developed methods still in use today include the Particle-In-Cell,

Vorticity-Stream function, and Marker-and-Cell methods, the k-epsilon turbulence model, and the Arbitrary Lagrangian-Eulerian methods [3]. D. Brian Spalding developed the k-epsilon model that is used today. Around this time, the second generation of CFD came into the picture, with calculations involving the governing equations that are so complex they require a computer. In the mid-1960s, the time-dependent technique helped shape flow field calculations [10].

Suhas V. Patanker published a book in 1980 which helped create a thousand CFD codes titled *Numerical Heat Transfer and Fluid Flow.* Around this same time, commercial CFD software came into use all over the world [3]. Today, CFD plays an essential role in studying fluid dynamics. Wendt [10] states that CFD is viewed alongside pure theory and pure experiment as the "third dimension" in fluid dynamics. Anderson, Jr. [12] also states that CFD makes up a "third approach" in the field of fluid dynamics. With every year, CFD is becoming more advanced, and it is an almost essential teaching in engineering courses. Pletcher et al. [4] stated that computational fluid dynamics development is related closely to the development of digital computers. With the availability of high speed computers in both academic and industrial settings, CFD has become a cornerstone in both research and testing of different engineering designs.

2.2 Computational Fluid Dynamics Capabilities

Computational fluid dynamics models are helpful analysis tools for engineers in the design and testing process. CFD is used in situations where engineers want to test a potential new design or the performance of an existing system. The procedure for using CFD involves modeling the design using a CAD program. This model may be a simplified

version of the actual design, or it may represent all of the features involved. Once the design has been modeled, it can then be imported into the CFD software for simulation. The simulation is setup by defining the different boundaries of the system and applying a computational grid, or mesh, for finite volume analysis. After creating the grid, the engineer will define the physical interactions occurring within the system. Upon setup completion, the simulation will then be run for as many iterations as necessary for suitable results. Any changes or improvements may be made as needed, and the simulation can be run multiple times. The process for preparing a model for simulation using computational fluid dynamics is discussed further in Chapter 3.1.

CFD is used around the world today in solving fluid problems beyond number. Studies can be anywhere from measuring the drag on a bicycle to determining the effect of water pressure on a new deep sea submarine design. Before delving into the various aspects of CFD, it is important to step back and understand its usefulness from the perspective of how resources like time and money will be conserved.

Thousands of engineering problems exist in the world today that require extensive time and grandiose budgets in order to solve. However, these constraints reduce the ability for engineers to solve problems to satisfaction, leaving room for error and even failure. The research community as a whole needs to bridge the gap between engineering ability and budget and time issues. One way to resolve this problem is to look for solutions outside of the experimental realm. Theoretical calculations can be backed up in more than one way. This calls for the use of computational software often used in industry today.

Finite element analysis and finite volume analysis software can be employed to help verify theoretical calculations. This type of software can take these calculations and iterate them in a timely manner so that the user may quickly find out answers to problems. Finite volume analysis and finite element analysis involves the use of discrete elements that make up a whole object, with the data being taken from each element and added together as a whole, much like a simple mathematic integral.

When it comes to thermodynamics and fluid mechanics analysis, these elements then become small 2-D or 3-D volume elements of the fluid being transferred, with the data from each one detailing what is occurring at that specific point in space. In this way, gas and liquid flows do not need to rely on carefully placed thermocouples and velocity sensors to determine their state. Instead, the computer can take the input conditions and give a mathematical solution to the element's state of being at a certain location in space or time. For fluids specifically, it is important to be able to track the particle's path and behavior.

Analyzing fluid flow and heat transfer can be done computationally using CFD. CFD takes into account the user set conditions to track individual fluid particles and return data for specific locations in space and time. The accuracy of Computational Fluid Dynamics relies greatly on the initial and boundary conditions set by the user, so care must be taken in order to best represent on the computer what is actually happening when the experiment is run in real life. This process involves detailed measurements of not only the size of the object, but also the temperature, pressure, and, in more detailed cases, the humidity, wind velocity, etc. that occur when the test is run experimentally. Any deviation from the actual measurements will result in the calculations being incorrect for the post-processing portion of the simulation. Therefore, the user must also make sure that the

measuring equipment used to determine the states is accurate as well as the person making the readings. These readings can then be imported into the simulation to set the conditions of the simulation being run.

Computational fluid dynamics can be used to run numerical simulations in parallel with experimental setups. Anderson, Jr. [12] stated that these simulations can help in interpreting the actual experiments by describing parts of the experiment that may not be easily seen. An example of this may be studying air flow, which can be difficult to visualize experimentally.

Anderson, Jr. [12] also points out the usefulness of CFD in the process of design. He makes the observation that computer programs for describing three-dimensional flow have become industry standards. By using CFD in the design process, the need for several costly prototypes may be significantly reduced. Designer engineers have the ability to instead test different setups of their design using CFD to see how changing one aspect of the system affects the results. Computational fluid dynamics can also help when researchers find it difficult to recreate specific flow types in the lab [13]. These flows can instead be simulated using CFD software. Because of its broad capabilities, a wide range of system types can modeled.

2.2.1 Benefits of Using CFD

Multiple industries benefit from the use of computational fluid dynamics. One such industry is the aerospace industry, discussed both by Wendt [10] and Anderson, Jr. [12]. An example of the use of CFD for the analysis of a space shuttle by NASA is shown in Figure 5. This figure shows the particle traces from takeoff based on the Mach number for

the shuttle. Cleaver, et al. [13] stated that both industry and government use computational fluid dynamics to help with significant cost savings on designing a weapons system. Other industries include the automobile and engine industries [12], which can use CFD to demonstrate the fluid flow through the engine and the external flow over the body of a vehicle. Environmental engineering is another discipline which can use CFD [12]. When designing HVAC systems, for example, the flow of air through air conditioners can be modeled, with both the velocity and temperature of the fluid easily described.

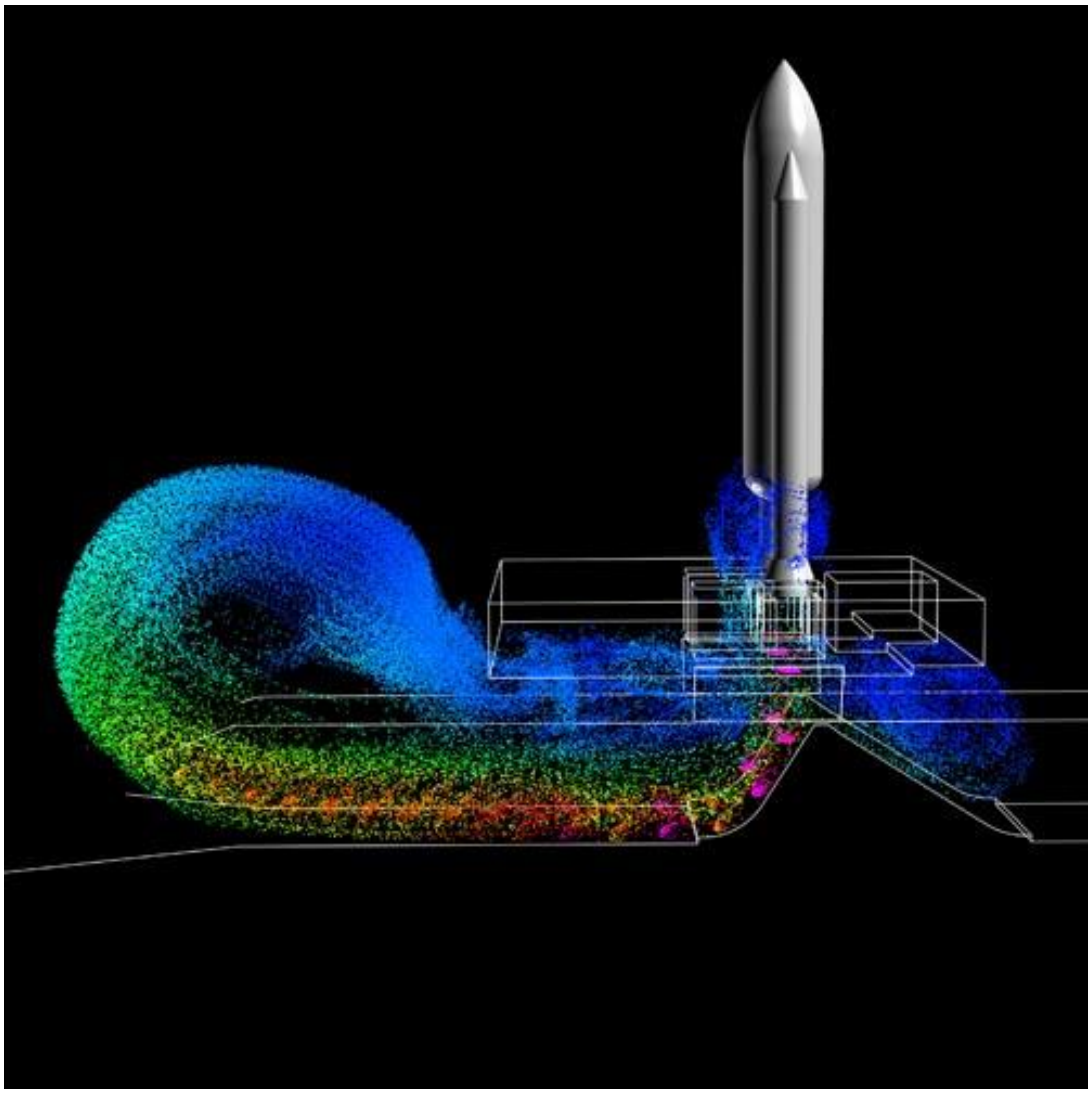

Figure 5: Visualization of Shuttle Flame Trench CFD Simulation Showing Instantaneous Particle Traces Colored by Mach Number [14]

The development of better supercomputers results in more powerful CFD abilities. Computational fluid dynamics is one of the main driving forces for the creation of new and improved computers [12]. Therefore, CFD is also indirectly the development of new technology by creating a demand for greater computer abilities. The illustration of three-dimensional flow is driving the development of computer graphics as well [12]. While one-

and two-dimensional flow are easily illustrated, the depiction of 3D flow is something that will continually be improved over the coming years. Although both the development of stronger computers and better graphics may not be directly related to CFD research, they are helping to drive the creation of better computers around the globe.

One of the biggest benefits of using computational fluid dynamics is the amount of time and resources saved from not needing to create several physical models for testing. Compared to using an actual experimental model, CFD can save anywhere from 20-40 percent of these resources [15]. This is due in large part to the amount of labor that goes into constructing a physical model that is not needed for a computational model. Included in this is the optimization of the design that can be accomplished using CFD. Instead of constantly creating new prototypes, designs can be tweaked easily in the computer simulation. However, CFD has some limits to its abilities.

2.2.2 Underlying Challenges of CFD

Although computational fluid dynamics is an essential tool in many design problems today, the field does have its drawbacks. The validity of a CFD simulation relies heavily on the user. If the setup of the problem does not include the correct physics formulation, then it cannot be reproduced successfully [10].

One of the biggest areas of concern with relation to the simulation formation is the presence of turbulence [10]. Turbulence is stated as being one of the biggest problems yet to be completely solved in the fluid dynamics and physics world [12]. Since just an approximation of the actual flow is used in turbulent simulations, there will always be inaccuracy. Both case studies in this research deal with turbulence, one involving

multiphase flows and one involving air flow through a heating duct for grain drying. The standard turbulence model chosen for both of these simulation setups was the k-epsilon turbulence model, which is described in Chapter 3, equations 3.5 and 3.6.

Another area where CFD solutions will be affected negatively is the uncertainty involved in chemically reacting flows [10]. Similar to turbulence, the computations involved in these flows may be limited by the physics knowledge and abilities of the software. For both of these situations, the user must rely on his/her own judgement in analysis.

The strength of the results of any computational fluid dynamics simulation rely heavily on the setup by the user. If any of the initial or boundary conditions are incorrectly specified, the outcome of the simulation will be negatively affected. Like the example discussed in section 2.3 from Figure 7(b), including incorrect model information or not refining the simulation enough will result in a complete misunderstanding of system behavior. The engineer may use the methods described in Section 2.3, where a simple model is tested first and refined further with successful iterations of the simulation. This may help reduce error and give an idea of how each step in model refinement may affect the outcome. Wendt [10] makes a good point in describing how solutions that may not be correct can in fact provide remarkable three-dimensional visuals. A model has the ability to completely misinterpret actual system behavior but may still seem to give valid results. Therefore, no matter how good a simulation solution may look, the numerical results must always be verified.

2.2.3 Commercially Available CFD Solvers

Numerous software packages exist today in the field of computational fluid dynamics. These solvers can be standalone packages or part of other software suites, including CAD modeling programs. A list of several different available programs is given in Table 1. This list is not comprehensive, but does include many of the more popular programs in use today.

Table 1: CFD Solvers and Capabilities

CFD Solver	Vendor	Features
STAR-CCM+™	Siemens™	Comprehensive meshing, solving, and post-processing. High performance computing.
STAR-CD™	Siemens™	Focus on internal combustion engine simulations
Fluent™	ANSYS®	Comprehensive meshing, solving, and post-processing
Chemkin-Pro™	ANSYS®	Gas phase and surface chemical reactions
CFX™	ANSYS®	Comprehensive package with a focus on turbomachinery
PolyFlow™	ANSYS®	Focus on polymers, glass, metals, and cement

COMSOL™ CFD Module	COMSOL™	Part of larger multiphysics solver
AcuSolve™	Altair™	Part of larger multiphysics solver
OpenFOAM®	ESI Group	Popular open source solver
Visual-CFD	ESI Group	User interface for OpenFOAM
Software Cradle	MSC™ Software Corporation	Packages specifically for polyhedral, structured and unstructured meshes
Autodesk® CFD	Autodesk®	CAD integrated solver

Figure 6 is a graphical representation of the computational fluid dynamics software preferences of different users. Fluent and STAR-CCM+ are by far the most popular options, followed by OpenFOAM [16]. This survey is not comprehensive, but it gives an idea of the leading packages in the industry. The more popular options will be discussed in greater detail.

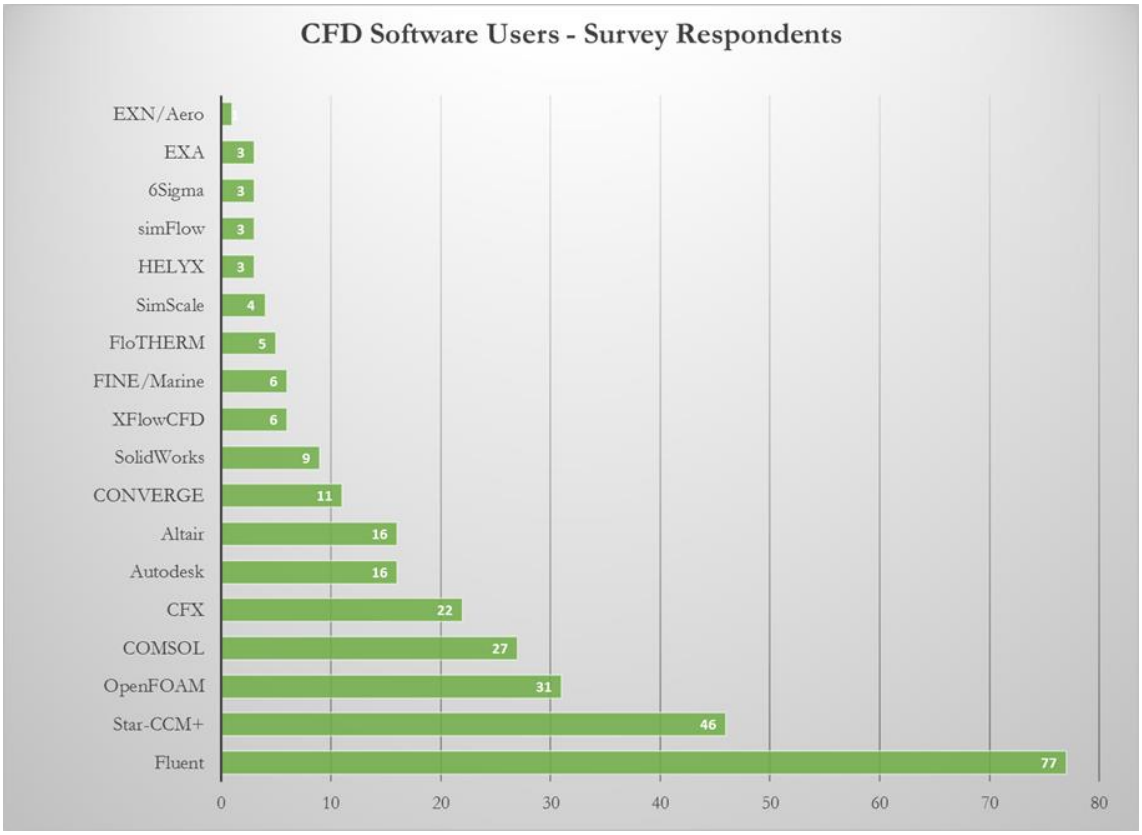

Figure 6: Graphical Results of CFD Software Preferences [16]

The four computational fluid dynamics packages discussed further include ANSYS Fluent and ANSYS CFX, STAR-CCM+ by CD-adapco, and OpenFOAM. These programs are all excellent tools when it comes to flow solvers, but each one has its strengths and weaknesses for different applications.

The first two packages are products of ANSYS. Fluent is a more general code solver for most types of systems, whereas CFX is focused on turbomachinery applications [17]. Fluent has almost comprehensive solvers available for single phase flows, heat transfer, multiphase flow types, multiphysics, and electro-thermal and fluid-structure interactions [18]. CFX has similar capabilities, but fewer in regards to reacting flows and electro-

thermal interaction. Fluent has solvers for comprehensive surface-kinetics, chemical and phase equilibrium, and can use the Model Fuel Library mechanisms, whereas CFX cannot. However, CFX has fully supported capabilities with transient blade rows, blade flutter analysis, and forced response analysis, while Fluent does not [18]. The solvers that are not supported in these packages were supported in other ANSYS software analysis tools.

STAR-CCM+ is a computational fluid dynamics package offered by Siemens. Its website [19] describes the software as an engineering process that can be used for heat transfer, stress, and flow problems. STAR-CCM+ uses a single code, making it user-friendly. It features many of the same solvers available in ANSYS Fluent and CFX. Some of the software's featured analysis tools include multiphase analysis of boiling, evaporation and condensation, melting and solidification, and a fast Fourier transform aeroacoustic analysis [20]. STAR has the ability to solve many different types of engineering problems.

The fourth CFD solver, OpenFOAM, takes a different approach to the analysis process. OpenFOAM uses a library of coding in order to solve different types of problems related to fluid dynamics [17]. If the user does not have the solver necessary for the situation being analyzed, the code can be added and edited using the C++ code library available. The standard solvers for OpenFOAM include multiphase flow, incompressible and compressible flow, combustion, particle tracking, heat transfer and buoyancy driven flows, and electromagnetics, to name a few [21]. Since OpenFOAM features a library of functions, the user does not need to write code from scratch [17]. However, the user may need to have a background in coding if the specific solver needed is not available. One of the perks of OpenFOAM is that it is a free software. In addition, many training courses can be found online to better understand this software.

The software that the engineer ultimately ends up choosing will be based not only on the capabilities within each package, but also the availability of each program. OpenFOAM is a free analysis tool that has the ability to be edited based on the needs of the engineer. Fluent and STAR-CCM+ are both comprehensive CFD packages but require the purchase of the software license to use. The resources that can be saved in the long run by using CFD will almost always offset the initial costs.

2.3 Design Process Analysis

With the use of CFD comes the use of models for analysis. Panchal et al. [9] used the quote by George Box in their paper, "All models are wrong, some models are useful." This statement is true in the development of any model, as simplifying assumptions must always be made, eliminating the ability to have a model that perfectly represents reality. This does not mean that these models are of no value, however. Instead, refinement techniques can be used in order to help increase the accuracy of the computational model.

Refinement is the process of adding more information into a model so that the outcome can better predict system behavior [9]. One example of a situation described by Panchal et al. [9] is the refinement of a pressure vessel simulation, and the value-of-information approach. The value-of-information approach weighs the benefits and costs of more information for improving the ability to make decisions with regards to design [22]. The decision outputs are studied with and without this extra information. Panchal et al.'s experiment involved comparing the appropriateness of the refinement of the material model to design the pressure vessel. As the model is refined, the accuracy of the material model is generally increased, but at an increased cost for more information. The purpose

is to find the level of imprecision in the material model that is acceptable for making decisions regarding the pressure vessel. A suitable stopping point for refinement is when there is low improvement potential [9]. Graphs comparing radius to overall payoff, or utility, weight to volume, weight to utility for weight, and unacceptable weight to Hurwicz Utility are all used in determining a good stopping point for refinement. In order to help visualize this concept, Panchal et al. [9] included two graphs that show the different potential for results based on using the predicted behavior of the system. These graphs show the danger in not knowing all the information about a model, as well as how refinement can help in making the recommended decision for the model payoff. Figure 7 (a) and (b) show the different payoffs achieved, with the predicted system behavior matching the actual behavior for ideal payoff, and not matching the actual behavior for an extremely low pay-off, respectively. In the first situation, the predicted system behavior has a maximum payoff at the same location as the actual system behavior. This exemplifies the right amount of refinement in the model. In Figure 7 (b), the predicted system behavior shows a maximum much earlier than the actual system behavior's maximum. The predicted maximum occurs at X_2, whereas the actual system behavior's maximum is located at X_1. If the engineer were to choose the point at X_2 in an attempt to achieve the most payoff, this would result in the lowest payoff for the actual system. The refinement in this case was either not thorough enough, or incorrect system information was used. In order to avoid such an extreme difference in system behaviors, careful study of the system must be performed. Although including more system information for refinement may be costly, the resources would not be wasted for this situation.

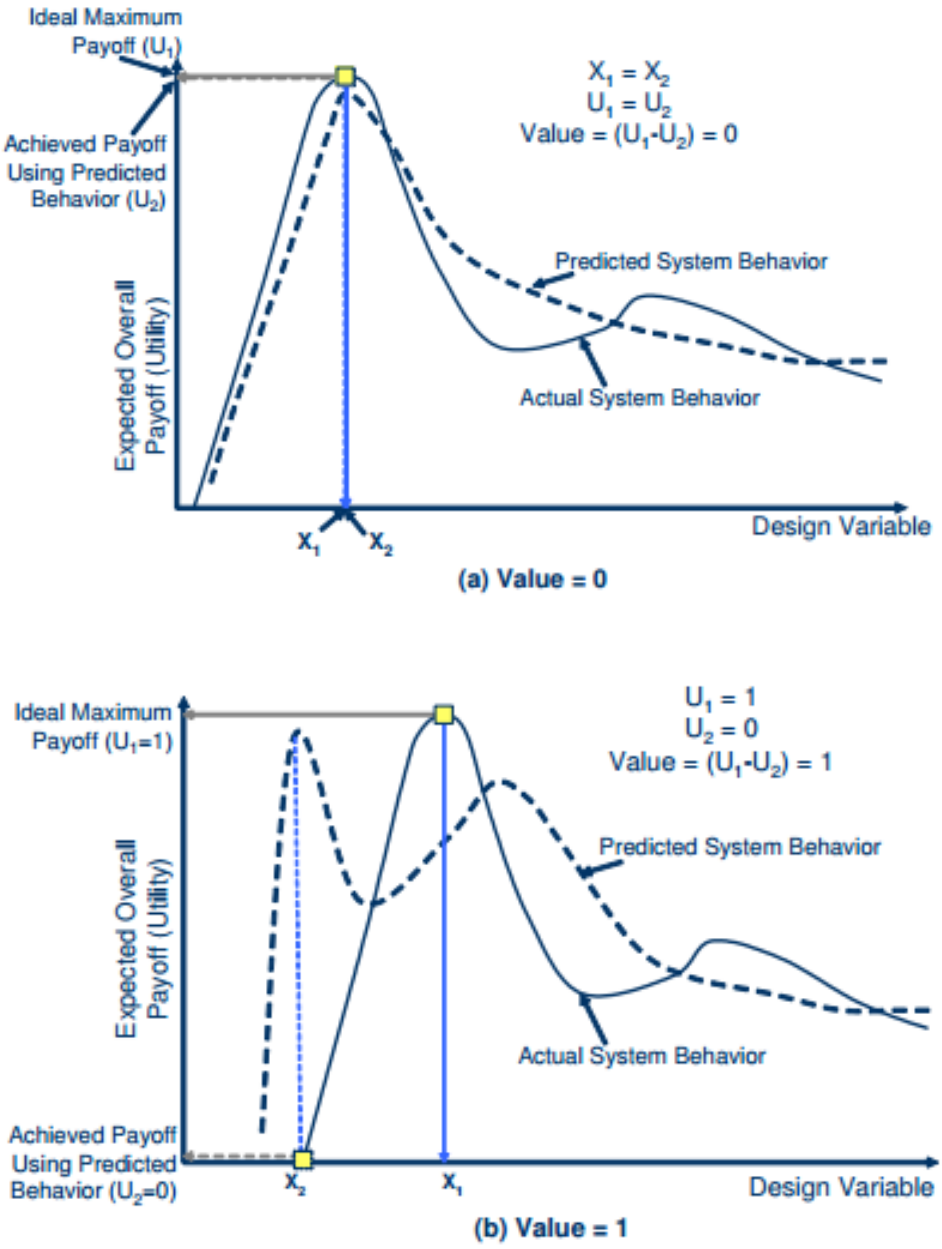

Figure 7: Two Extreme Scenarios of Value of Perfect Information [9]

Panchal et al. [23] defines the Hurwicz criterion as a decision criterion that is created from both optimistic and pessimistic criteria. In order to calculate this criterion, a weighted average is used that involves a coefficient of pessimism, α. An α value of 1 is

considered completely pessimistic, while a value of 0 is considered completely optimistic. The value 0.5 is used unless stated differently [23]. The Hurwicz criterion is used for finding the value-of-information of the model. It can help show the amount of improvement potential to be gained by refining the simulation further. If this improvement potential in the utility is low, then refinement of the system can be stopped.

The pressure vessel problem involves increasing the accuracy of the model by including more information about the material microstructure. The drawback of adding more information to the system is the increased cost of the experiments [9]. The purpose is then to find the amount of imprecision that is acceptable in this situation for making decisions. The engineer set the material strength with a lower and upper bound. The maximum and minimum value of the utility based on the Hurwicz criterion are found using these upper and lower bounds of material strength, and the improvement potential is found from the difference in these utilities. Once this improvement potential is "sufficiently low," the refinement can be considered complete. This means that refining the model further would not actually improve the predicted system outcome. Since obtaining more information about the material strength requires costly testing, it is best to stop the refinement as soon as this potential is low enough. The authors go on to refine based on density information for the pressure vessel as well.

While this is an excellent example for simulations and refinement methods, the pressure vessel situation is not a real life experiment that is performed. It is instead an example of using the design process analysis for refinement. These refinement procedures can be applied to experiments and simulations in use today and help in decision making.

Since the process of design can use a large amount of resources, it must be included in design decisions, especially when it comes to refinement [22].

2.3.1 Applying Design Process Principles to CFD Research

The principles discussed in the previous section can be applied to computational fluid dynamics simulations. One important note with using CFD is its validity. Great care should be taken with selecting all conditions and equations that apply to the simulation. Proper refinement techniques are essential, but as stated before, only a certain amount of refinement may be necessary before the costs outweigh the benefits.

One method of applying these refinement procedures is the systematic approach using the value-of-information process performance indicator suggested by Messer et al. [24]. With this method, the engineer would use the least complicated but valid model first, and refine the model continually until a recommended model is achieved. System complexity can be increased by further refining the computational grid, which creates more data points for analysis. Another way to refine the simulation would be to add either more information into the system, as in the case of the material strength data in the pressure vessel situation, or adding more features to the simulation. This can be accomplished by using more detailed geometry or by adding more parts to the system, including things like nuts and bolts or more fan blades, for example.

The US Air Force used design of experiments (DOE) methods along with CFD when developing missiles [13]. The concept of DOE is similar to the design process principles discussed. It is a method where the relationship between process factors and process output are determined [25]. The inputs of the process are analyzed in order to

maximize the output. Both DOE and design process analysis look to change the process of design in order to optimize results. Computational fluid dynamics was used in this study to determine the forces and moments on a missile through different speeds and attack angles. They used DOE to find the effect of the flight conditions on the aerodynamic force and moment coefficients of a missile. Cleaver, et al. [13] discussed the concern that modeling turbulent flow using a highly refined mesh would require several days or weeks to complete the simulation. Since the system being analyzed was so complex, the Air Force Research Lab used a supercomputer with 87,424 cores [13]. The use of DOE was found to be beneficial when the factors affecting the output were carefully selected. The authors also note the computer model needs to be validated using computational and experimental results.

A similar method for design process analysis in regards to refinement was used when evaluating the CFD simulations for the two case studies in this research. A simplified model of the system was used first for both the photobioreactor analysis and the grain dryer analysis. As these simulations were run successfully, additional parameters was introduced into the models to better represent the experimental tests that corresponded to these situations. Once reasonable results were obtained for the more complex models, variations on the original setups for each case study were then simulated, giving different results for varying initial conditions.

The design process principles discussed in this chapter are applied to the designs studied in this thesis. In order to accurately represent real-life systems, the proper modeling procedure should always be followed, and is discussed in detail in Chapter 3. Methods for

setting up the simulation and proper refinement are also studied further. The governing equations used by the simulation software are presented in detail.

2.4 Summary

This chapter discussed the basics of computational fluid dynamics and its strengths and areas for improvement. Design process analysis was also studied as it relates to modeling and simulation.

The first calculations that resembled CFD took weeks to complete. Today, the same calculations can be done in a matter of hours. This improvement was largely due to the advent of the computer age. CFD gives users the ability to design and test and variety of systems. It helps to streamline the design process as computational models can easily be changed and tested. Flow fields that in the past were difficult to visualize can be represented in CFD. Potential areas for improvement with CFD include the analysis of chemically reacting and turbulent flows. CFD also relies heavily on the user, so care must always be taken when using it to analyze a system.

Design process analysis helps to decrease the potential for user error through the use of model refinement. Model refinement can be accomplished either by starting with a simple system and adding more features with successful iterations or by refining the computational grid. Many studies exist on the process of using these methods in theoretical situations.

This research seeks to bring together the use of CFD on real life systems with the process of model refinement. By comparing results of CFD simulations with varying levels of refinement and experimental setups, a recommended system for computational

modeling can be achieved. This will bridge the gap between using model refinement on theoretical systems and actual systems. The research will also give examples of using design process analysis within CFD simulations.

Chapter 3: Methodology

The basic methods for creating models and preparing them for simulation are discussed in this chapter. In addition, the relevant governing equations involved with CFD are described. Depending on the goal of the research, a system can be modeled several ways. This chapter gives insight into these methods.

3.1 Steps for Creating an Appropriate Model and Simulation

In order to construct a simulation for use with CFD, a representation of the system must be created using a computational model. The model is then imported into the CFD software and used in the analysis, with the proper initial and boundary conditions incorporated into the setup. The flow chart in Figure 8 shows the step-by-step process for setting up and simulating a model. This process is the basis for the methods described in this section.

The procedure for modeling and simulating a design discussed in this thesis are general guidelines and may vary based on the engineer and the system being analyzed. Based on the flow chart in Figure 1, this process falls under the step involving developing and testing models. However, since simulations allow the engineer to determine the effectiveness of a design, the steps involving improving and redesigning and making a design decision could also be accomplished using this method. For any simulation, the setup, boundary, and physical conditions should be verified for the actual system. As stated before, a completed simulation may seem like it gives great results, but these results are meaningless if the model does not accurately represent the design. With an effective

simulation, the design can easily be modified to show the engineer how changes will affect the results. This helps to cut down on the costs associated with prototype development and testing. The engineer can then compare the different system setups and make a design decision based on the outcomes of the simulations.

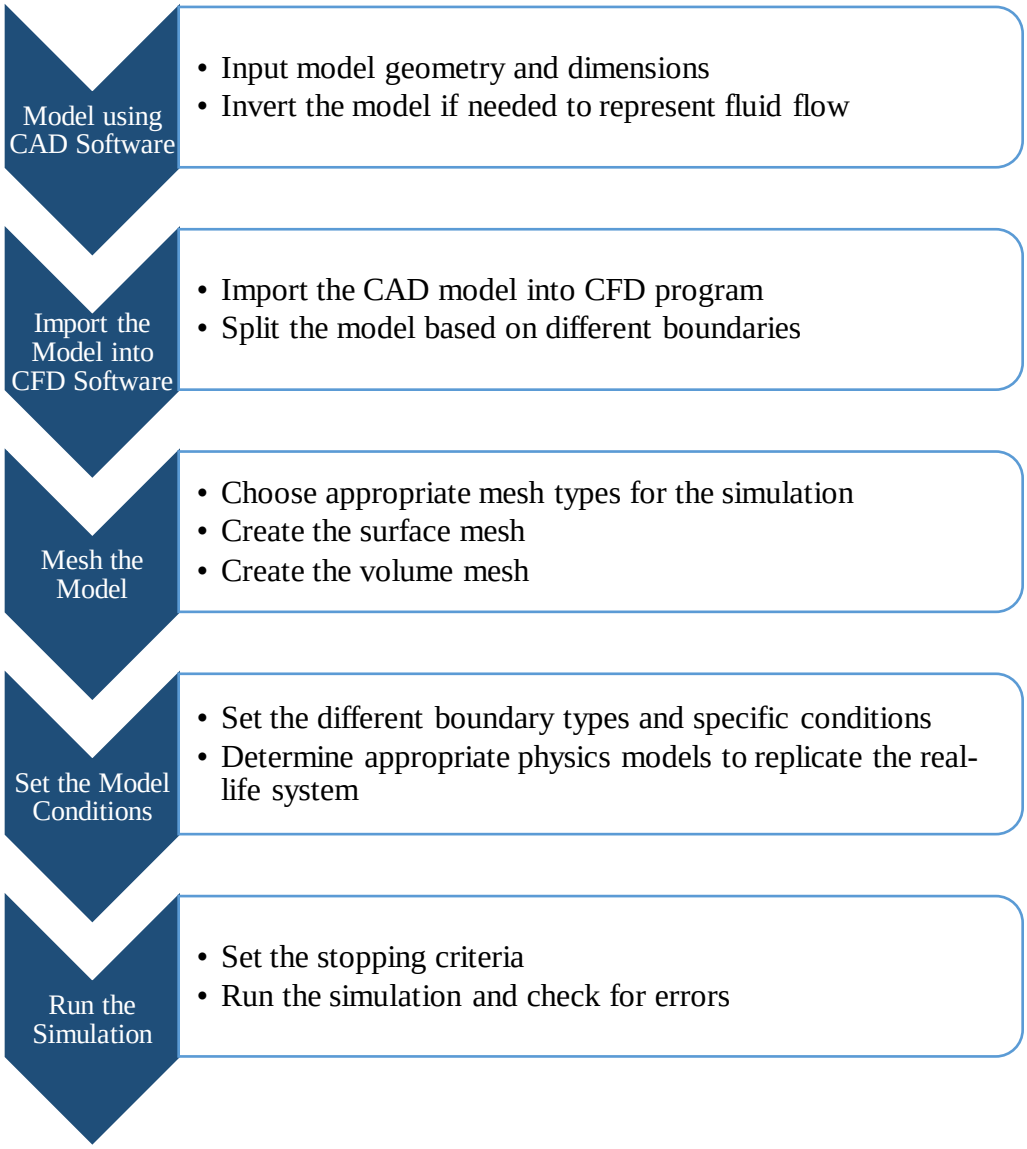

Figure 8: Flow Chart of Modeling and Simulation Process

3.1.1 Modeling Using CAD Software

Modeling is an essential part of the simulation process, as an appropriate model is required to be able to represent what is occurring in real life. The model can be created using any of a variety of different Computer Aided Design (CAD) software programs. The models used in this analysis were created using Creo Direct 2.0® and SolidWorks 2014®, for the photobioreactor study and grain dryer simulation, respectively. Both modeling programs are excellent, the choice for each was made based on convenience of access. In order to create these models in CAD software, the user must first measure the dimensions of the object to be analyzed in real-life. Depending on the goal of the simulation, such intricate details, e.g., fasteners, may not be required to be included in the measurements and model. Once the measurements have been recorded, the user can use a relevant CAD program to create a model of the object to be simulated.

When using computational fluid dynamics, an important note to keep in mind is that the model being created is generally not a model of the solid part of the object. While this is not how the models are created in all cases, for the photobioreactor and grain dryer case studies, this is how the CAD models were designed. The models should be the geometry of the fluid flow area. Oftentimes, this means that the model the engineer would generally create when designing a product will be inverted, and the solid regions will become the hollow regions, and the space where the fluid flows will now be modeled as a solid. When the desired model has been created using CAD software, it can then be imported into the computational fluid dynamics software of choice.

3.1.2 Importing the Model into CFD Software

In this research, the CFD software STAR-CCM+ version 11.04 was used. Upon opening the CAD model in the CFD interface, the user must split the object into its different boundaries in order to specify the purpose of each. For example, in a heat exchanger, the model must be split so that the inlets, outlets, and walls are clearly defined. This way any inlet and outlet velocities and pressures may be set, as well as the temperatures of the different walls. Any boundaries that have the same conditions, for example the walls of an air duct, can be combined for simplicity. Once the proper boundaries are selected and set, the mesh, which is the basic tool for finite element analysis, may be created.

3.1.3 Meshing the Model

Meshing is one of the most important tools used in CFD analysis. It allows the user to be able to gain an understanding of the interactions occurring at each point in space or time. The mesh is generally divided into two parts: a surface mesh and a volume mesh. The surface mesh goes around the outside of the object and allows for analysis at each finite point based on the size set by the user. The surface mesh is required in order to create a volume mesh. For poorer quality CAD models, the surface wrapper can be used. Otherwise, the surface remesher, which retriangulates the surface of the model, is selected [26]. Once the surface has been meshed, the volume mesh can be created.

The volume mesh is used for a more detailed analysis, as it involves a 3-D calculation process. Each volume element is taken into account when running the simulation, and this gives the user the ability to determine the interactions occurring at any point in the experimental setup. The different volume mesh types are as follows: trimmed,

polyhedral, tetrahedral, prism layer, advancing layer, extruder, thin, and generalized cylinder meshers [26]. CD-adapco [26] lists the following as considerations for choosing a volume mesh: time require to create the mesh, solution accuracy desired, available memory, quality of the initial surface mesh, convergence rate, single or multi-region mesh, and if the geometry is thin or not. All of these factors need to be considered when choosing the right mesh for the design problem.

Each mesh has its strengths for specific design problems. The tetrahedral mesh builds quickly and uses little memory, but is not as accurate as the other mesh types. It requires more cells to produce the same quality results as other volume meshes. Polyhedral and trimmed meshes are two types that will give more accurate results compared to the tetrahedral mesh [26]. The polyhedral and tetrahedral mesh types are similar in that their accuracy relies on the quality of the starting surface, unlike the trimmed meshing model. However, both the tetrahedral and polyhedral volume meshes are recommended for situations where a multi-region grid exists and a conformal mesh is required at the interfaces. The prism layer mesher and advancing layer mesher work similarly in that they both produce prismatic cell layers near wall boundaries. The prism layer mesh is used with a core volume mesh, whereas the advancing layer mesh creates a mesh based off the initial triangulated surface, then extrudes the prismatic layers into the volume. The extruder mesh type is used for inlets and outlets to extend the mesh past the initial surface [26]. The generalized cylinder mesher is used with the polyhedral mesher to make an extruded mesh along cylindrical parts. Lastly, thin surface geometries do best with the thin mesher, which makes a prismatic mesh [26].

For the case studies in this research, the polyhedral volume mesh was chosen based on its flexible shape and applicability to complex mesh problems [26]. Both the grain dryer and the photobioreactor have rectangular and cylindrical aspects in the models. If the model were mainly made up of rectangular shapes, the trimmed mesher may be more appropriate as it has small, cube shaped elements. The polyhedral mesher involves polyhedral-shaped cells, which conform better to the structure of the two models. An illustration of a polyhedral mesh is shown in Figure 9. This figure demonstrates the appearance of the volume cells that make up the model. When viewed from the outside, the model appears to have a web-like covering to it. These polyhedral cells make up the entirety of the mesh for analysis. The volume mesh in Figure 9 shows only a portion of the full model in order to demonstrate the three-dimensional shape of the cells. A smaller base size for the cells will result in more points for analysis, generally improving the accuracy of the simulation. However, more cells in the simulation also means more time and computer resources are required. As discussed in Chapter 2, the engineer must make a trade-off between an over-complicated simulations that take excessively long to run versus an under-refined simulation that does not give good results. Generally, a good guideline is to start out with a coarser mesh and refine it further as the simulation is run successfully.

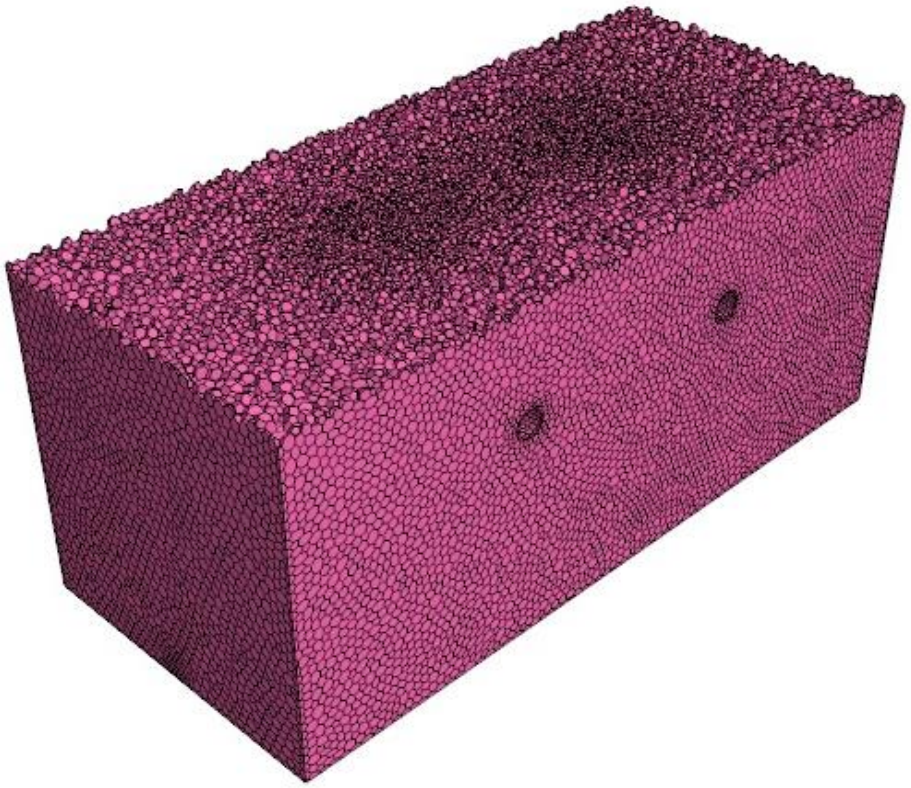

Figure 9: Example of Photobioreactor Polyhedral Core Mesh

3.1.4 Setting the Boundary and Physics Conditions

Once the volume mesh has been created, the boundary conditions and physics models for the simulation are set to replicate the experimental setup as closely as possible. The boundary and initial conditions can be set for each region depending on what type of boundary is specified. For example, if the thermal specification for an inlet is set to constant temperature, this temperature can be input into the simulation. If the thermal specification is set to a heat flux instead, the appropriate heat flux needs to be assigned.

The physics models are specified for the different types of fluid and solid regions, and different regions can have different models. When selecting the models, the engineer

must consider how he or she wishes the analysis to proceed. If the fluid region is set to be a gas, for example, the gas can behave as an ideal gas, real gas, incompressible, or compressible. Other aspects of the simulation that may be of importance include the turbulence specification, the inclusion of gravity, and an energy analysis, to name a few.

Within the physics models, the actual material being analyzed, whether it is a solid, liquid, or gas, can be input by the user. STAR-CCM+ has an extensive material database, and the user can manually input a certain material into this database if it is not already included. In addition to this, the different properties of the materials can also be changed if necessary.

The different interfaces may also be changed based on how the user would like for them to interact. In the grain dryer case study, a porous interface exists between the heating duct and the duct that contains the grain. The porosity of a region is defined by how much of the space is taken up by empty volume. It is generally a fractional or decimal value. For a porous interface, the porosity can easily be set and changed in the software.

By setting all of the initial and boundary conditions needed in the simulation, the user is telling the CFD program what equations and calculations are appropriate for the analysis. These calculations are based on equations that make up the structure of computational fluid dynamics.

3.2 Governing Equations

The ability to use CFD for analyzing the system saves much time because the analysis would normally be done step-by-step using complicated calculus relations. CFD helps to streamline these calculations.

CFD has several governing equations that provide a basis for the intense calculations that take place during its run time. According to Wendt [10] the "cornerstone" of CFD is the governing fluid dynamics equations: continuity, momentum, and energy. Wendt [10] also specifies these as statements of the three fundamental physical principles of fluid dynamics: mass is conserved, Newton's second law, and energy is conserved. Many different equations govern computational fluid dynamics software. For the sake of this research, the main fluid governing equations and any equations related to the specific case studies will be discussed.

The main governing equations within CFD are the Navier-Stokes equations. The following are the complete Navier-Stokes equations in their conservation form from Wendt [10]:

$$\frac{\partial(\rho u)}{\partial t}+\frac{\partial(\rho u^2)}{\partial x}+\frac{\partial(\rho uv)}{\partial y}+\frac{\partial(\rho uw)}{\partial z}=-\frac{\partial p}{\partial x}+\frac{\partial}{\partial x}\left(\lambda\nabla\cdot\vec{V}+2\mu\frac{\partial u}{\partial x}\right)+\frac{\partial}{\partial y}\left[\mu\left(\frac{\partial v}{\partial x}+\frac{\partial u}{\partial y}\right)\right]+\frac{\partial}{\partial z}\left[\mu\left(\frac{\partial u}{\partial z}+\frac{\partial w}{\partial x}\right)\right]+\rho f_x \quad (3.1a)$$

$$\frac{\partial(\rho v)}{\partial t}+\frac{\partial(\rho uv)}{\partial x}+\frac{\partial(\rho v^2)}{\partial y}+\frac{\partial(\rho vw)}{\partial z}=-\frac{\partial p}{\partial y}+\frac{\partial}{\partial x}\left[\mu\left(\frac{\partial v}{\partial x}+\frac{\partial u}{\partial y}\right)\right]+\frac{\partial}{\partial y}\left(\lambda\nabla\cdot\vec{V}+2\mu\frac{\partial v}{\partial y}\right)+\frac{\partial}{\partial z}\left[\mu\left(\frac{\partial w}{\partial y}+\frac{\partial v}{\partial z}\right)\right]+\rho f_y \quad (3.1b)$$

$$\frac{\partial(\rho w)}{\partial t}+\frac{\partial(\rho uw)}{\partial x}+\frac{\partial(\rho vw)}{\partial y}+\frac{\partial(\rho w^2)}{\partial z}=-\frac{\partial p}{\partial z}+\frac{\partial}{\partial x}\left[\mu\left(\frac{\partial u}{\partial z}+\frac{\partial w}{\partial x}\right)\right]+\frac{\partial}{\partial y}\left[\mu\left(\frac{\partial w}{\partial y}+\frac{\partial v}{\partial z}\right)\right]+\frac{\partial}{\partial z}\left(\lambda\nabla\cdot\vec{V}+2\mu\frac{\partial w}{\partial z}\right)+\rho f_z \quad (3.1c)$$

Where $\vec{V}$ is the vector velocity field in Cartesian space given by:

$$\vec{V}=u\vec{\imath}+v\vec{\jmath}+w\vec{k} \quad (3.2)$$

The u, v, and w are the x, y, and z components of velocity given by:

$$u = u(x, y, z, t)$$

$$v = v(x, y, z, t)$$

$$w = w(x, y, z, t)$$

The term $\nabla \cdot \vec{V}$ is the time rate of change of the volume of a moving fluid element, per unit volume. The ρf_x, ρf_y, and ρf_z terms are the body forces per unit mass acting on the fluid element by $\vec{f}$, with each component in its respective direction. The term λ is the bulk viscosity coefficient, and μ is the molecular viscosity coefficient, with:

$$\lambda = -\frac{2}{3}\mu \tag{3.3}$$

In equations 3.1a-c, the density is given by ρ, with the scalar density field being:

$$\rho = \rho(x, y, z, t)$$

In addition to this, t is the function of time in these equations.

The continuity equation for used to solve the Navier-Stokes equations is [27]:

$$\frac{\partial \rho}{\partial t} + \nabla \cdot \left(\rho \vec{V}\right) = 0 \tag{3.4}$$

Compared to the conservation form of the Navier-Stokes equations, the non-conservation form is found by applying the fundamental physical principle to a fluid element that is moving.

The realizable k-epsilon turbulence model is used to describe the turbulence in both the photobioreactor and the grain dryer simulations. The transport equations for this model are as follows [26]:

$$\frac{d}{dt}\int_V \rho k dV + \int_A \rho k(v - v_g)\cdot da = \int_A (\mu + \frac{\mu_t}{\sigma_k})\nabla k \cdot da + \int_V \left[f_c G_k + G_b - \rho((\varepsilon - \varepsilon_0) + \Upsilon_M) + S_k\right]dV \quad (3.5)$$

$$\frac{d}{dt}\int_V \rho \varepsilon dV + \int_A \rho \varepsilon(v - v_g)\cdot da = \int_A (\mu + \frac{\mu_t}{\sigma_\varepsilon})\nabla \varepsilon \cdot da + \int_V \left[f_c C_{\varepsilon 1} S\varepsilon + \frac{\varepsilon}{k}(C_{\varepsilon 1} C_{\varepsilon 3} G_b) - \frac{\varepsilon}{k+\sqrt{\nu\varepsilon}} C_{\varepsilon 2}\rho(\varepsilon - \varepsilon_0) + S_\varepsilon\right] dV \quad (3.6)$$

Where S_k and S_ε are user-specified source terms, ε_0 is the ambient turbulence value in the source terms that counteracts turbulence decay, and f_c is the curvature correction factor [26]. G_k is defined as the turbulent production term and is calculated as follows:

$$G_k = \mu_t S^2 - \frac{2}{3}\rho k \nabla \cdot v - \frac{2}{3}\mu_t(\nabla \cdot v)^2 \quad (3.7)$$

Where $\nabla \cdot v$ is defined as the velocity divergence and S as the modulus of the mean strain tensor:

$$S = |\mathbf{S}| = \sqrt{2\mathbf{S}:\mathbf{S}^{\mathrm{T}}} = \sqrt{2\mathbf{S}:\mathbf{S}} \quad (3.8)$$

And:

$$\mathbf{S} = \frac{1}{2}(\nabla v + \nabla v^T) \quad (3.9)$$

G_b is the production term due to buoyancy defined by:

$$G_b = \beta \frac{\mu_t}{\sigma_t}(\nabla T \cdot \mathbf{g}) \quad (3.10)$$

Where β is the coefficient of thermal expansion, ∇T is the temperature gradient vector, **g** is the gravitational vector, and σ_t is the turbulent Prandtl number. Ideal gases use the following relation:

$$\beta = -\frac{1}{\rho}\frac{\partial \rho}{\partial T} \tag{3.11}$$

The coefficient $C_{\varepsilon 3}$ is calculated according to Henkes et al. [28] by:

$$C_{\varepsilon 3} = tanh\frac{|\mathbf{v}_b|}{|\mathbf{u}_b|} \tag{3.12}$$

Where $\mathbf{v}_b$ is the velocity component that is parallel to **g**, and $\mathbf{u}_b$ is the velocity component perpendicular to **g**. For this formulation, the coefficient is generally set to zero outside the natural convection boundary layers. Another formulation sets $C_{\varepsilon 3}$ as constant everywhere, or specified by [26]:

$$C_{\varepsilon 3} = \begin{cases} 1 \; for \; G_b \geq 0 \\ 0 \; for \; G_b < 0 \end{cases} \tag{3.13}$$

Υ_M is the dilatation dissipation and is modeled according to Sarkar and Balakrishnan [29] as:

$$\Upsilon_M = \frac{C_M k \varepsilon}{c^2} \tag{3.14}$$

Where $C_M = 2$ and c is the speed of sound.

The turbulent viscosity is calculated by:

$$\mu_t = \rho C_\mu \frac{k^2}{\varepsilon} \tag{3.15}$$

Where C_μ is given by:

$$C_\mu = \frac{1}{A_0 + A_S U^{(*)} \frac{k}{\varepsilon}} \tag{3.16}$$

With:

$$U^{(*)} = \sqrt{\mathbf{S}:\mathbf{S} + \mathbf{W}:\mathbf{W}} \tag{3.17}$$

Where S is the modulus of the mean strain rate tensor given in equation 3.9 and $\mathbf{W}$ is the rotation rate tensor given by:

$$\mathbf{W} = \frac{1}{2}(\nabla \mathbf{v} - \nabla \mathbf{v}^{\mathrm{T}}) \tag{3.18}$$

The coefficients are given by:

$$A_s = \sqrt{6} cos\phi \tag{3.19a}$$

$$\phi = \frac{1}{3}\mathrm{acos}(\sqrt{6}W) \tag{3.19b}$$

$$W = \frac{S_{ij}S_{jk}S_{ki}}{\sqrt{S_{ij}S_{ij}}^3} \tag{3.19c}$$

A_0 = 4.0 for this model.

The coefficient $C_{\varepsilon 1}$ is calculated by:

$$C_{\varepsilon 1} = \max(0.43, \frac{\eta}{5+\eta}) \tag{3.20}$$

Where:

$$\eta = \frac{Sk}{\varepsilon} \tag{3.21}$$

The remaining model coefficients have values given in Table 2 [26]:

Table 2: K-Epsilon Model Coefficient Values

Coefficient	Value
$C_{\varepsilon 2}$	1.9
σ_k	1.0
σ_ε	1.2

For the photobioreactor simulation, the general Navier-Stokes equations for incompressible Newtonian fluids were used from [30]:

$$\rho(\partial V/\partial t + V \cdot \nabla V) = -\nabla p + \rho g + \mu \nabla^2 V \qquad (3.22)$$

Where V is the fluid velocity, p is the pressure, g is gravity, and μ is the dynamic viscosity.

The photobioreactor simulation involves the analysis of small particles, or bubbles. With such a small diameter, these bubbles are assumed to be internally homogenous. Mortuza et al. [31] made the same assumption. This assumption gives a small Biot number of less than 0.1. The following equation was used:

$$m_p c_p \, (dT_p/dt) = Q_t + Q_{rad} + Q_s \qquad (3.23)$$

Where m_p is the mass of the particle, c_p is the particle's specific heat, and T_p is the particle temperature. Q_t is the rate of convective heat transfer, Q_{rad} the rate of radiative heat transfer, and Q_s the rate of heat transfer from other sources. Q_t is given by:

$$Q_t = fhA_s(T - T_p) \qquad (3.24)$$

With T being the continuous phase temperature, h is the heat transfer coefficient, A_s is the surface area of the particle, and f is a mass transfer coefficient. El Wakil et al. [32] gives the relation for f as:

$$f = z/(e^z - 1) \tag{3.25}$$

Where:

$$z = (-m_{pr}c_p)/(hA_s) \tag{3.26}$$

With m_{pr} as the rate of mass transfer to the particle.

In order to find the drag force, the particle Reynolds number was calculated according to the following equation [30]:

$$Re_p = \rho V D_p/\mu \tag{3.27}$$

Where D_p is the particle diameter. In addition to the particle Reynolds number, the particle Nusselt number was calculated to find the heat transfer in PBR. This equation is based on the Ranz-Marshall correlation [33]:

$$Nu_p = 2\left(1 + 0.3{Re_p}^{1/2}Pr^{1/3}\right) \tag{3.28}$$

Where Pr is the Prandtl number of the continuous phase for water (7.07).

3.3 Representation of Models and CFD

Computational fluid dynamics uses the governing equations in order to replicate the interactions occurring within the system. This includes both the different boundary

conditions of the model and the fluid and heat transfer interactions that occur when running a simulation. Proper model representation is necessary to receive acceptable to results.

Taking the ideas discussed in Chapter 2 Section 2, the design process analysis can be applied to simulations involving CFD. The different principles for model generation and analysis help to determine the tradeoff between system complexity and the validity of the results.

For each system that is modeled, the mesh, or computational grid, must be created. Generally, a simple mesh is created at first, with the base size for the cells continually decreased in order to increase the precision. A smaller base size for the cells means more cells in the overall simulation. The increased time required by the computer to run the simulation can be measured and compared to the difference in simulation results.

A different method for analyzing the model representation involves studying a system that is initially modeled with fewer features. Additional time is required as more information is added into the system, either in the form of data or parts. A simplified system will not replicate the real-life structure very well, and the results may not even be applicable for the given situation. However, it may be necessary to start with such a simplified model in order to ensure that each part of the system is behaving correctly. As simulations are successfully completed, additional features can be added to the model. This technique can be repeated until a model that closely represents the actual system is achieved. Similar to the grid refinement technique, more features will translate into more time required by the computer for both setting up the model and for running the simulation. Some features may not be relevant to the results needed for the system. Another tradeoff analysis can be

performed to determine the recommended model representation in CFD for the given situation. The engineer can conserve resources effectively using this method.

Both of these methods will be applied to two case studies analyzed in this research. The main focus will be on the method of adding more features to the system, with grid refinement throughout. Through the use of these refinement methods, the recommended models for the two systems are obtained. These models can then be used to test design changes and to give more information about the system.

Chapter 4: Case Study 1 – Photobioreactor

The first research study in this thesis involved a photobioreactor system. An overview of PBRs is given, along with the relevant research studies pertaining to them. The system being analyzed and the modeling process is discussed. Results from the simulations are described.

4.1 Overview of Photobioreactors

In order to meet the rising energy demand around the world today, we must turn to the renewable sources of energy available. Without biofuels, there is little chance to meet this demand sustainably [34]. Although other sources besides imported petroleum exist to help offset this demand, using fossil fuels like coal and shale is not an environmentally sound and permanent solution to the problem. Different types of biofuels are available and constantly being researched and improved. These include ethanol from such crops as corn, potatoes, and wheat, biodiesel produced from different types of oils and fats, solids such as wood or corn stover, and second-generation biofuels, including cellulosic ethanol and algae biofuels, to name a few [35]. For this case study, algae-based biofuels are studied specifically. Microalgae were first studied by the U.S. government in the 1970s with the Aquatic Species Program, which was shut down in 1996, but a new era of research into this type of fuel was started in 2006 [34]. These biofuels are produced by using photobioreactors, which are controlled systems in which the algae grows.

4.1.1 Function of a Photobioreactor

Photobioreactors are tanks used to grow microalgae, and they rely on a carefully balanced ecosystem. The algae growth depends on a delicate balance involving the mixing of the tank, proper oxygen and carbon dioxide amounts, sufficient light, and nutrients. Some of these properties are more easily managed than others, and the ability to reach an ideal balance for the specific type of PBR given varies greatly.

Several different types of photobioreactors are in use today, each with its own benefits and drawbacks. One such example is the open pond raceway PBRs [36]. This type of PBR is open to the environment and uses direct sunlight to grow the algae. These have the capability for large amounts of microalgae to be produced, but factors such as light, contamination, carbon dioxide, etc. are not easily controlled.

Instead, closed loop photobioreactors can still produce large yields of algae with the ability to change the growing conditions relatively easily. This type of PBR usually involves artificial light for the growth of algae and uses tanks the prevent contamination from the environment. According to Massart et al., [37] "A photobioreactor is a closed transparent device which maintains a controlled environment within the microalgal culture…" Among the closed system PBRs, several types exist: vertical-column, flat-plate, and tubular. Recently, most research has been on these three types of PBRs, with the light being applied to the outside of the tank [38]. Each type has its costs and benefits. However, according to Nauha and Alopaeus [39], adequate fluid dynamics analysis plays the most essential role in the success of a design of a PBR. Column photobioreactors, the type studied in this research, have an advantage in that they provide superior mixing and

volumetric gas transfer rates [38]. The mixing in this type of photobioreactor is often supplied by a bubble column which diffuses carbon dioxide bubbles into the fluid mixture. This research focuses specifically on a closed loop bubble column PBR.

4.1.2 Advantages and Limitations of Photobioreactors

Photobioreactors have the potential to mass produce microalgae for biofuel. Algae, unlike grain ethanol, is capable of producing yields of 1,100 to 15,000 gallons per acre (grain has the potential of only 620-930 gallons per acre). Photobioreactors have an advantage in that they do not require fertile land to grow the microalgae for fuel [34]. Therefore, they can utilize previously unused or unsuitable land without taking away from the agricultural market. This is a concern for most grain-based ethanol. In order to be effective, PBR design needs to be optimized for producing large quantities of algae.

One area for improvement in PBRs is mixing. Although mixing is an essential part of the algal growth process, it also requires a delicate balance. When the algal culture is properly stirred, the algae gets adequate exposure to the light and nutrients within the column. The yield of algae can be increased by the exposure to light and dark cycles [40]. In order for all of the algae to get the exposure to the light it needs, they need to continuously be circulated throughout the column. Otherwise, shading can occur from the algae closest to the light source, preventing the algae in the darker middle region of the PBR from getting the necessary light for photosynthesis. Too much or too forceful mixing can affect negatively affect the growth of algae, however. When the rate of diffusion in the column is too high, shear can occur, which has the potential to damage or kill the cells [40, 41]. One advantage of the vertical column photobioreactor, in this case, is the ability to

mix the fluid without any moving parts, providing homogeneous shear [41]. Although higher volumetric flow rates for aeration may provide better mixing, the potential for shear also limits this aspect. A suitable balance between mixing of the algae and the rate at which the bubbles are sparged into the column is required.

Another factor that affects the growth of algae is the amount of light applied to the fluid column. As stated previously, algae need light in order to photosynthesize. This can be problematic, as many photobioreactors are limited by the light only being applied externally to the photobioreactor. The algae closest to the outside of the tank will receive the most light and grow, but their growth can then cause shading to the algae in the middle of the photobioreactor.

4.1.3 Related Research on Photobioreactors

Several studies have been performed In order to help increase light penetration in PBR tanks. Luo and Al-Dahhan [42] suggest using the flashing light effect as one solution to this problem, by helping to reduce photoinhibition in those cells that are close to the outside walls. Other ways to help solve the problem of insufficient light throughout the PBR include increasing the mixing, changing the geometry of the PBR in order to improve the light distribution, and adding light penetration in the column. Using light guides is a method of increasing light penetration in the fluid column. Light guides are placed within the fluid and help illuminate dark regions in the dense algal culture. One research study by Zijffers et al. [43] involved the design of the Green Solar Collector used to add light penetration through the use of optical fibers. This research did not take into account how these light guides would affect the mixing and flow patterns within the photobioreactor.

Massart et al. [37] also discuss the consideration of the fluid flow in PBRs and uses CFD to help in designing PBRs since it cuts down on time required for analysis. This research involved the analysis of an airlift photobioreactor, where the CO_2 was introduced along the bottom of the PBR, similar to the system analyzed in this thesis. However, the software Fluent® was used. Both software packages have similar methods for analysis.

4.1.4 PBR Research at South Dakota State University

The photobioreactor model used in this research was based off of the same PBR studied by Bari et al. [44, 45] and Mortuza et al. [31, 46]. The basic PBR tank setup can be seen in the illustration shown in Figure 10. Their previous research involved the study of a photobioreactor of the same geometry. Mortuza et al. [31, 46] first studied photobioreactors within CFD, with his papers specifically focusing on the heat transfer and bubble circulation patterns in the PBR, respectively. Bari et al. [44, 45] expanded on his research by testing different bubble sparger shapes and placements and spacings, respectively. The works of these two graduate students provided a basis for this paper's research study.

4.2 Photobioreactor System for Analysis

The research mentioned in the previous section is expanded upon in this thesis, with the inclusion of the effects of introducing structural members into the PBR flow. These members represent the geometry of light guides being added to the fluid column, disrupting the flow [47]. A basic diagram of a PBR system is shown in Figure 10. Figure 11 shows an example of the CFD model of the basic tank without light guides. Figure 12 shows a PBR with a 3×3 array of light guides penetrating the tank.

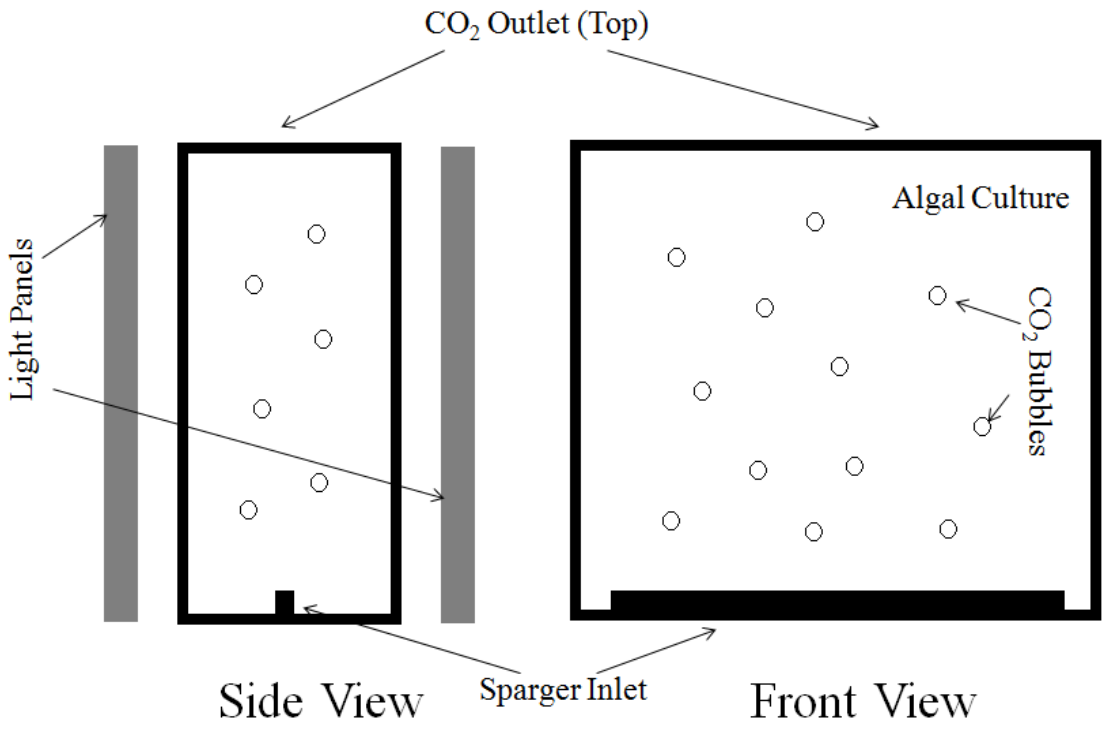

Figure 10: Schematic of Side and Front View of PBR [47]

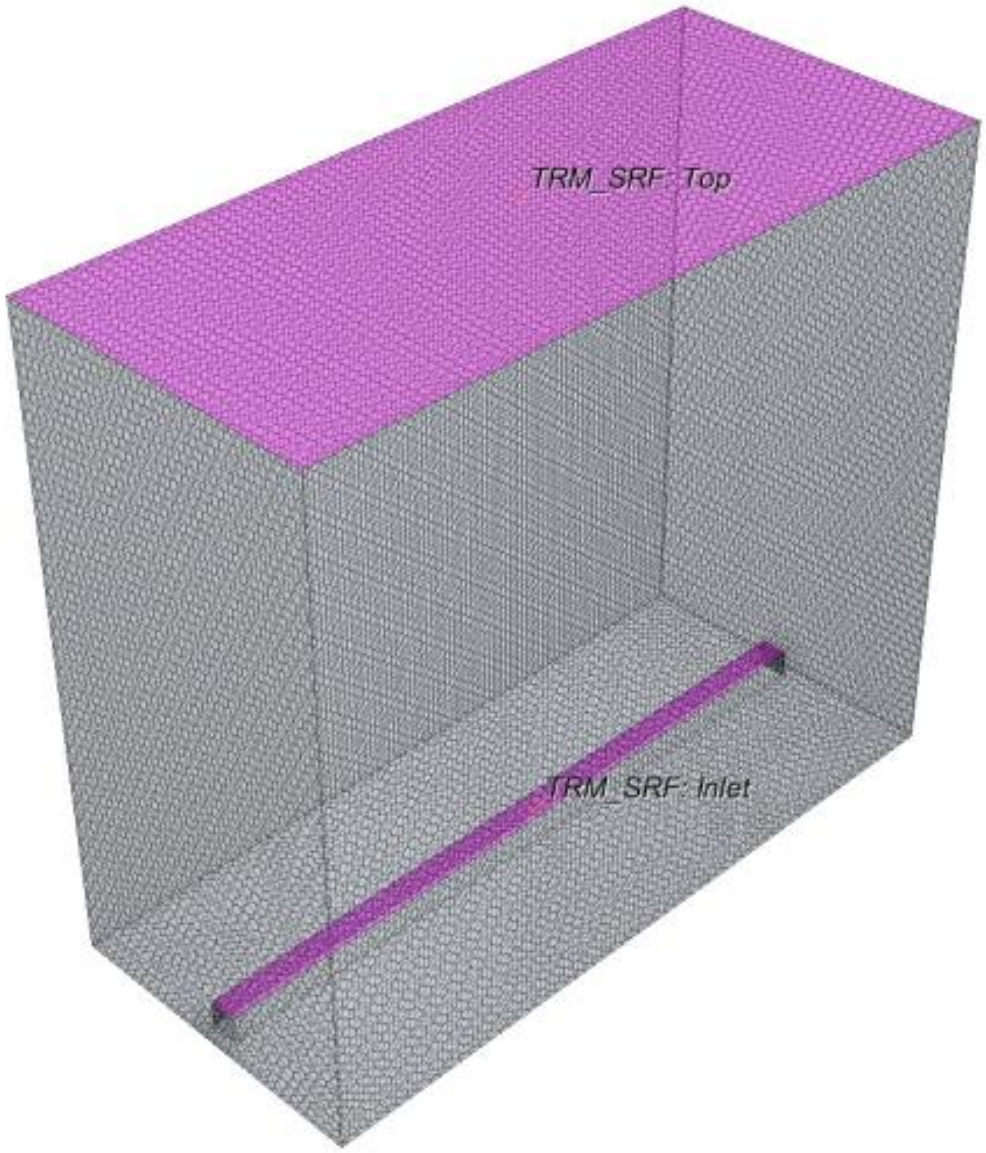

Figure 11: Photobioreactor without Light Guides [47]

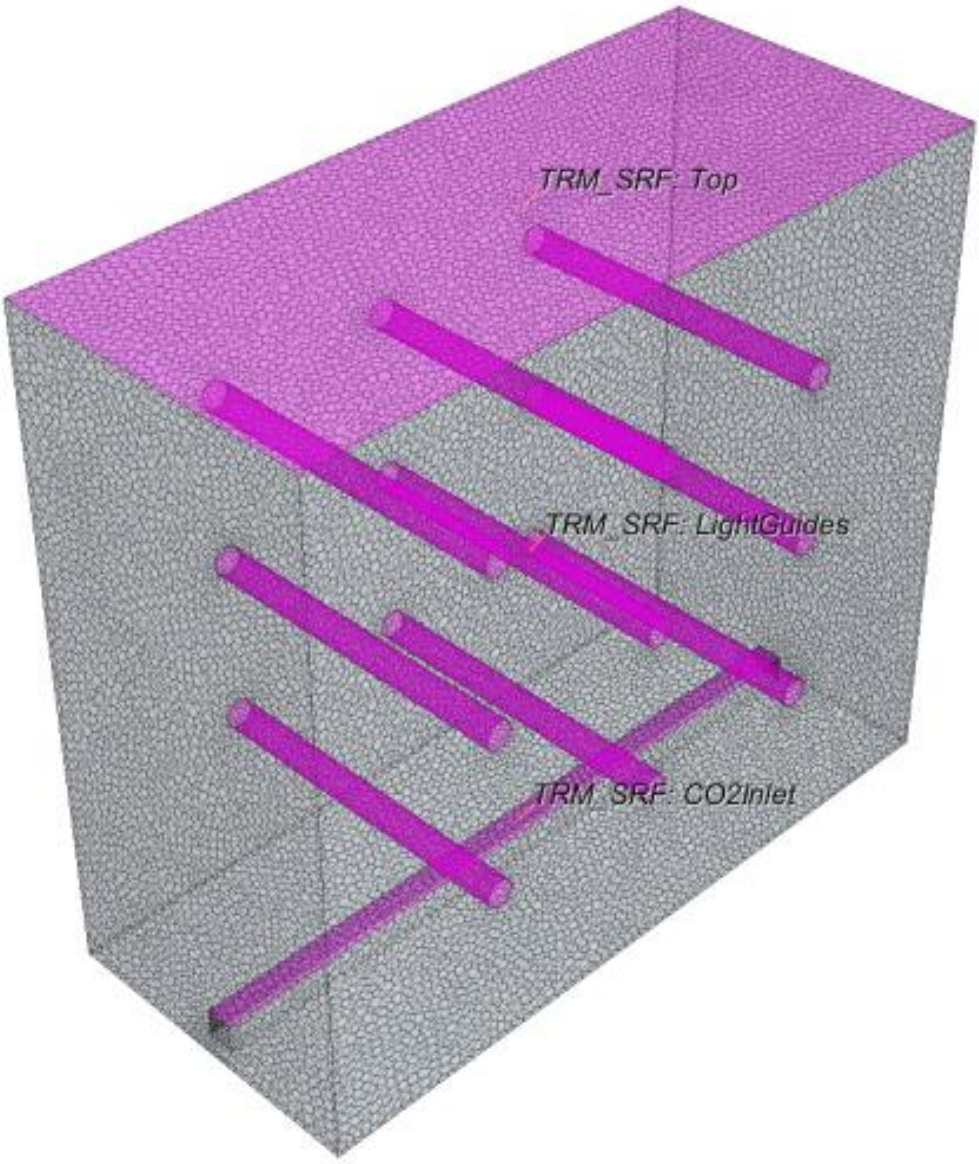

Figure 12: Photobioreactor with 3×3 Light Guide Array [47]

The structural members modeled were 0.5 inches in diameter and penetrated the full width of the fluid column. Carbon dioxide bubbles were sparged in from an inlet along the base of the PBR. These provided the mixing at several different volumetric flow rates. The fluid was modeled as water. Since this study was only based on the effect on the flow

rate and heat transfer of adding cylindrical structures through the middle of the fluid column, light spectrification was not included in the simulation. Five different types of light guide arrays were modeled, including a setup of 2×2, 3×3, and 4×4, and staggered arrays of 2-3-2 and 3-2-3 changing vertically. The visual representation of these arrays is shown in Figure 13.

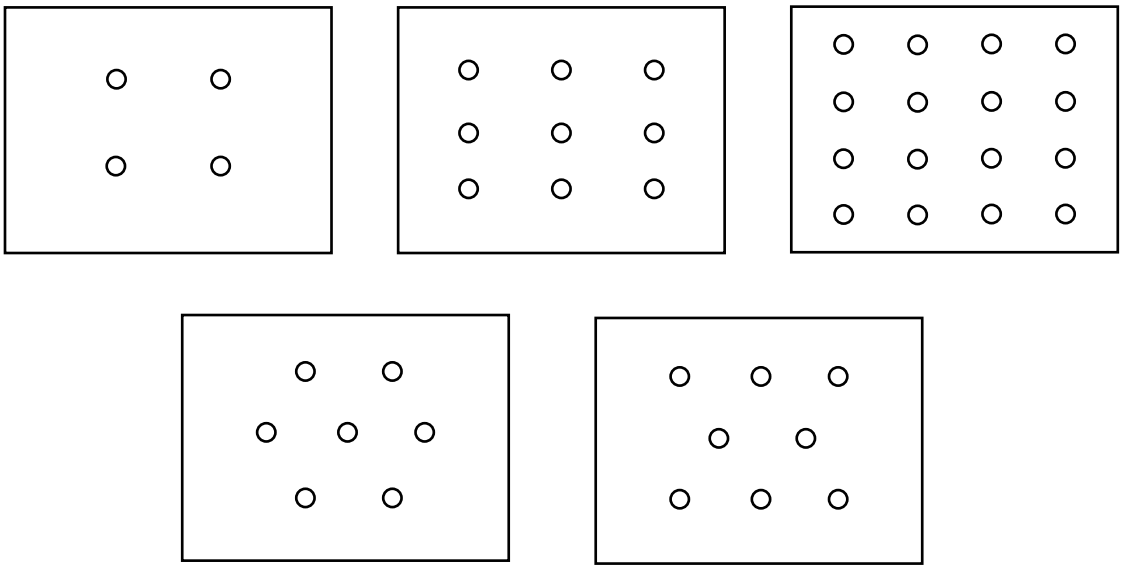

Figure 13: Schematic of Different Light Guide Arrays (side view)

Anderson et al. [48] did a similar research study experimentally involving acrylic light guides of 9.5 mm (0.374 inches) that penetrated the PBR width 38.1 mm (1.5 inches). Although the light guides do not penetrate the full width of the fluid column, both setups will involve similar fluid dynamics results. This PBR was also slightly smaller in size, with a size of 273 mm length × 51 mm width × 271 mm depth. The test apparatus only had a carbon dioxide flow rate of between 0.8 L/min and 1.1 L/min, whereas the flow rates in this research's simulations ranged from 1 L/min to 20 L/min. The results from the research

study by Anderson et al. [48] compared to the simulation results to help demonstrate the effectiveness of computer modeling.

4.2.1 Modeling the Photobioreactor

In order for the simulation to be consistent with the photobioreactor being analyzed, all of the same dimensions were used in creating the model. The PBR tank has base dimensions of 34.29 cm long × 15.25 cm wide × 34.29 cm tall. The actual height of the fluid column is only 30.48 cm tall, and this is the height that was used in the analysis, since the fluid and not the tank is being analyzed in CFD. The bubble diffuser that runs along the base of the PBR is 33.02 cm, almost the entire length of the bottom. The height and width of the diffuser are both 1.27 cm. The light guides modeled in the fluid column are also 1.27 cm, or 0.5 inches, in diameter.

The use of CFD allows for the testing of many different light guide arrays at any number of volumetric flow rates. For this research, five different arrays were tested. These models were created using the Creo CAD software version 5.0. Once the fluid columns with the light guide arrays were modeled in Creo, they were ready to be imported into the CFD simulation software.

4.2.2 Preparing the PBR Model for Simulation

For the analysis in CFD, STAR-CCM+ version 4.04 was used. One of the first steps involved in setting up the conditions of the simulation is to define the different boundary types. For examples, the diffuser is the inlet for the carbon dioxide bubbles. This section can be set as the velocity inlet and injector where the user can choose the velocity of the entering bubbles and the surface that acts as the inlet. Another condition that can be

specified during simulation setup is the initial temperature. Table 3 gives a description of the different surfaces of the PBR and their initial and boundary conditions.

Table 3: Boundary Conditions and Initial Temperature of Photobioreactor

Surface	Boundary Condition	Initial Temperature (K)
CO_2 Inlet	Velocity Inlet	291
Light Guides	Wall	301
Top	Pressure Outlet	300
Bottom	Wall	300
Front	Wall	301
Back	Wall	301
Right Side	Wall	295
Left Side	Wall	295

In addition to the boundary conditions, a mesh must be chosen in order to analyze the system. For the photobioreactor system, a polyhedral volume mesh with a surface remesher was chosen. The polyhedral shape of the mesh helps account for both the rectangular shape of the PBR tank and sparger, while also taking into account the cylindrical shape of the light guides. The size of the mesh varied based on the number of light guides in the arrays, but the base size was typically around 0.01 m. Because the number of light guides in the arrays varied, the number of volume mesh cells for each simulation varied as well. The values ranged from 350,000 to 370,000 total cells.

The fluid mixture within the PBR was treated as a multiphase mixture of water and carbon dioxide bubbles. Although the algae is not grown in pure water and is instead a mixture of the nutrients, algae, and water, water was the best simplification for this scenario. For this mixture, the heat transfer and fluid properties would not change significantly by adding these components.

The carbon dioxide bubbles had a specific size of 1 mm diameter. They were also set as material particles being injected into the fluid column. The rate of injection from the CO_2 inlet was determined by the different volumetric flow rates that were tested. The interaction of the bubbles was set as a rebound boundary condition within the photobioreactor. The carbon dioxide bubbles also have a slightly lower initial temperature, so the inlet was set to 291 K initially, as stated in Table 3. The eight different volumetric flow rates tested for each array were: 1, 3, 5, 8, 10, 12, 15, and 20 L/min. Overall, forty total simulations were tested.

4.3 Applying Design Process Principles to Photobioreactor Simulations

The photobioreactor simulations were completed using the design process ideas discussed in Chapter 2. Initially, a very simple tank was modeled and meshed with few features and cells. With successful iterations, a square structural member, or light guide, was added to penetrate the tank. Both initial test simulations were run at 1 L/min. The more complex simulations used for analysis involved cylindrical tubes that ran through the width of the PBR.

First, a basic photobioreactor was modeled and imported into STAR-CCM+. This photobioreactor only had the basic features and was similar to the PBRs studied previously

at SDSU. The modeled system included a velocity inlet for the carbon dioxide diffuser, a pressure outlet for the top of the tank, and simple walls. No light guides were included in the initial simulation. The simple, meshed photobioreactor can be seen in Figure 14.

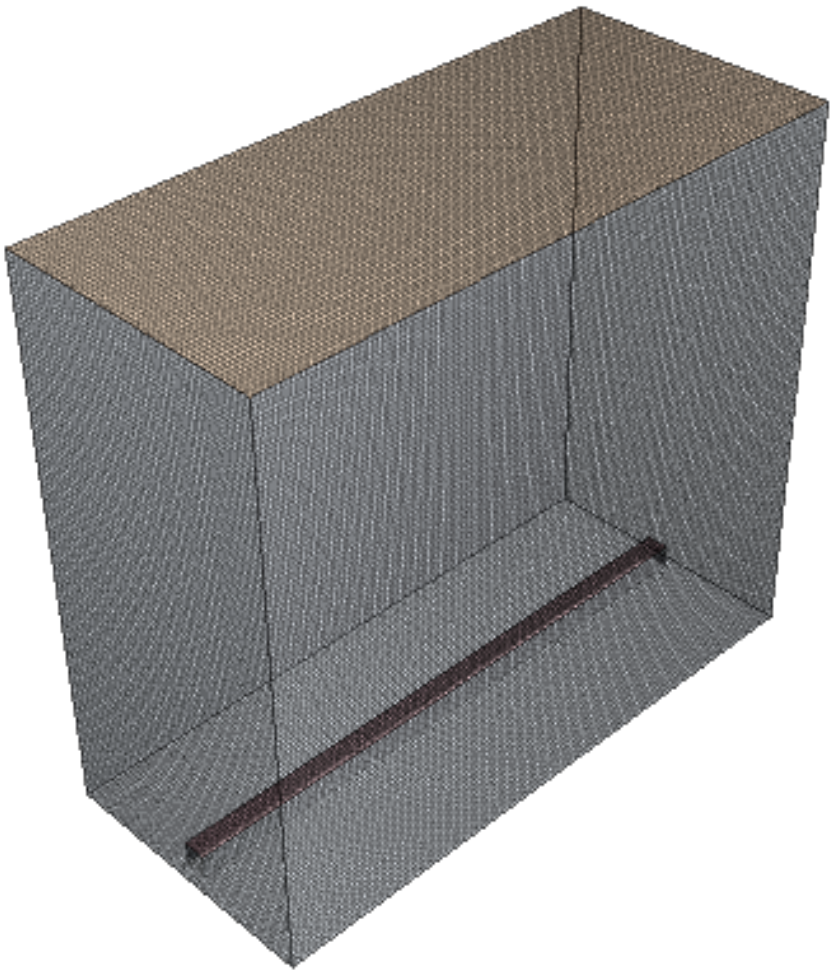

Figure 14: Initial Photobioreactor Volume Mesh

The mesh for analysis with this model was chosen as both a surface remesher and a trimmed mesh. As discussed in Chapter 3, the trimmer mesh breaks the volume into small cubic elements for analysis. This shape was appropriate for the simple PBR as it contains

only rectangular geometry. The mesh was fairly unrefined, with only 162,096 cells and a base cell size of 0.00475 m. The simulation was run in order to determine the effectiveness of the simulation methods and to have a basis with which to compare future simulations.

Previous simulations with no light guides and a similar diffuser geometry run by Mortuza et al. [46] show the expected flow pattern for a PBR without structural members. Their results are shown in Figure 15 for a side view. Similarly, the side view for the photobioreactor analyzed in this research is shown with its flow pattern in Figure 16. A comparison of the two simulation pictures shows the same flow pattern. This flow pattern also matches the experimental flow pattern. The front view of the PBR flow pattern is shown in Figure 17. The distribution is fairly even as it goes up the fluid column.

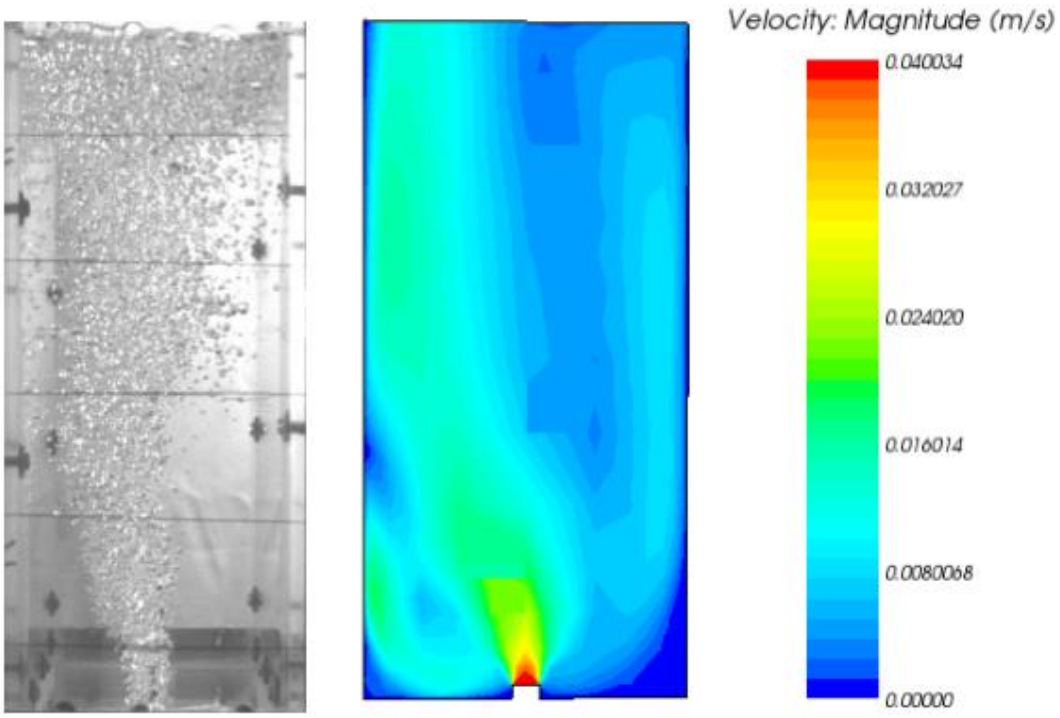

Figure 15: Flow Pattern from Side View Experimentally (Left) and Computationally (Right) [46]

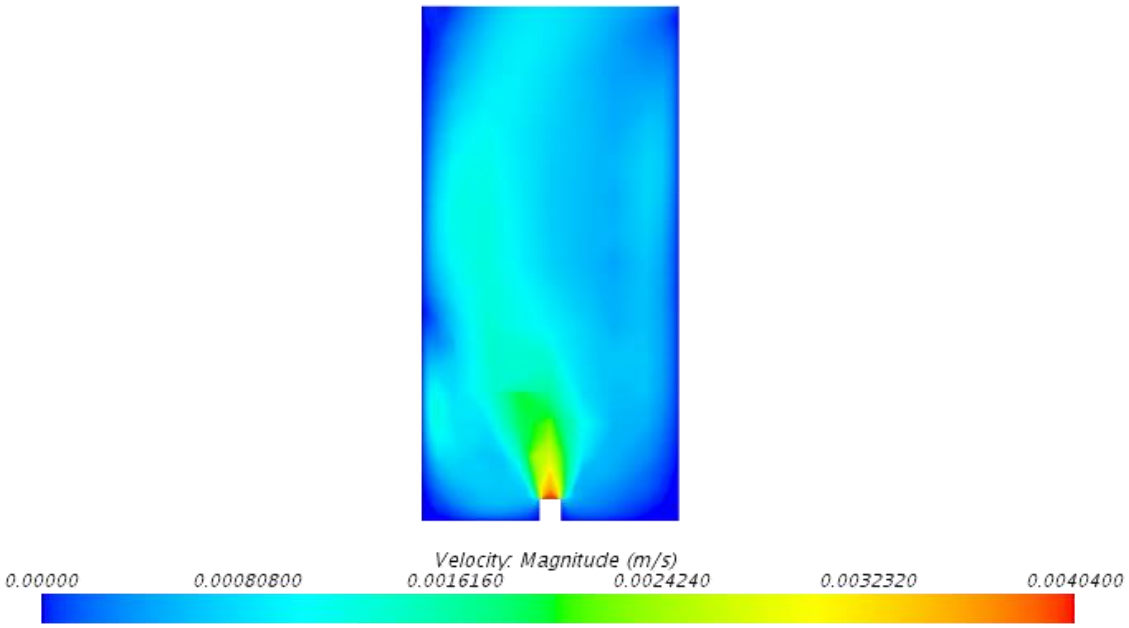

Figure 16: Side View of Initial Photobioreactor Flow Pattern at 1 L/min

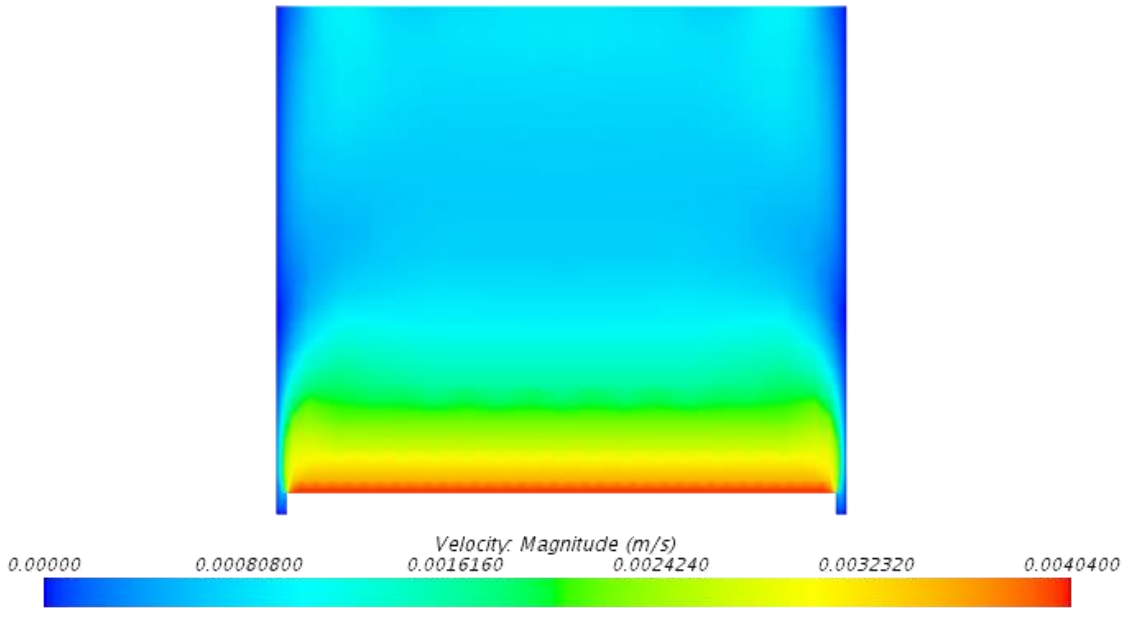

Figure 17: Front View of Initial Photobioreactor Flow Pattern at 1 L/min

Simulation data for the PBR without light guides is given in Table 4. When compared to the work of Mortuza et al. [46], the mass flow in and out of the PBR is the same, approximately 0.017 kg/s. The bubble velocity in [46] is 0.12 cm/s, versus 0.112 cm/s in this research, which is a small difference. Although these findings are similar, the initial photobioreactor was only run for about 220 iterations, so the system may not be in equilibrium just yet.

The temperature and heat transfer in a bubble column photobioreactor were also studied by Mortuza et al [31]. Temperature distributions were found for both fluorescent light panels and LED light panels being applied to the fluid column. The front temperature distributions from Mortuza et al. [31] are shown in Figure 18, compared to the front temperature distribution of this research in Figure 19. The temperature initial conditions for the LED light panel are similar to those for the photobioreactors in this research, with most being within a few degrees of each other. However, as can be seen when comparing the two figures, the initial simulation has a higher temperature along the sides of the photobioreactor instead of the front, giving it an almost opposite distribution from the research done by Mortuza et al. [31]. This could be due to differing volumetric flow rates from the injector.

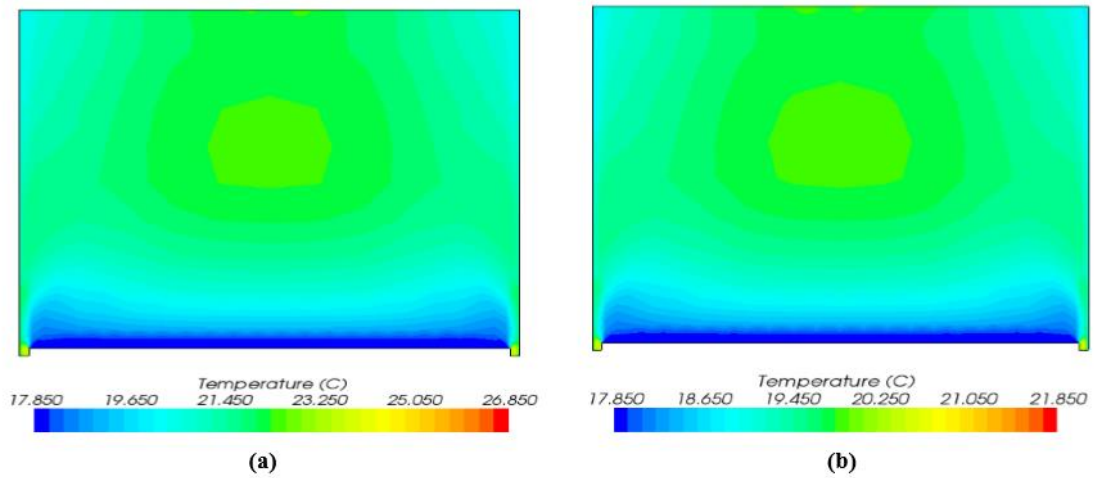

Figure 18: Temperature Distribution Inside PBR from Front View for Fluorescent Light Panel (a) and LED Light Panel (b) [31]

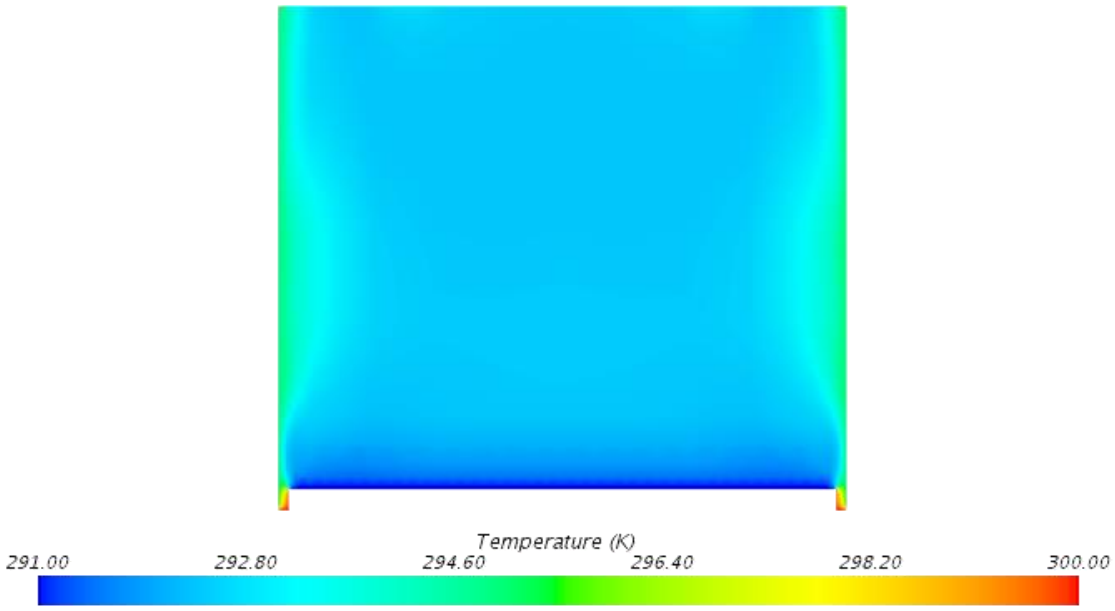

Figure 19: Front Temperature Distribution of Initial PBR Simulation

With the similar results from this simulation compared to previous research, the initial basic simulation was considered successful. In addition, the residuals from the simulation show a convergence pattern, as can be seen in Figure 20. The system was run for about 220 steps. The main goal of the first simulations was to have them run without any issues from the software and to give reasonable results.

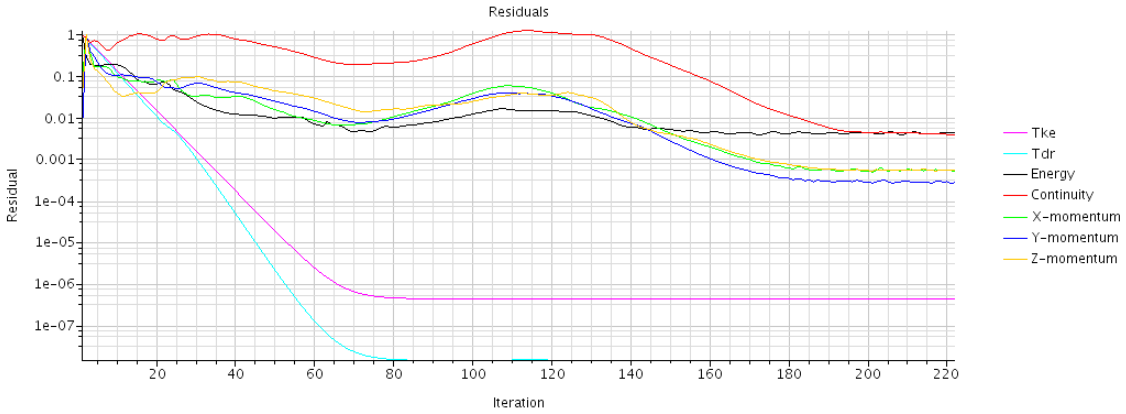

Figure 20: Residuals for Initial Photobioreactor Simulation

Table 4: Bubble Averages and Mass Flow Data of Initial Simulations

Property	Initial PBR
Reynolds Number	0.0908
Temperature (K)	292.44
Particle Velocity (cm/s)	0.112
Mass Flow In (kg/s)	0.0166
Mass Flow Out (kg/s)	0.0166

The second iteration of the photobioreactor simulations included the same PBR geometry with a square structural member added to the middle of the fluid column. The volume mesh for this simulation is shown in Figure 21. The square light guide runs from one side to the other of the photobioreactor and has dimensions of 0.5 in × 0.5 in. Once again, the trimmed mesh was chosen for this simulation based on the rectangular geometry. The volume mesh was made up of more cells, 206,460, and a smaller base size, 0.0045 m. The increased refinement allows for greater accuracy, especially with the addition of the structural guide.

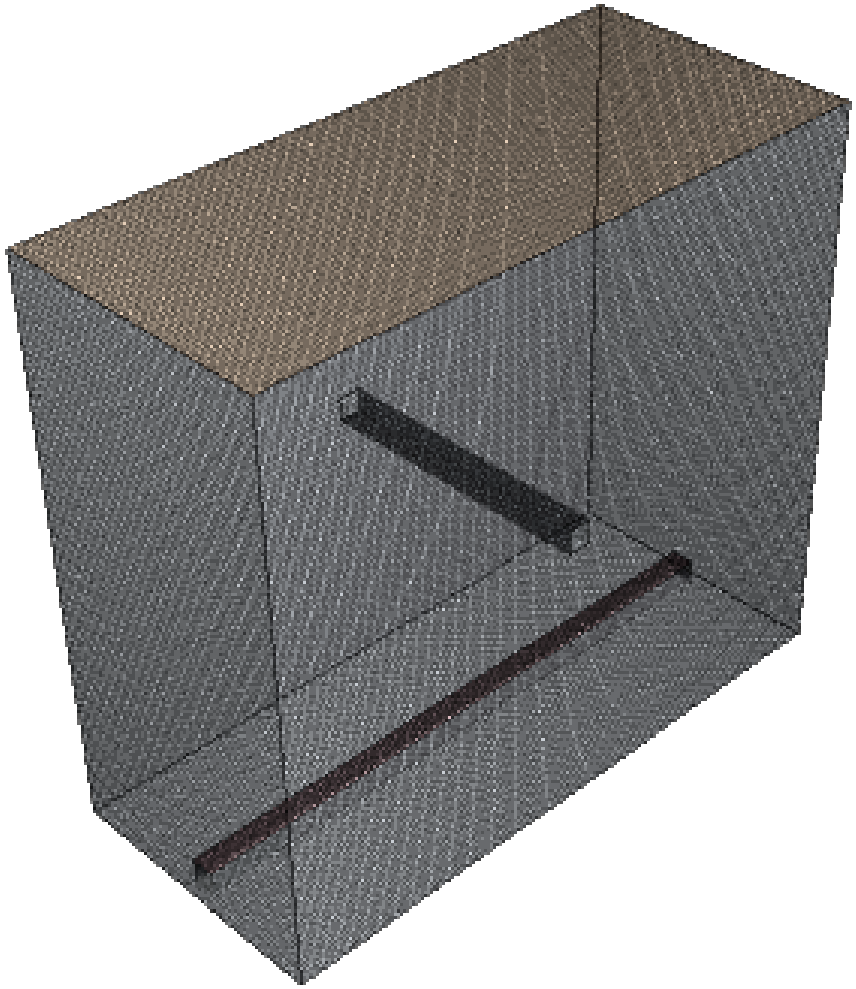

Figure 21: Photobioreactor Volume Mesh with a Square Light Guide

Temperature distributions and flow patterns were also obtained for this simulation. The velocity scenes for the PBR are shown in Figure 22 (side view) and Figure 23 (front view). This simulation was also a test simulation to determine if the addition of the structural member would cause any issues with the simulation. It was only run for about 37 iterations before the decision was made to move forward with modeling a more accurate system. Since so few iterations were run, the flow pattern are not completely developed.

This and the addition of the light guide to the center of the tank accounts for the difference in velocity scenes. Also, this simulation only looked at the flow of the fluid, so the bubble particles were not given an initial velocity. In future simulations, the particles were more accurately depicted with a starting velocity.

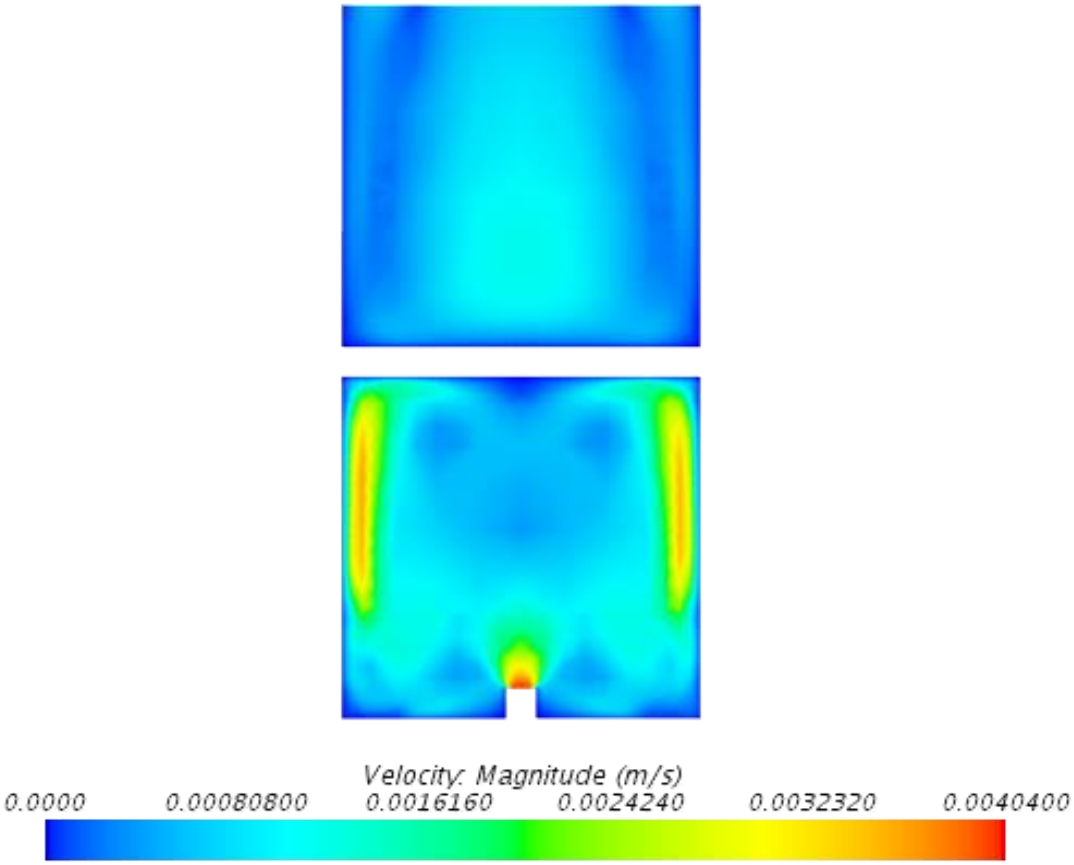

Figure 22: Side Velocity Distribution of PBR with a Square Light Guide

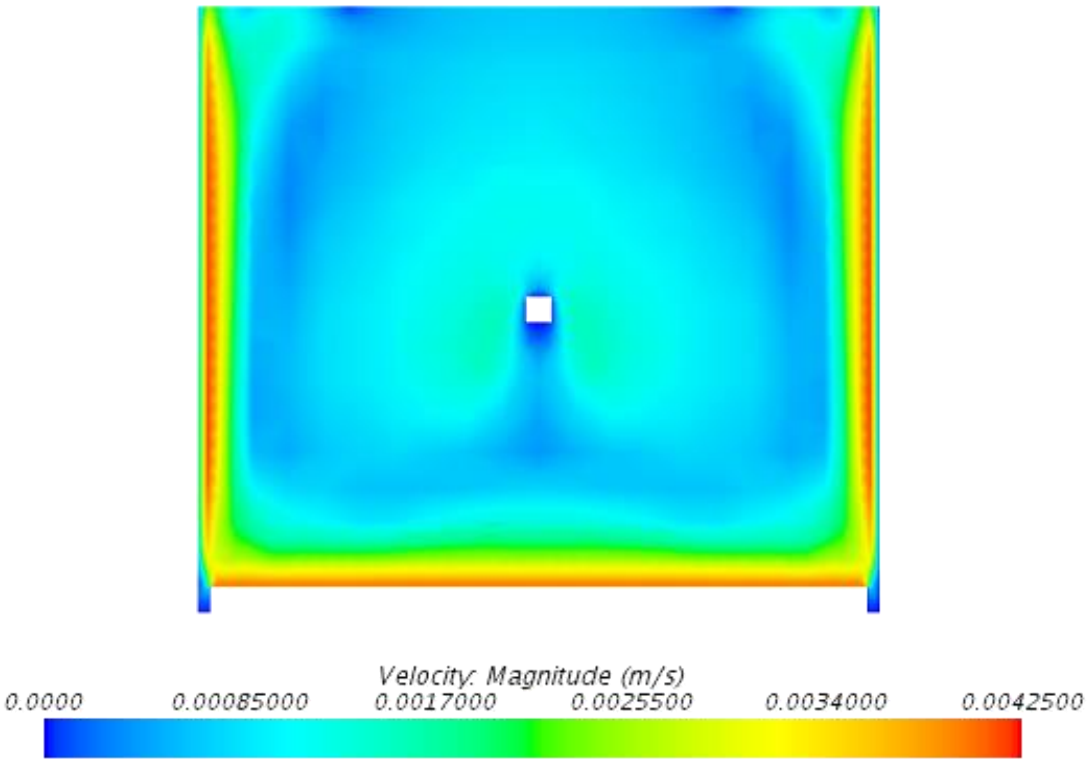

Figure 23: Front Velocity Scene of PBR with a Square Light Guide

Moving forward, the next simulations that were used for research included more cells in their meshes, around 350,000. The mesh type was also changed to better interpret the circular geometry of the light guides. The results from these simulations are discussed in the following section.

4.4 Analyzing the Photobioreactor Simulation Results

The photobioreactor was tested with five different light guide arrangements and eight different CO_2 injection rates. All of the simulations were run for 1000 iterations to check for validity. The higher the volumetric flow rate, the fewer simulations converged under the expected accuracy of 0.001. The effects the different light guide arrays had on

the bubble velocity, temperature distribution, Reynolds and Nusselt number, and bubble flow patterns were all analyzed.

First, the temperature distribution for the front of the photobioreactors was studied. In general, this temperature profile was uniform. The initial temperatures for each of the different regions in the simulation are given in Table 3. For the square arrays, this front temperature distribution showed little variation. For the staggered light guide arrangements, the temperature distribution tended to be warmer overall, with the cooler regions being closest to the bubble sparger. A side-by-side comparison of the different temperature profiles at 10 L/min is shown in Figure 24.

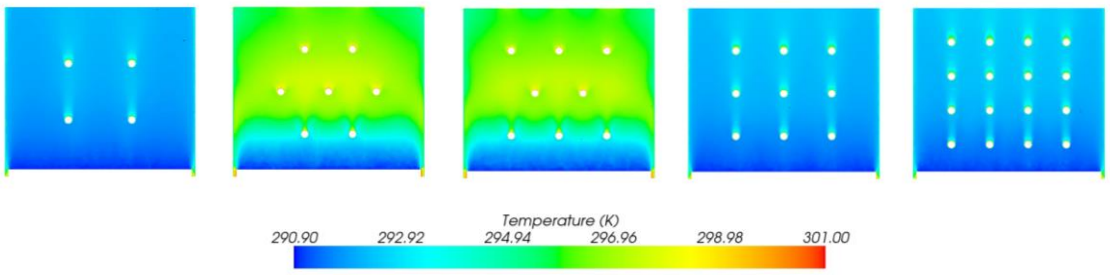

Figure 24: Front Temperature Distributions for Different Light Guide Arrays at 10 L/min

The average bubble temperatures for each of the different arrays and sparger volumetric flow rates are given in Table 5, Table 6, and Table 7. Between the different types of light guide arrangements, the temperature of the bubbles did not vary significantly. However, with the square arrays, the temperature of the bubbles tended to increase with

increasing volumetric flow rate. The Nusselt number also tended to increase with increasing bubble inlet velocity for all of the arrays.

The side temperature profiles were not as evenly distributed as the front profiles. The light guides have a tendency to block the flow of the fluid vertically. Higher temperatures are seen where the velocity is higher at the CO_2 inlet in the photobioreactor. The temperature distributions that are shown in Figure 25 are taken from a point where the light guides are penetrating the fluid column. The light guides in this situation are split in half lengthwise. This results in the rectangular look of the light guides shown in Figure 25.

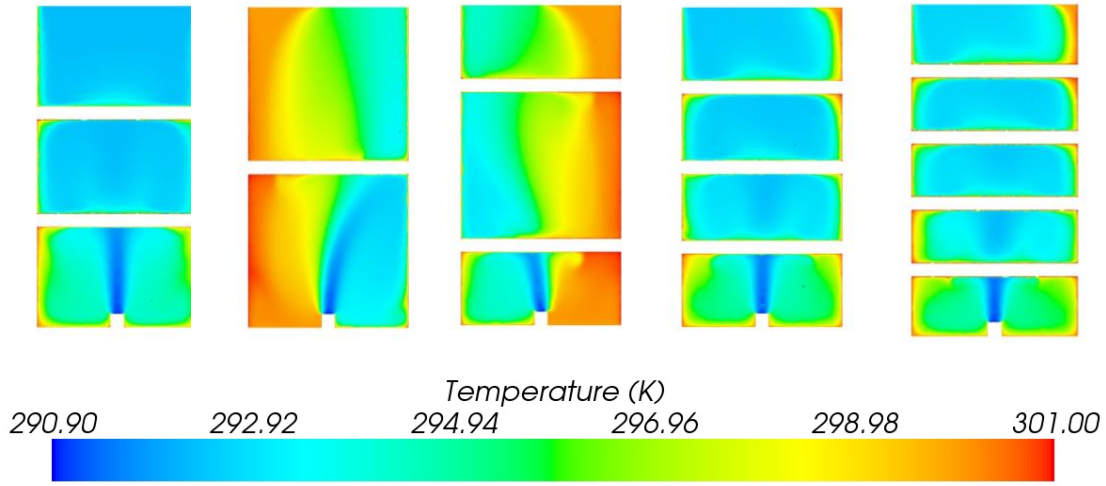

Figure 25: Side Temperature Distributions for Different Light Guide Arrays at 10 L/min

With the three square array photobioreactors, the side temperature distributions are fairly consistent, with the highest temperature seen along the walls. The staggered arrays in Figure 25 show a higher temperature along the walls. Since there are fewer light guides penetrating the center of the column at this point, the flow is more direct from bottom to

top. The highest temperature boundaries are along the front and back walls and the outer surfaces of the light guide structures.

Table 5: Bubbles Averages for 2×2 and 2+3+2 Arrays

	2×2			2+3+2		
Volumetric Flow Rate (L/min)	**Nusselt Number**	**Reynolds Number**	**Temperature (K)**	**Nusselt Number**	**Reynolds Number**	**Temperature (K)**
1	2.176	0.0329	292.95	2.210	0.0438	293.30
3	2.208	0.0544	292.94	2.201	0.0457	293.07
5	2.510	0.284	293.61	2.424	0.226	293.50
8	2.589	0.412	293.18	2.808	0.716	293.91
10	2.832	0.925	292.99	3.054	1.365	293.47
12	2.893	0.968	293.13	3.074	1.414	293.29
15	2.854	0.830	293.46	3.305	1.914	293.91
20	2.873	0.729	294.21	3.445	2.668	293.15

Table 6: Bubbles Averages for 3+2+3 and 3×3 Arrays

	3+2+3			3×3		
Volumetric Flow Rate (L/min)	**Nusselt Number**	**Reynolds Number**	**Temperature (K)**	**Nusselt Number**	**Reynolds Number**	**Temperature (K)**
1	2.206	0.0430	293.21	2.204	0.0448	293.36
3	2.194	0.0429	293.10	2.217	0.0553	293.18
5	2.502	0.266	293.67	2.503	0.278	293.62
8	2.946	0.882	293.83	2.654	0.482	293.03
10	3.108	1.349	293.74	2.797	0.846	293.08
12	3.118	1.255	294.09	2.953	1.152	293.04
15	3.591	2.833	293.40	2.961	1.025	293.21
20	3.181	1.726	292.72	3.432	3.052	294.11

Table 7: Bubbles Averages for 4×4 Array

	4×4		
Volumetric Flow Rate (L/min)	**Nusselt Number**	**Reynolds Number**	**Temperature (K)**
1	2.263	0.0724	293.46
3	2.357	0.1290	293.72
5	2.537	0.300	293.45
8	2.624	0.429	293.21
10	2.877	1.106	293.05
12	2.901	0.856	293.21
15	2.892	0.868	293.06
20	3.149	1.411	293.26

The staggered light guide array photobioreactors tended to have warmer temperature distributions compared to the square arrangements of light guides. The velocity profiles of the staggered arrays are not as evenly distributed, as is shown in Figure 26, so the cooler bubbles from the sparger are not mixed as well. This results in an overall higher PBR temperature. This can be seen in Figure 24 and Figure 25. However, the temperature is also increased with an increasing number of light guides. A more even temperature profile is seem in the square light guide arrays.

Table 5, Table 6, and Table 7 describe the average bubble Nusselt number for the different arrays. This number describes the heat transfer occurring in the multiphase mixture and is calculated within STAR-CCM+. In general, an increasing volumetric flow rate resulted in an increasing Nusselt number. This increase happened sooner for the staggered arrays than for the square arrays. The Nusselt number for the bubbles is important as it describes the heat transfer interactions between the bubbles and the fluid mixture. Algae are very sensitive to temperature differences, so it is important to understand how

the light guides affects the temperature distribution. Microalgae growth can be affected by too much or too little heat transfer.

Another important aspect of the photobioreactor is the Reynolds number, which is also described in Table 5, Table 6, and Table 7. The Reynolds number in all of the light guide configurations increased with increasing volumetric flow rate. Since the Reynolds number is directly proportional to velocity, a higher volumetric flow rate will mean a higher Reynolds number. These higher volumetric flow rates also resulted in less stable results for the Reynolds number due to convergence issues. This issue may be solved by running additional simulations.

The bubble velocities provide some of the most applicable and easy to visualize results. The sparger inlet velocity was changed directly for each of the eight volumetric flow rates tested. The average particle velocity for each of the different light guide arrangements varies. The light guides inhibit the flow so more light guides results in more flow disruption. The lower volumetric flow rates resulted in the arrays having similar particle velocities. The 2×2 light guide configuration had the highest average particle velocity of 3.443 cm/s at the 20 L/min volumetric flow rate. On the other hand, the 4×4 light guide array had the slowest maximum velocity of 2.008 cm/s. Compared to the other arrays, there are 16 light guides in the 4×4 array to disrupt the flow, which is almost double and even four times as many light guides as the other arrangements. Table 8, Table 9, and Table 10 give a summary of the different light guide configurations and their corresponding bubble velocities, the percentage of bubbles in reverse flow, and the carbon dioxide mass flow rates for the different volumetric flow rates.

Table 8: Bubble Velocity, Reversed Flow, and Mass Flow Rate for 2×2 and 2+3+2 Arrays

	2×2				2+3+2			
Volumetric Flow Rate (L/min)	**Particle Velocity (cm/s)**	**Reversed Flow (%)**	**Mass Flow In (kg/s)**	**Mass Flow Out (kg/s)**	**Particle Velocity (cm/s)**	**Reversed Flow (%)**	**Mass Flow In (kg/s)**	**Mass Flow Out (kg/s)**
1	0.209	0.00	0.0166	0.0166	0.215	0.07	0.0166	0.0166
3	0.440	4.32	0.0499	0.0499	0.454	1.76	0.0499	0.0499
5	0.695	8.45	0.083	0.0831	0.711	6.26	0.0831	0.0831
8	1.227	10.15	0.133	0.133	1.336	7.59	0.133	0.133
10	1.601	10.85	0.166	0.166	1.655	9.64	0.166	0.166
12	1.860	13.51	0.200	0.199	1.709	16.36	0.200	0.199
15	2.588	11.33	0.249	0.249	2.122	17.30	0.249	0.249
20	3.443	11.55	0.332	0.332	2.388	23.25	0.332	0.332

Table 9: Bubble Velocity, Reversed Flow, and Mass Flow Rate for 3+2+3 and 3×3 Arrays

	3+2+3				3×3			
Volumetric Flow Rate (L/min)	**Particle Velocity (cm/s)**	**Reversed Flow (%)**	**Mass Flow In (kg/s)**	**Mass Flow Out (kg/s)**	**Particle Velocity (cm/s)**	**Reversed Flow (%)**	**Mass Flow In (kg/s)**	**Mass Flow Out (kg/s)**
1	0.225	0.00	0.0166	0.0166	0.219	0.04	0.0166	0.0166
3	0.460	1.97	0.0499	0.0499	0.437	6.21	0.0499	0.0499
5	0.719	6.39	0.083	0.0831	0.666	11.42	0.0831	0.0832
8	1.302	9.31	0.133	0.133	1.018	17.32	0.133	0.133
10	1.552	13.58	0.166	0.166	1.281	18.73	0.166	0.166
12	1.689	18.35	0.200	0.200	1.533	20.26	0.200	0.199
15	2.383	13.28	0.249	0.249	2.043	18.42	0.249	0.249
20	2.112	25.19	0.333	0.332	2.258	27.05	0.332	0.332

Table 10: Bubble Velocity, Reversed Flow, and Mass Flow Rate for 4×4 Array

	4×4			
Volumetric Flow Rate (L/min)	**Particle Velocity (cm/s)**	**Reversed Flow (%)**	**Mass Flow In (kg/s)**	**Mass Flow Out (kg/s)**
1	0.231	0.11	0.0166	0.0166
3	0.455	6.77	0.0499	0.0499
5	0.680	10.25	0.083	0.0832
8	0.978	17.38	0.133	0.133
10	1.197	20.33	0.166	0.166
12	1.279	23.50	0.200	0.199
15	1.476	24.39	0.249	0.249
20	2.081	24.39	0.332	0.333

For the percentage of bubbles in reversed flow, the number of particles with negative velocity is divided by the total number of bubbles in the simulation. The velocities for the bubbles can be found using the particle tracks of the completed simulations. In general, as the number of light guides is increased, so is the number of bubbles in reversed flow. This is true of the 4×4 light guide array, where the 12, 15, and 20 L/min flow rates had approximately 25% of the bubbles reversed. For the 2×2 array, the percentage of particles in reversed flow was a fairly consistent number. However, the other four arrays had an increase in bubbles in reversed flow with a higher volumetric flow rate. This is due to the fact that more light guides will result in more of the bubbles' flow being obstructed, sending them into reversed flow. If less flow interruption is desired, fewer light guides should be used. Another aspect to consider is the shear caused by the reversed flow. If the shear rate is safe for the specific strain of algae, an increase in reversed flow may be desirable for better mixing.

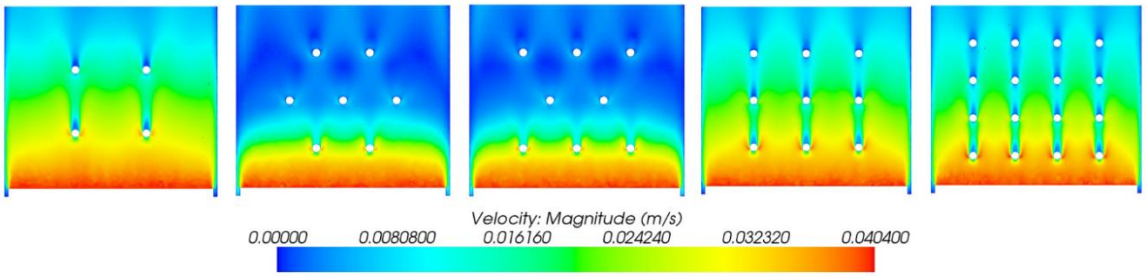

Figure 26: Scalar Velocity Profiles of Different Light Guide Arrays at 10 L/min

The staggered light arrangements tended to have higher average bubble velocities compared to the square arrays, but their velocity profiles were less consistent, as shown in Figure 26. This figure shows the velocity distributions of each different light guide configuration from the front at 10 L/min. For the 2+3+2 and 3+2+3 arrays, the velocity almost drops off completely after the first row of light guides. The decrease in velocity is more gradual for the square configurations. For the staggered arrays, the second row of light guides are placed in a way that inhibits the already decreased bubble motion. The fluid velocity after the second row of light guides is basically zero. In every configuration, there is a wake zone of zero velocity at the top of each light guide.

The square light guide arrays all had less area of zero velocity because the light guides are in the same position going vertically up the column. This means the bubbles will only have their path obstructed in one position, which helps them to reach the top of the fluid column and not drop off so greatly in velocity. The CO_2 sparger along the bottom of the PBR gives the bubbles their highest velocity, and the velocity at the top of the column is at its lowest. The number of light guides does not affect the flow patterns as much as the

arrangement of these structural members. The more complex geometry of the staggered arrays obstructs the flow the most. Instead, the square arrays help in having a less obstructive effect on the bubble flow.

Anderson et al. [48], in future work, demonstrated experimentally that staggered light guide arrays result in a decreased vertical velocity as predicted by the simulations. They state that this is desirable for light penetration and mass transfer, as it increases the residence time of the bubbles in the PBR. It is noted that the light guides in the work of Anderson et al. [48] only penetrate half the width of the PBR, compared to the full width as described in this work.

This photobioreactor study is an example of how model refinement can be used to determine a suitable representation for a system. The results from this study can also be used to help predict system behavior, which simplifies the design process. By comparing the simulation setup to previous baseline simulations and experiments, changes to the system can be made easily.

Chapter 5: Case Study 2 – Grain Dryer

The second system studied in this research involved a laboratory-scale grain dryer. An overview of grain dryers is given, including the different types available today. Related research to this topic is discussed. Then, the design process for creating CFD simulations of the system is walked through, and relevant results are described.

5.1 Overview of Grain Drying

After grain has been harvested, it needs to be prepared for storage and sale. Grain drying is one of the greatest energy consuming steps out of the entire process to grow and harvest corn, possibly accounting for up to 60 percent of the energy used [49]. At a time when energy costs and demands are high, much improvement potential exists in this part of the process. With the help of CFD simulations, the drying system can be furthered analyzed and areas for improvement found.

5.1.1 Need for Grain Drying

Grain drying is a delicate process. It actually starts in the field, after the grain has matured [50]. The time the grain is harvested after it has stopped maturing will affect the amount of drying it needs later. It is up to the farmer how long to leave the grain in the field before harvesting. The risks involved in leaving the grain out in the field include potential losses from both wildlife and weather [51]. The secondary part of the drying process comes after the grain has been harvested and needs to be prepared for market or storage. The farmer uses grain dryers in this case to bring the grain to the desired moisture

content. Although drying is essential, care needs to be taken that too little or too much drying does not occur.

If the grain is not dried enough, the quality will deteriorate due to mold and insect damage [51]. This affects how long the grain can be stored and how much yield it will produce in the next year if it is to be used for planting. In addition, underdrying can result in a price decrease when sold [50]. The price of grain is set by weight per bushel. If the grain holds more moisture than the standard, it will weigh more, skewing the price. This will result in a penalty on the sale price for farmers. Typically, a moisture content of around 15% or less is desired [52]. Since grain that is dried artificially can contain close to the maximum allowable water content, this will actually result in a better payoff for the farmer [51]. However, it is equally important to consider how much drying is needed.

Over-drying of grain also presents a problem. Since grain is sold by weight, too much drying will result in the farmer selling their yield at a lower price than they could get. A base moisture content is used to price grain. Any drying beyond this moisture content is detrimental to the farmer's profit as it results in less weight. If the grain has a moisture content below the standard for sale, the farmer is considered to be "giving away" dry matter [53]. Another problem with excessive heating is that energy is being wasted to dry the grain [50]. Not only will the farmer lose money on the extra drying costs, but also on the decrease in sale price if the grain is not going to storage. In addition, during the heat and mass transfer process of drying, contraction occurs in the kernels. This contraction can cause a stress crack within the kernel [54]. These cracks then make the grain susceptible to insects and also affect the germination. When this occurs, the corn is reduced in value and may

not even be sellable [55]. The farmer needs to find a good balance in drying in order to make the most profit from the grain.

5.1.2 Classification of Grain Dryers

The type of grain dryer used will also affect the drying process. Three main types of heated air dryers used for grain include bin, batch, and continuous flow dryers [51]. Each dryer has its strengths and weaknesses depending on the application, with continuous flow dryers becoming a more popular option due to their efficiency [55].

Bin dryers involve loading the grain as a batch, with the grain being stationary during the drying process [51]. With this type of dryer, not as much supervision is necessary. Bin dryers can use low temperature air for the drying [56]. Less energy use is required, saving money on the drying process. However, this can also increase the drying time required [55]. Depending on the harvest time, climate, and drying needs of the farmer, this may not be ideal.

Batch dryers involve drying a set amount of grain, and can be recirculating or non-recirculating. The batch dryer type requires more supervision, and the effectiveness depends on whether or not the dryer is recirculating. A batch dryer with recirculation will dry the grain more uniformly than a non-recirculating dryer [51]. This involves the same amount of grain to be cycled through the dryer until the desired moisture content is achieved [57]. The air in these dryers can also be low temperature, but this presents the same constraints as the bin dryers discussed above.

The third type of heated dryer is the continuous flow grain dryer. With this dryer type, the grain is flowing continuously through a perforated column [55]. The heated air in

these dryers can flow in multiple directions. In cross-flow dryers, it blows perpendicular to the grain flow. With concurrent-flow, it blows parallel. A counter-flow air stream will blow in the opposite direction [55]. This dryer type is often preferred as it allows grain to be dried without needing to stop for each batch. Continuous flow dryers can help reduce required drying time. However, a more complex setup may be required with loading and unloading equipment and supervision to ensure that drying is uniform [51]. The initial costs may be offset by the efficiency of these dryers.

5.1.3 Related Research

For this research, the concept of a cross-flow grain dryer is studied on a laboratory-scale. Although cross-flow grain dryers are typically continuous flow, the experimental setup for testing involves drying one stationary batch of corn at a time.

In order to model the mini grain dryer, the fluid flow simulation software STAR-CCM+ was used again. In order to determine the relevance of the model as well as compare the results to past research, research into similar studies was conducted. Different software and meshing techniques have been used for similar fan simulations. However, the overall research projects have methods that are comparable.

5.1.3.1 Centrifugal Fan Modeling

Karanth and Sharma [58] conducted an analysis on a centrifugal fan based on the radial gap's effect on the impeller and diffuser. Similar to most models reviewed with centrifugal fans, the duo developed a simulation using the k-ε turbulence model and a sliding mesh. The simulation was also set as unsteady. The pair studied the radial gap in a centrifugal fan, which is the area between the impeller exit and diffuser entry. Based on the

velocity profiles, fan efficiency, and pressure loss coefficient, among others, an optimum gap between the impeller and diffuser was found for converting energy and transferring it.

Singh et al. [59] performed a similar analysis of centrifugal fans to that done in this research paper, using the same simulation software, a steady simulation, and a rotating mesh technique. However, the research done by this team was in relation to cooling internal combustion engines. The purpose of their research was to be able to match up the experimental tests to the simulation set up in STAR-CCM+. One of the findings of this study was that as the CFD simulations were run at higher speeds, results tended to diverge from the experimental numbers. However, at lower speeds, the results were in good relation to the experiment. Overall, Singh et al. [59] found that more blades in a centrifugal fan was good for power, but not as conducive for flow efficiency. The group also found that backward curved blades were preferable to forward curved blades for the application of the centrifugal fan in question.

5.1.3.2 Full Grain Dryer Modeling

Computational fluid dynamics and finite element methods have been applied to grain dryer research in recent years. Sitompul et al. [60] used two-dimensional models to analyze a deep-bed grain dryer. The models they used involved the conservation of both momentum, mass, and energy and heat and mass in the grain. These mathematical models were solved with finite-differencing methods and compared to an experimental setup. They showed that the simulated and experimental results closely resembled one another. The air velocity was also shown to have a small effect on the drying rate, leading to the conclusion that the main drying mechanism is the diffusion of moisture.

Research done by Weigler et al. [61] discussed using numerical and experimental analyses on a mixed-flow dryer. They looked at both horizontal and diagonal air ducts in the dryer system and used an experimental setup for testing. The dryer they studied had vertical drying shafts and controlled, batch grain flow. To simulate the air flow in the grain dryer, they used ANSYS CFX, a CFD program discussed in Chapter 2. Similar to this thesis research, Weigler et al. [61] modeled the grain bed as porous. Through their research, they found that inconsistent drying of grain can occur from airflow dead zones in the dryer, faster grain flow at the center of the dryer versus the walls, and air duct setups that are not ideal. They recommended increasing air velocity in areas of greater grain velocities.

Scaar et al. [62] also studied mixed-flow dryers, looking at the airflow patterns in the grain bed. The grain types tested in this study were dry wheat and rapeseed. In order to study the distribution of airflow, the pressure drop, air velocity, and residence time were measured. ANSYS CFX was used in this research study as well, and the grain bed was modeled as porous. Scaar et al. [62] found that with the increase in particle size and porosity from rapeseed to wheat, the pressure drop decreased. They were able to achieve good agreement between experimental and computational results and validate that their CFD model could be used to help study and predict the airflow in the dryer.

5.1.4 Grain Dryer Research at South Dakota State University

Suess et al. [55] previously researched the drying efficiency of the same laboratory-scale dryer with corn kernels as the grain analyzed. The team performed tests to determine how changing air inlet conditions effect dryer efficiency, energy efficiency throughout the drying process, and drying time to recommended moisture content. This study found that

dryers have high efficiency right after pre-heating occurs, and the efficiency drops off as the corn nears the desired moisture content. Also, the energy efficiency and drying time are generally inversely related, showing that a tradeoff exists for farmers [55]. The data from this study helps to describe this research.

5.2 Grain Dryer System for Analysis

5.2.1 Modeling the Grain Dryer

The laboratory-scale grain dryer used in this research can be seen in Figure 27. The fan is located on the left with heating coils downstream, and the drying chamber of corn is on the right. A simplified setup of this was modeled using SolidWorks.

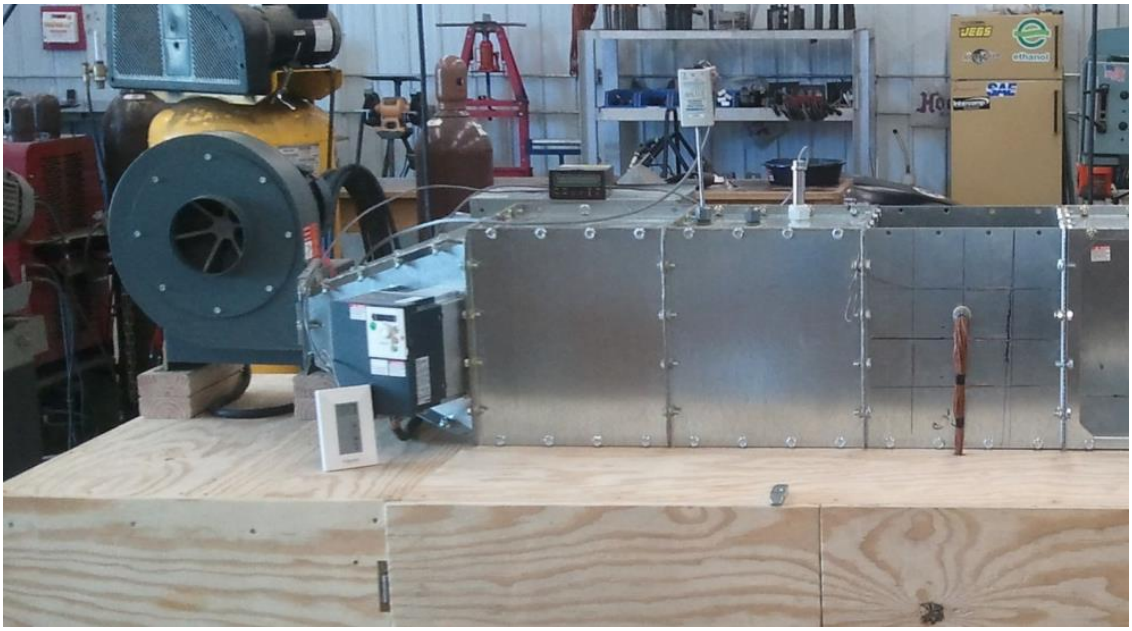

Figure 27: Laboratory-Scale Grain Dryer

For the simulation testing of the grain dryer, the measurements of the different components of the system were taken and used in creating the SolidWorks CAD models. These measurements were determined directly from the experimental setup of the grain dryer. The different parts of the system include:

- Fan model with six blades (Dayton Blower 2C820) – 8.875 in diameter
- Fan rotor – 0.5625 in diameter
- Fan housing – increasing radius from 5.75 in to 7.75 in
- Long duct with heating coils (modeled as cylinders) – 4 ft long
- Corn chamber (porous duct) – 1 ft square

The CAD models of these different parts are shown in Figure 28:

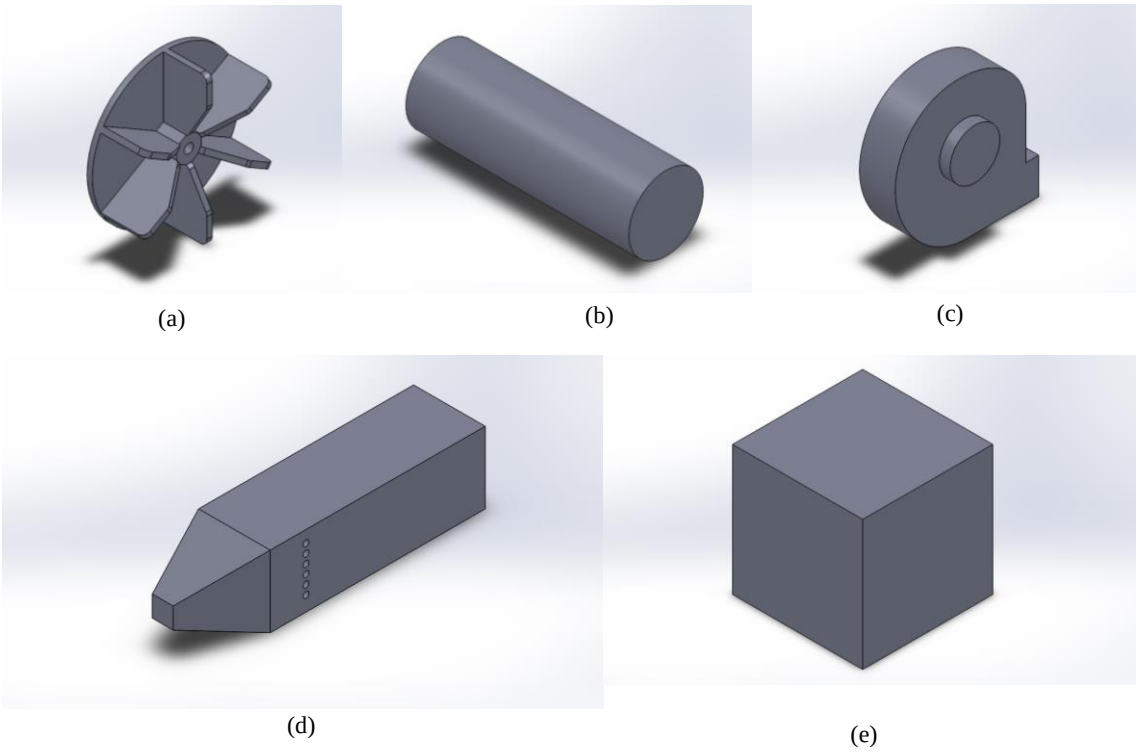

Figure 28: Corn Dryer Components (a) Fan (b) Rotor (c) Housing (d) Heating Duct (e) Grain Duct

The fan and its housing are shown in Figure 29, both in the actual system (a) and modeled using CAD (b). In the model, the fan was initially set to only have two blades in order to simplify the first simulations. With the more complex iterations, six blades were eventually added to the system.

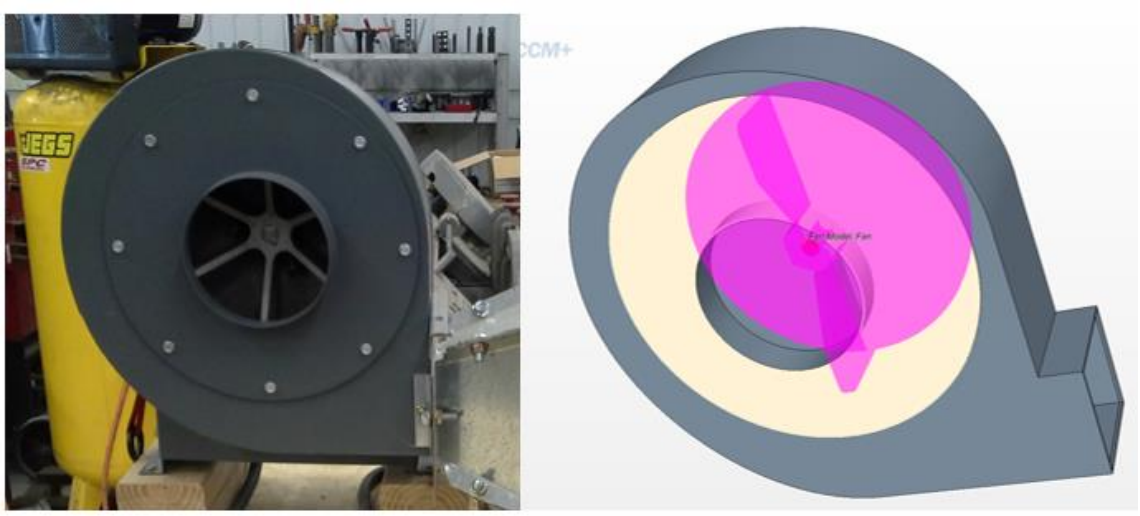

Figure 29: (a) Actual Fan and (b) CAD Model of Fan for Laboratory-Scale Grain Dryer

5.2.2 Preparing the Grain Dryer Model for Simulation

The different parts of the lab-scale grain dryer's system were imported into STAR-CCM+ as separate files that made up an entire dryer. Initially, only the fan and its housing were analyzed. With successful simulation runs, more parts of the system were added.

In order to make the files ready for simulation, interfaces were created between the different dryer parts. Perhaps the most important interfaces were the open interface between the fan housing and the heating duct, and the porous interface between the heating duct and the grain chamber. Mesh consistency was also important for creating these interfaces.

Different regions of the system required different types of physics conditions. The fan and rotor were set as solid materials. The housing for the fan, heating duct, and porous chamber all were set to be fluids to demonstrate the air flow in the system.

5.3 Applying Design Process Principles to the Grain Dryer Simulation

The first step in the simulation process for the laboratory-scale grain dryer was to model the fan and then its housing. The fan analyzed in this research was a Dayton Blower 2C820. The measurements for this fan were taken from the experimental system and modeled using SolidWorks 2014®. The fan was then imported into STAR-CCM+ in an attempt to simulate air flow. A polyhedral mesh was chosen for the geometry of the fan to account for the different geometries. The volume mesh of the fan is shown in Figure 30. As is shown in this representation, the initial model of the fan included only two blades. The actual fan has six blades. However, the goal of the first few simulations was to successfully simulate the fan rotating and then increase the complexity of the system. This version of the fan was never simulated, as the air flow around it needs to be defined. As it is, the fan is just a solid rotating member. The next step was to add the fan's housing to the system.

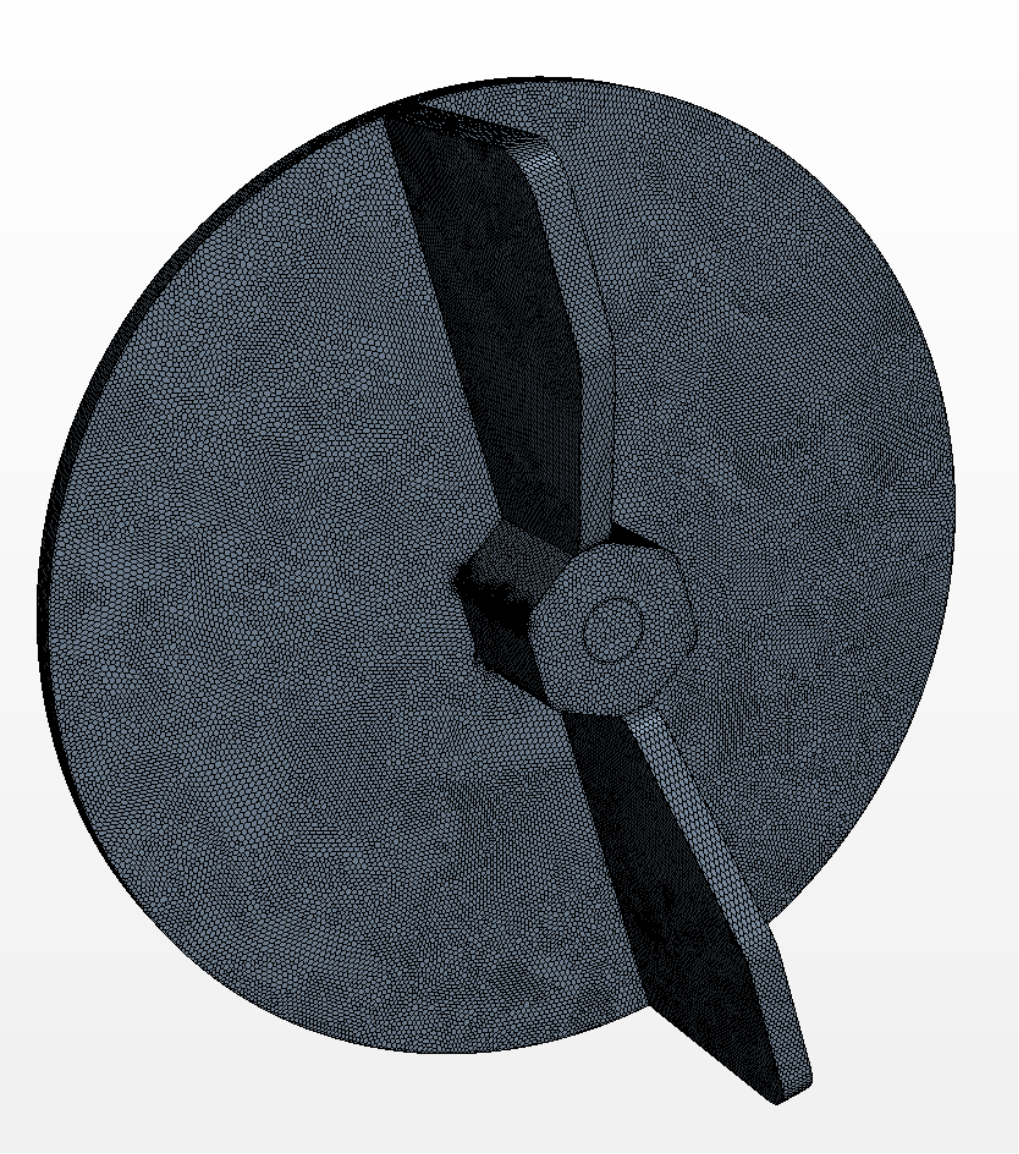

Figure 30: Volume Mesh Representation of the Laboratory-Scale Dryer Fan

The shell that encased the fan can be seen in Figure 29 (a) and (b). As is shown in the model in (b), such things as the screws holding the front of the fan housing together were not necessary to include in the simulation. This is an example of how simplifying the model will increase the efficiency of the simulation without compromising the results.

First, the meshing was completed for the fan and its housing. The fan shell was modeled fairly coarsely at first, with only 90,250 volume cells. The base size for the cells for the different regions was the same at 0.005 m. A representation of the volume mesh is shown in Figure 31. The fan was set to be a rotating region, rotating counterclockwise at 3450 rpm. In order to simulate the air flow into the fan housing, the inlet was set as a velocity inlet, with an initial velocity of 1.0 m/s. The simulation was run to 1000 iterations.

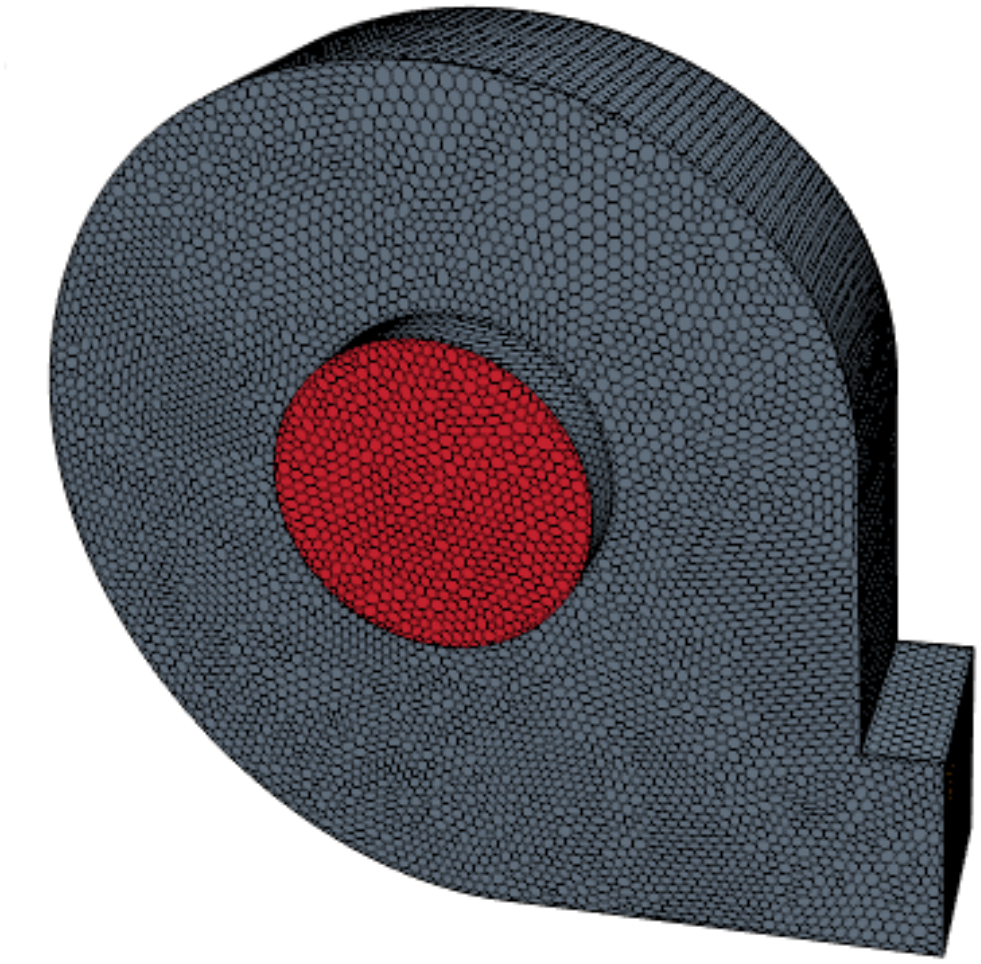

Figure 31: Volume Mesh of Initial Fan Shell Simulation

The purpose of the initial fan and shell setup was to determine the proper way to model the air flow before adding the different drying chambers to the system. The way this was determined was by testing to determine the velocity at the outlet of the housing. The velocity scene is shown in Figure 32. The flow pattern shows an increase in the velocity at the exit, as expected. The data for this simulation is compared in Table 11. The average velocity at the outlet was found to be 1.524 m/s.

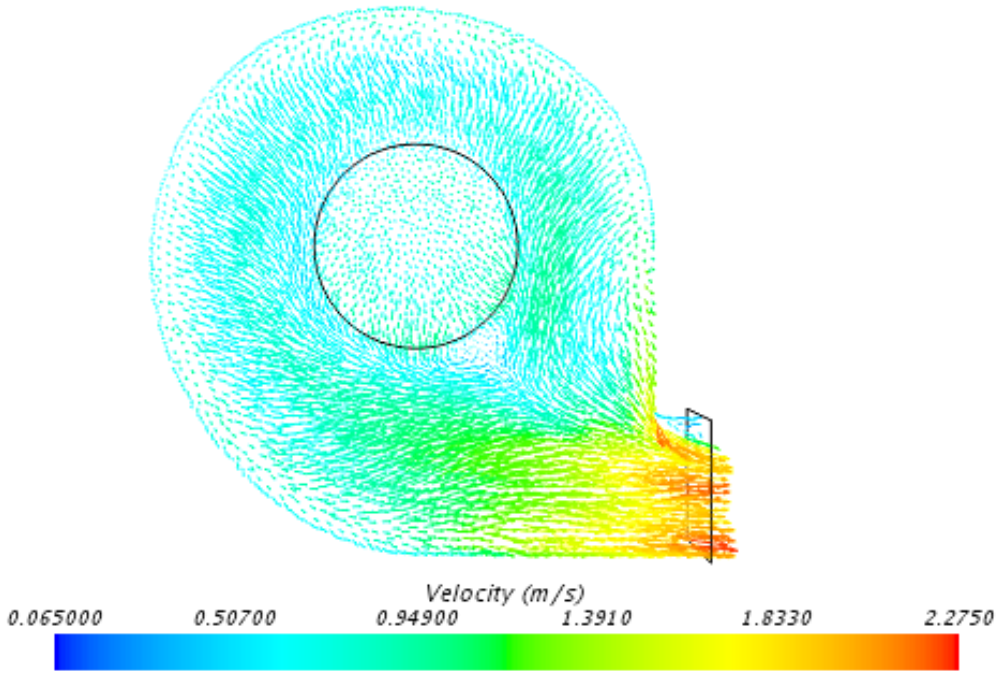

Figure 32: Velocity Vector Scene for Initial Fan Shell Simulation

After the initial fan and housing simulation, the mesh was further refined to 598,282 cells, more than 500,000 cells more than the first simulation. The volume mesh was once again chosen to be polyhedral. The volume mesh of this simulation is given in Figure 33. As can be seen in this representation, the cells are much smaller in size, giving many more

data points for analysis. The base cell size for the different mesh regions were as follows: 0.0025 m for the fan shell, 0.00075 m for the rotor, and 0.002m for the fan.

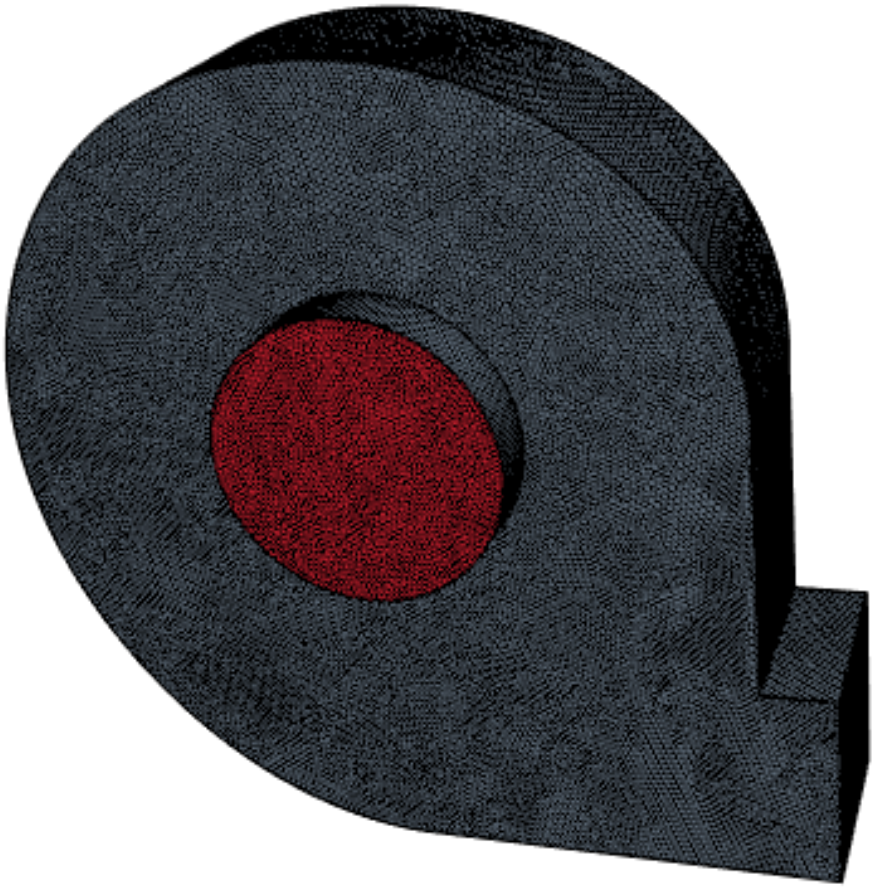

Figure 33: Refined Volume Mesh of Fan Shell Simulation

The distribution of the velocity was also determined for the refined housing simulation. This can be seen in Figure 34. Compared to Figure 32, there are many more vectors corresponding to the increase in volume mesh cells. However, the pattern of the vectors and the overall velocity is very similar.

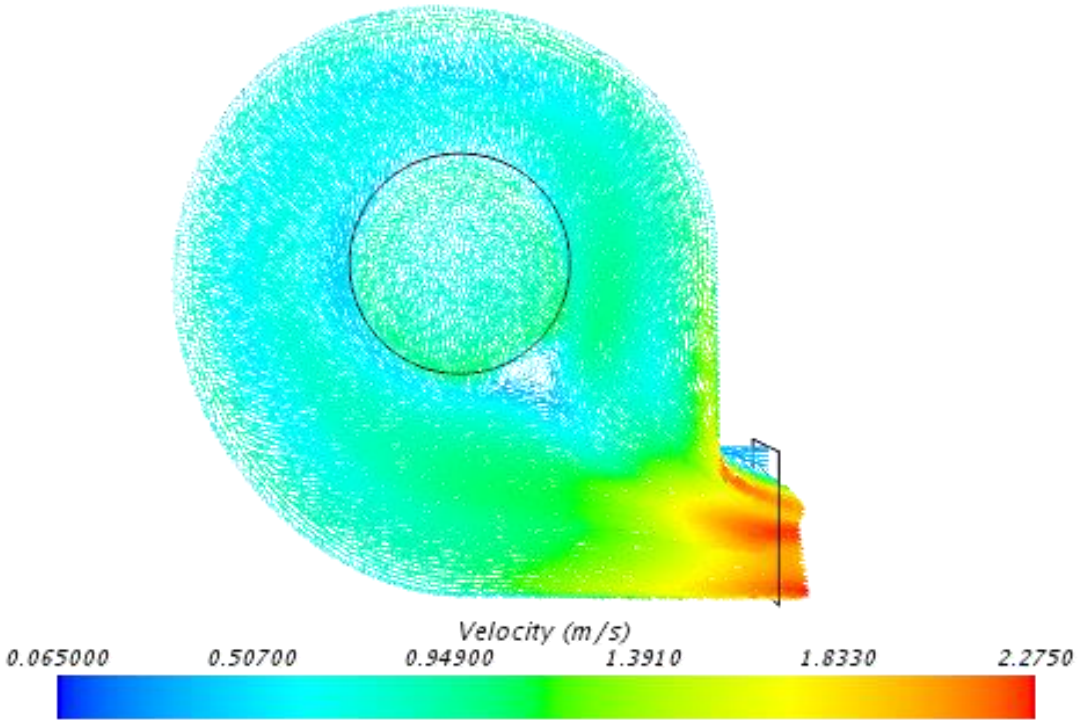

Figure 34: Velocity Vector Scene for Refined Fan Shell Simulation

As described in Table 11, although the difference in number of cells in the volume mesh between these first two simulations is over 500,000, the resulting outlet velocity is not greatly affected. In fact, the percent difference is only 0.03136 %. This is important to take into account as more parts of the system are included in the model. The fan and its housing does not need to be very refined, which helps keep the computation time and the complexity of the entire system manageable.

Table 11: Mesh Data and Velocity Values for Fan-Only Simulations

Property	Initial Simulation	Refined Simulation
Cells in Volume Mesh	90,250	598,282
Velocity at Inlet (m/s)	1.0	1.0
Average Velocity at Outlet (m/s)	1.5238	1.5242

The next phase of the simulation process involved adding the drying ducts and porous chamber to the modeled system. Velocity profiles and area averages were still the main focus, so temperature initial conditions were not yet included. The heating coils were also not modeled in this phase. The dryer system that was simulated is described in Figure 35.

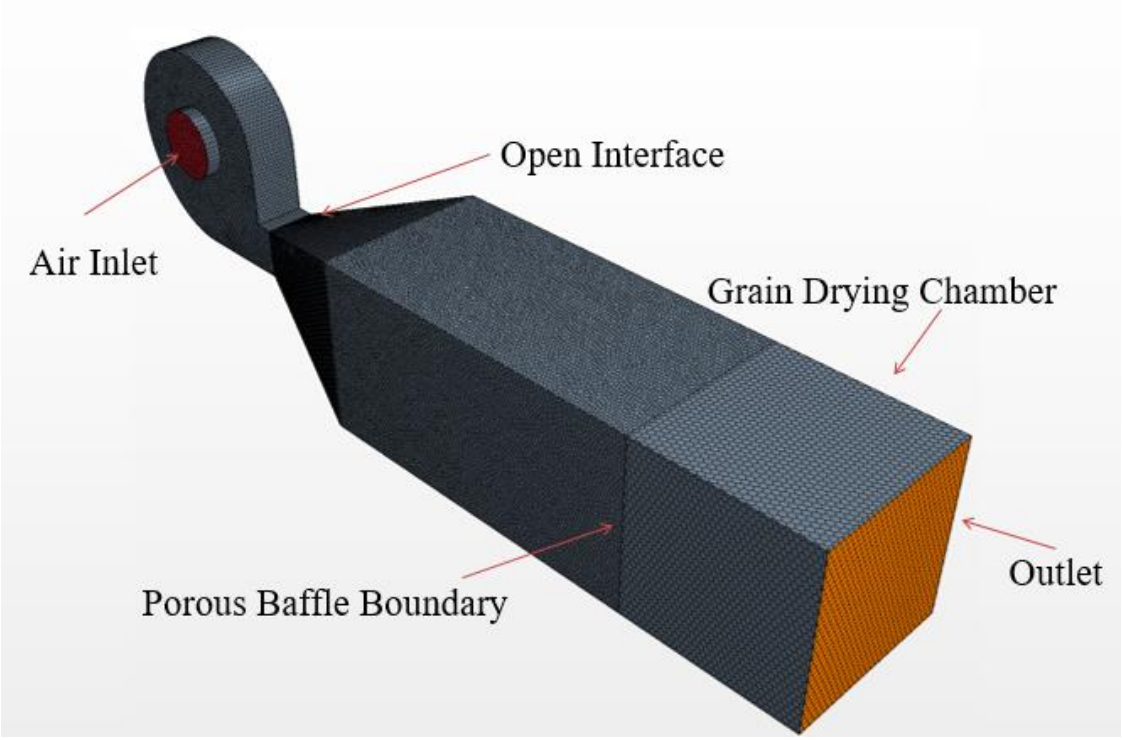

Figure 35: Initial Full Dryer System Model

In this iteration of the system, the air inlet was again considered a velocity inlet and the outlet was set to be a pressure outlet. The size of the cells in the mesh varied by region. The mesh for the heating duct, fan, and fan housing all had a base cell size of 0.0075 m. The fan rotor mesh had a smaller base size of 0.0025 m. For the porous duct that contained the grain, the mesh base size was also smaller at 0.007 m. A polyhedral volume mesh was chosen for the entire system. These iterations had a total of 266,923 cells in the mesh.

The first simulation of the entire system was run with a velocity at the inlet of 1.0 m/s. This is the same velocity that was used in testing the models with only the fan, rotor, and fan housing. Table 12 describes the different velocities obtained at different points in the system, including just after the fan shell, at the interface of the heating duct and porous chamber, and at the pressure outlet of the porous chamber. The pressure drop across the porous chamber is also given in this table. The porosity of this chamber was set to 0.37 for the packed bed of corn.

Once the first full system was run for 1000 iterations and shown to converge, the velocity at the inlet was changed to better match experimental testing. Since the air flow rate ranged between 75 – 125 CFM per bushel (0.0836 – 0.139 m^3/min per kg corn), a value within that range was chosen: 3.5 m/s. This equates to approximately 89.3 CFM (0.124 m^3/min per kg corn). With this inlet velocity, the simulation was run twice to determine the different velocity profiles and values along the system. Table 12 gives these numbers and compares them for all three simulations.

Table 12: Velocities and Pressure Drops for Initial Full Dryer Simulations

Property	Initial Full Dryer	Adjusted Velocity 1	Adjusted Velocity 2
Inlet Velocity (m/s)	1.0	3.5	3.5
Shell Outlet Velocity (m/s)	1.501	5.279	5.285
Porous Chamber Inlet Velocity (m/s)	0.1232	0.4497	0.3199
Porous Chamber Outlet Velocity (m/s)	0.1294	0.4536	0.4534
Pressure Drop Across Porous Chamber (Pa)	26.21	186.7	189.1

The velocity distribution for the simulation at 3.5 m/s is shown in Figure 36. The flow pattern this simulation is fairly typical for all of the grain dryer simulations that were run. As expected, the peak velocity occurs the exit of the fan housing, and the velocity drops off once the air reaches the porous region of the system. The velocity peak is approximately 9.3 m/s for the system. Larger velocities also occur in the area of the rotating fan.

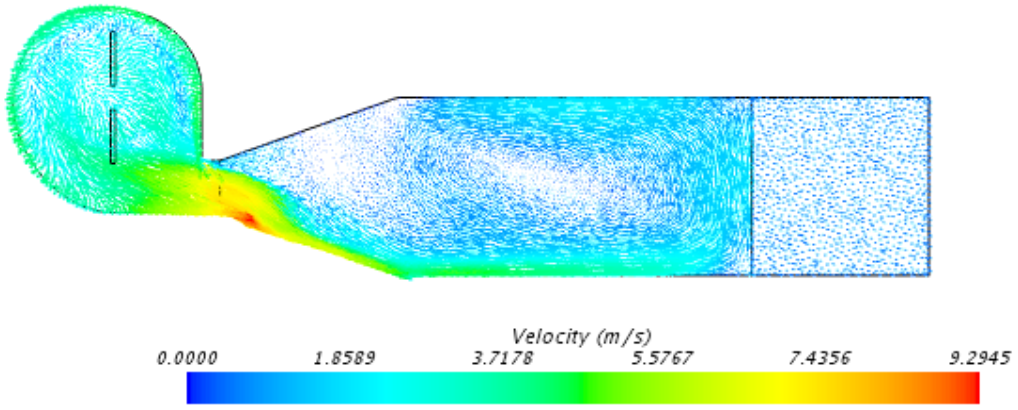

Figure 36: Full Dryer Adjusted Velocity Vector Scene

The next step in the model refinement involved the addition of the heating elements to the simulation. In the actual grain dryer system, these heating elements are coils that span the width of the duct. Initially, these coils were modeled with similar geometry to the heating coils. These coils can be seen in Figure 37. However, the meshing of such a small and complicated geometry was a very difficult and time-consuming process. In the interest of time, the decision was made to model these coils as cylinders.

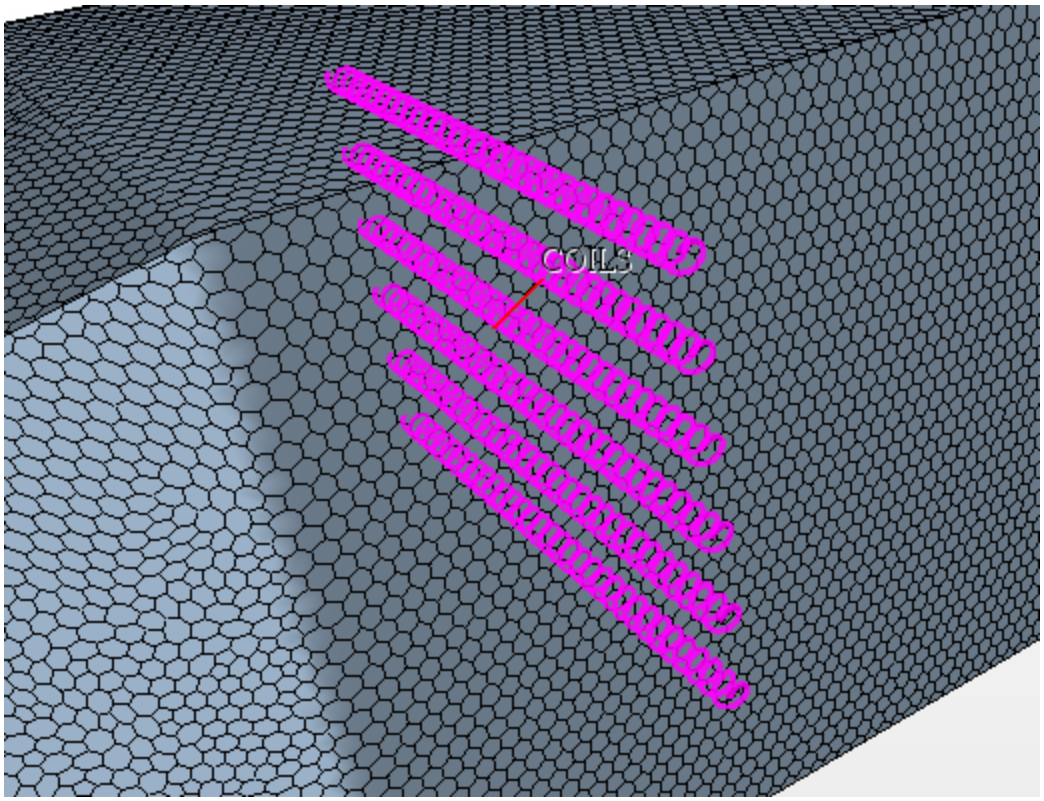

Figure 37: Coils in the Heating Duct of Grain Dryer

The length of the drying chamber was also changed from 0.914 m to 1.219 m to better match the experimental system. Figure 38 shows the updated system for analysis, featuring both the cylindrical heating elements and elongated duct. The fan in this system still only has two blades. Initially, the heating elements were given a boundary condition of constant temperature, ranging from 873.15 K to 1673.15 K. For the set of tests involving this setup, the inlet velocity was once again 3.5 m/s. One change that was made was the flow setting was tested as coupled rather than segregated. The coupled solver is more robust and uses more computational resources, while the segregated solver uses less memory and solves each of the momentum equations successively [26].

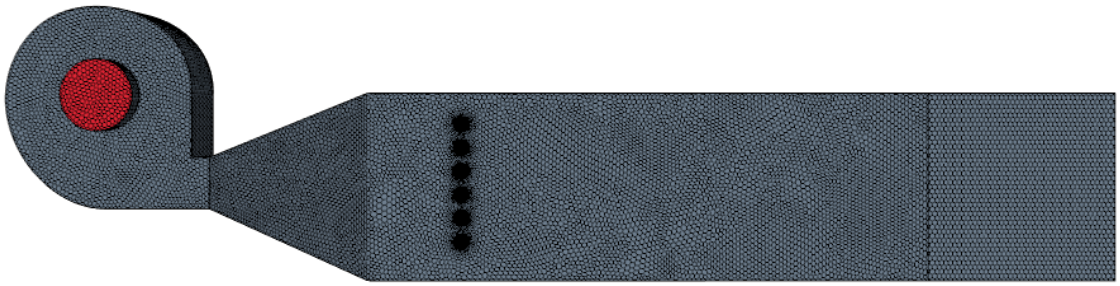

Figure 38: Updated Dryer Setup

The described setup was run five times to 3000 iterations, each time with a different temperature boundary conditions on the heating elements. These five simulations had a total of 975,201 cells each. The average temperature at the inlet of the porous chamber was then found. This data is given in Table 13. Compared to the experimental data available for the grain dryer, these inlet temperatures are similar. Temperatures tended towards 190-200 °F (360.9 K - 366.5 K) in experimental studies. The temperature variance was chosen with the goal of reproducing experimental findings at the entrance to the grain duct. However, this condition was changed to a heat flux in subsequent simulations, as this more accurately represents the heating mechanism in the grain drying system.

Table 13: Temperature Data from Updated Initial System Setup

Temperature of Heating Coils (K)	Inlet Velocity (m/s)	Average Temperature at Porous Inlet (K)
873.15	3.5	333.28
1273.15	3.5	350.42
1373.15	3.5	362.45
1473.15	3.5	362.66
1673.15	3.5	374.69

The same system setup was tested again, with a change in the inlet conditions to the fan housing. Instead of having an inlet velocity, the system was given a stagnation inlet. The pressure generated by the motion of the fan should then be the main mechanism for the flow. However, the simulations tested with this inlet condition did not converge correctly and the velocity was actually shown to go in the opposite direction of predicted. For the sake of time, a velocity inlet was chosen for the rest of the simulations.

The last step in refining the simulation before the recommended setup was achieved was to increase the number of blades on the fan from two to six. The cells in the volume mesh totaled 637,659 this time. The simulation was run for 3000 iterations, and the temperature data obtained is given in Table 14.

Table 14: Temperature Data from Updated Fan System

Temperature of Heating Coils (K)	Inlet Velocity (m/s)	Average Temperature at Porous Inlet (K)
873.15	3.5	331.79

The grain dryer system used for analysis took features from these different simulations in order to come up with a recommended balance of complexity and time. The solver was chosen to be segregated instead of coupled, as it requires less computer resources. Cylindrical heating elements were modeled instead of coils, as they still gave similar results for heating values. A heat flux was chosen for the heating elements instead of a static temperature in order to better represent the actual system.

5.4 Analyzing the Grain Dryer System Results

The system for analysis is shown as transparent in Figure 39. This setup features the elongated drying duct, the six blade fan, and a porous chamber for the grain. In addition, the heat flux was calculated for this system based on the geometry of the cylindrical heating elements. For the velocity inlet speed of 3.5 m/s, the inlet diameter of 0.1238 m, density at the average temperature of 70 °C of 1.029 kg/m^3, and six heating elements of 0.0254 m diameter, the heat flux is calculated to be 20.84 kW/m^2. Since 3.5 m/s is in the range of 0.0836 to 0.139 m^3/min per kg corn (75 CFM to 125 CFM per bushel), this heat flux value was used on all the simulations.

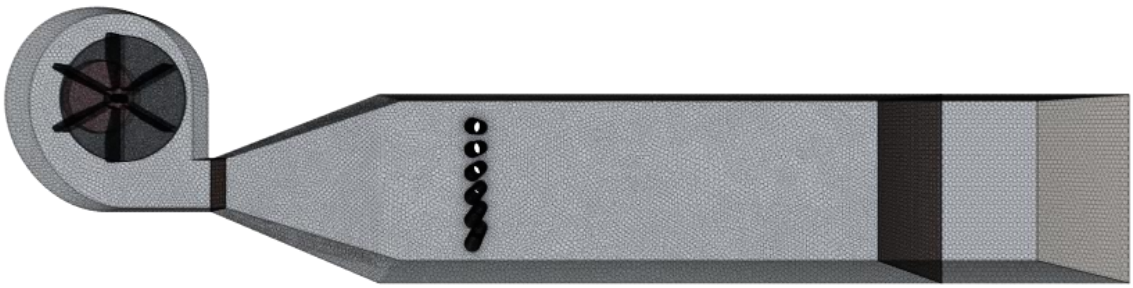

Figure 39: Transparent View of Grain Dryer System for Analysis

The mesh for this system was a surface remesher with a polyhedral volume mesh. The refinement of the mesh was based on the different system parts. The fan and rotor had a finer mesh, with a base size of 2.5 mm. The fan housing, heating duct, and porous duct base size was 7.5 mm. Both the fan and rotor were defined as solid regions, with the remaining regions given fluid (gas) physics conditions. The air was set to behave as an

ideal gas, and the segregated flow solver was used. A rotational boundary condition was given to the fan with a value of 3500 rpm counterclockwise. The interfaces between the fan housing and heating duct and heating duct and porous chamber were set to be porous baffle boundaries. For the first interface, the porosity was set to 1 so that it would be completely open. For the second interface, the porosity was set to 0.37 to represent the porous nature of the packed corn kernels.

Seven different simulations were run based on the inlet airflow rate. The first was run at 3.5 m/s, and the remaining six were run from 75 to 125 CFM per bushel, increasing by 10 CFM (0.0836 to 0.139 m^3/min per kg corn increasing by approximately 0.0111 m^3/min per kg corn). All had a heat flux on the heating elements of 20.84 kW/m^2. The data obtained from these simulations is given in Table 15. In general, as the flow rate increased, the inlet temperature at the porous duct tended to decrease.

Table 15: Temperature Data for Varying Flow Rate Simulations

Inlet Flow Rate (CFM/bu)	Inlet Flow Rate (m^3/min/kg corn)	Inlet Velocity (m/s)	Heat Flux on Coils (W/m^2)	Porous Inlet Temp (K)
75.00	0.08361	2.362	20839.06	390.45
85.00	0.09476	2.677	20839.06	371.59
95.00	0.1059	2.992	20839.06	375.53
105.0	0.1171	3.307	20839.06	357.51
111.1	0.1239	3.500	20839.06	361.91
115.0	0.1282	3.622	20839.06	354.82
125.0	0.1393	3.937	20839.06	353.39

Experimental tests were performed for this same setup. The data from these tests is given in Table 16. The flow rate in most of these tests was determined to be 90 CFM per

bushel (0.100 m^3/min per kg corn), with the last test having a flow rate of 110 CFM (0.123 m^3/min per kg corn). The two shaded rows indicate tests that had incorrect inlet conditions, so the data is not valid. The temperatures from Table 15 follow the same pattern as those in Table 16, showing a decrease in inlet temp with an increase in air flow rate.

Table 16: Experimental Data for Laboratory-Scale Grain Dryer

Test #	CFM/bu (Nominal)	m^3/min/kg corn (Nominal)	Average Inlet Temp (K)
1	90.00	0.1003	366.7
2	90.00	0.1003	366.0
3	90.00	0.1003	365.7
4	90.00	0.1003	366.2
5	90.00	0.1003	366.4
6	90.00	0.1003	367.9
7	90.00	0.1003	366.4
8	110.0	0.1226	357.7

The temperatures from both the experimental findings and simulated results were averaged and the similar air flow rates were compared. These are shown in Table 17. The inlet temperature shows close alignment between the simulation and experimental data. A 7.0 K temperature difference exists for the 0.100 m^3/min per kg corn tests, and there is only a 1.5 K difference for the tests at 0.123 m^3/min per kg corn CFM.

Table 17: Comparison of Experimental and Simulated Temperature Data

Data Source	Inlet Temp (K)
Average of 0.09476 and 0.1059 m^3/min/kg corn (Simulation)	373.7
Average of Tests 1, 2, 5, 6, 7 (Experimental)	366.7
Temperature Difference	7.0

Average of 0.1171 and 0.1282 m^3/min/kg corn (Simulation)	356.2
Test 8 (Experimental)	357.7
Temperature Difference	1.5

The temperature distribution in the drying chamber is another area of interest in this research. It was predicted that the temperature would be evenly distributed at the entrance to the packed grain bed. Figure 40 shows the temperature along the dryer. The area of highest temperature is at the heating elements and in a portion of the back flow from them. As the air flows further down the duct, it does tend to have a more uniform temperature. From Table 15, the average temperature at the inlet to the porous duct is 361.9 K.

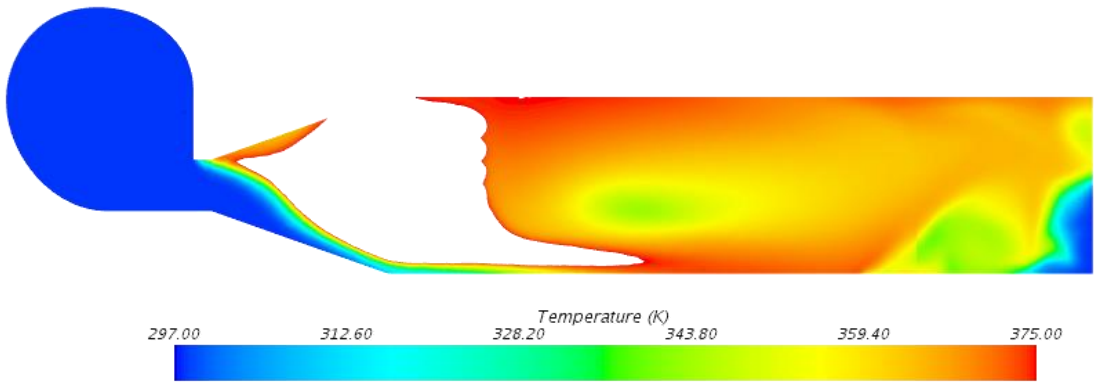

Figure 40: Temperature Distribution of Simulated Dryer at 3.5 m/s

The grain dryer simulation process demonstrates both aspects of model refinement. First, the refinement of the computational grid was studied with the fan and its housing.

Then, the system complexity increased as more parts of the grain dryer were included. Final model refinement came through modifying the simulation parameters to find the recommended analysis setup. This model can be used in the future for changes in the system design. Testing can easily be done for these designs using computational fluid dynamics.

Chapter 6: Conclusions and Future Work

6.1 Conclusions

In this thesis, a laboratory-scale photobioreactor and laboratory-scale grain dryer were simulated and analyzed in order to demonstrate the process of model refinement within computational fluid dynamics simulations. The results were compared to similar experiments to determine the effectiveness of the simulations. When modeled accurately, these systems can easily be changed and improved using computer software.

6.1.1 Case Study 1 – Photobioreactor

The photobioreactor in this case study was modeled using CAD software and computational fluid dynamics. First, a simple tank was modeled with no structural members in the fluid column. Then, the complexity of the simulation was increased by incorporating a square structural member and using more cells for analysis. Once this simulation was run successfully, the desired system setup could be tested.

Five different arrangements of light guides were tested under varying volumetric flow rates. Square arrangements included 2×2, 3×3, and 4×4, and staggered arrangements included rows of 2+3+2 and 3+2+3. The volumetric flow rates tested were 1, 3, 5, 8, 10, 12, 15, and 20 L/min. The addition of the structural members interrupted the flow from the bubble sparger as expected. The staggered arrays of light guides tended to interrupt the flow more, resulting in a warmer temperature distribution and more area of zero velocity. This interruption of the flow may be desirable as it increases the residence time of the bubbles, increasing mass transfer and light penetration.

6.1.2 Case Study 2 – Grain Dryer

A laboratory-scale cross-flow grain dryer was analyzed in order to determine the air flow patterns and the temperature stratification in the drying chamber. The drying system was modeled step-by-step using different model refinement techniques. First, only the centrifugal fan and its housing were modeled. This was done first with a coarse mesh, and then a refined mesh. Only a 0.032 % difference was found between the outlet velocities of these two setups. The remainder of the dryer system was added with successful iterations, including heating elements, more fan blades, and heat flux. The recommended system for a balance of valid results and system complexity included cylindrical heating elements, a velocity inlet, and a segregated flow solver.

The temperature distributions and average temperature at the inlet to the porous grain duct were found for flow rates from 0.0836 to 0.139 m^3/min per kg corn. Results were compared to experimental research at 0.100 m^3/min per kg corn and 0.123 m^3/min per kg corn. The simulation results showed good alignment with experimental data, with only a 7.0 K and 1.5 K temperature difference, respectively. Using this model, potential changes to the drying system could be made and tested computationally.

The model refinement process for the laboratory-scale grain dryer system involved both increasing the refinement of the computational grid and adding more features to the dryer with successful iterations. Increased refinement of the grid with the fan, rotor, and housing did not significantly affect the outlet velocity. This was taken into consideration with proceeding simulations, as a coarser mesh did not require as much computational time to run.

The goal of this research was to demonstrate using model refinement to answer specific design questions. In order to determine the air flow patterns and temperature stratification at the packed bed, the centrifugal fan rotation, heat flux from the heating elements, and the geometry of the duct needed to be consistent with the experimental setup. However, the model did not require a very refined computational mesh or complicated heating coil geometry. If other features of the system were being studied, the required refinement criteria may be changed.

6.2 Future Work

The case studies in the research demonstrate the idea of applying model refinement to CFD simulations. Potential future work involving both of these systems is discussed in this section.

6.2.1 Case Study 1 – Photobioreactor

The photobioreactor system tested included light guides that penetrated the full width of the fluid column. In the future, guides that only span half the width could be simulated and compared to the work of Anderson et al. [48]. Different arrangements of the bubble sparger could also be tested with the light guides to determine a good balance for fluid flow.

The simulation setup could also be used to predict the light penetration to the fluid. Further heat transfer analysis could give an idea of the temperature reaching the algae. In addition, the properties of the algae/water mixture could be tested, as this research uses only the properties of water for analysis.

6.2.2 Case Study 2 – Grain Dryer

Future simulations of the laboratory-scale grain dryer could test different grain types. This could be accomplished by changing the porosity of the grain bed. The heat and mass transfer that occurs from the drying process could also be added to the system. A better prediction of the temperature at the outlet of the porous grain region could then be found.

The heating elements could be modeled as coils in order to better represent the actual system. This would help decrease the backflow caused by the cylindrical shape. In addition, the inlet conditions could be modified to be stagnation pressure at the inlet. With more time, any simulation issues could be fixed. The fan could also be modeled as a fan interface using the STAR-CCM+ feature.

References

[1] G. E. Dieter and L. C. Schmidt, Engineering Design, Fourth Edition, New York, NY: McGraw-Hill, 2009.

[2] AMWEL Enterprises, "A brief history of CFD," CMD, 2008. [Online]. Available: http://www.amwel.com/history.html.

[3] M. P. Rumpfkeil, "University of Dayton," 2014. [Online]. Available: http://academic.udayton.edu/MarkusRumpfkeil/CFDcourse/Intropresentation.pdf.

[4] R. H. Pletcher et al., Computational Fluid Mechanics and Heat Transfer, 3rd ed., Boca Raton, FL: Taylor & Francis Group, LLC, 2013.

[5] Siemens Product Lifecycle Management Software Inc., "What is PLM software?," Siemens, 2017. [Online]. Available: https://www.plm.automation.siemens.com/en_us/plm/. [Accessed 17 Mar. 2017].

[6] Dublin City Schools, "Ten stages of the engineering design process," n.d.. [Online]. Available: http://www.dublincityschools.us/userfiles/433/Classes/13738//userfiles/433/my%20files/engineering%20design%20process%20-%2010%20stages%20-%20present%20this.pdf?id=8047. [Accessed 10 June 2016].

[7] Teach Engineering, "Engineering design process," n.d.. [Online]. Available: https://www.teachengineering.org/k12engineering/designprocess#Ask. [Accessed 10 June 2016].

[8] M. Rossi et al., "Engineering and design best practices in new product development: an empirical research," *Procedia CIRP*, vol. 21, pp. 455-460, 2014.

[9] J. H. Panchal et al., "A value of information based approach to simulation model refinement," *Eng. Optimization*, vol. 40, no. 3, pp. 223-251, 2008.

[10] J. F. Wendt, Ed., Computational Fluid Dynamics: An Introduction, 3rd Ed., Rhode-Saint-Genèse, Belgium: Springer-Verlag Berlin Heidelberg, 2010.

[11] CD-adapco, "CD-adapco engineering simulation software - CAE and CFD software," n.d.. [Online]. Available: http://www.cd-adapco.com/.

[12] J. D. Anderson, Jr., Computational Fluid Dynamics: The Basics with Applications, New York, NY: McGraw-Hill, Inc., 1995.

[13] T. A. Cleaver et al., "Using design of experiments methods for applied computational fluid dynamics: a case study," *Quality Eng.*, vol. 28, no. 3, pp. 280-292, 2016.

[14] D. Ellsworth, "NASA @ SC08," 24 June 2014. [Online]. Available: http://www.nas.nasa.gov/SC08/FlameTrenchMach.html. [Accessed 7 May 2016].

[15] K. W. Linfield and R. G. Mudry, "Pros and cons of CFD and physical flow modeling," Aug. 2008. [Online]. Available: http://www.airflowsciences.com/sites/default/files/docs/Pros-and-Cons-of-CFD-and-Physical-Flow-Modeling.pdf.

[16] Resolved Analytics, "A Comparison of CFD Software Packages," Apr. 2017. [Online]. Available: https://www.resolvedanalytics.com/theflux/comparing-popular-cfd-software-packages. [Accessed 19 Apr. 2017].

[17] M. R. Haghgoo, "A comparison of CFD Software packages to find the suitable one for numerical modeling of gasification process," Rep. CMPT 898(02), 2013.

[18] ANSYS, Inc., "ANSYS capabilities brochure 17.2," 2016. [Online]. Available: http://www.ansys.com/-/media/Ansys/corporate/files/pdf/product/release-highlights/ansyscapabilities172.pdf. [Accessed 30 Sept. 2016].

[19] CD-adapco, "STAR-CCM+®," n.d.. [Online]. Available: http://www.cd-adapco.com/products/star-ccm%C2%AE. [Accessed 30 Sept. 2016].

[20] CD-adapco, "Comprehensive simulations," n.d.. [Online]. Available: http://www.cd-adapco.com/products/star-ccm%C2%AE/comprehensive-simulations. [Accessed 30 Sept. 2016].

[21] OpenCFD Ltd (ESI Group), "OpenFOAM," 2016. [Online]. Available: http://www.openfoam.com/documentation/user-guide/standard-solvers.php. [Accessed 3 Oct. 2016].

[22] S. C. Thompson and C. J. J. Paredis, "An investigation into the decision analysis design process decisions," *J. Mech. Design,* vol. 132, pp. 121009-1-121009-9, 2010.

[23] J. H. Panchal et al., "Managing design-process complexity: a value of information based approach for scale and decision decoupling," *J. Computing and Inform. Sci. in Eng.,* vol. 9, pp. 021005-1-021005-12, 2009.

[24] M. Messer et al., "Model refinement decisions using the process performance indicator," *Eng. Optimization,* vol. 43, no. 7, pp. 741-762, 2011.

[25] K. Sundararajan, "Design of experiments – a primer," iSixSigma, 2016. [Online]. Available: https://www.isixsigma.com/tools-templates/design-of-experiments-doe/design-experiments-%E2%90%93-primer/. [Accessed 6 Oct. 2016].

[26] CD-adapco, "STAR-CCM+ user guide," n.d.. [Online]. Available: file:///C:/Program%20Files/CD-adapco/STAR-CCM+11.02.009/doc/en/online/index.html#page/connect%2Fsplash.html. [Accessed 18 Apr. 2016].

[27] COMSOL Inc., "Navier-Stokes equations," 2016. [Online]. Available: https://www.comsol.com/multiphysics/navier-stokes-equations. [Accessed 2 May 2016].

[28] R. A. W. M. Henkes et al., "Natural convection in a square cavity calculated with low-Reynolds number turbulence models," *Int. J. Heat and Mass Transfer*, vol. 34, pp. 1543-1557, 1991.

[29] S. Sarkar and L. Balakrishnan, "Application of a Reynolds-stress turbulence model to the compressible shear layer," ICASE Rep. 90-18, NASA CR 182002, Hampton, VA, 1990.

[30] B. R. Munson et al., Fundamentals of Fluid Mechanics, 6th ed., Hoboken, NJ: John Wiley & Sons, Inc., 2009.

[31] S. M. Mortuza et al., "Computational and experimental investigation of heat transfer within a column photobioreactor," in *ASME 2011 Int. Mechanical Engineering Congr. & Expo.*, Denver, CO, 2011.

[32] M. M. El Wakil et al., "A theoretical investigation of the heating-up period of injected fuel droplets vaporizing in air," NACA Tech. Note 3179, Washington, 1954.

[33] W. E. Ranz and W. R. Marshall, "Evaporation from drops parts I and II," *Chem. Eng. Prog.*, vol. 48, no. 3, p. 141, 1952.

[34] R. C. Brown and T. R. Brown, Why are We Producing Biofuels?: Shifting to the Ultimate Source of Energy, Ames, IA: Brownia, LLC, 2012.

[35] Biofuel.org.uk, "Biofuels: the fuel of the future," 2010. [Online]. Available: http://biofuel.org.uk/types-of-biofuels.html. [Accessed 15 Apr. 2016].

[36] Z. Yang et al., "An experimental investigation on the multiphase flows and turbulent mixing in a flat-panel photobioreactor for algae cultivation," *J. Appl. Phycology,* vol. 26, no. 5, pp. 2097-2107, 2014.

[37] A. Massart et al., "Experimental characterization and numerical simulation of the hydrodynamics in an airlift photobioreactor for microalage cultures," *Algal Research,* vol. 6, no. B, pp. 210-217, 2014.

[38] N. T. Eriksen, "The technology of microalgal culturing," *Biotechnol. Lett.,* vol. 30, no. 9, pp. 1525-1536, 2008.

[39] E. Nauha and V. Alopaeus, "Modeling method for combining fluid dynamics and algal growth in a bubble column photobioreactor," *Chemical Eng. J.,* vol. 229, pp. 559-568, 2013.

[40] A. M. Kunjapur and R. B. Eldridge, "Photobioreactor design for commercial biofuel production from microalgae," *Ind. & Eng. Chemistry Res.,* vol. 49, no. 8, pp. 3516-3526, 2010.

[41] L. Xu et al., "Microalgal bioreactors: challenges and opportunities," *Eng. in Life Sci.,* vol. 9, no. 3, pp. 178-189, 2009.

[42] H.-P. Luo and M. H. Al-Dahhan, "Airlift column photobioreactors for porphyridium sp. culturing: part I. effects of hydrodynamics and reactor geometry," *Biotechnol. and Bioeng.*, vol. 109, no. 4, pp. 932-941, 2011.

[43] J.-W. F. Zijffers et al., "Design process of an area-efficient photobioreactor," *Marine Biotech.*, vol. 10, no. 4, pp. 404-415, 2008.

[44] G. S. Bari et al., "Predicting hydrodynamic and heat transfer effects of sparger geometry and placement within a column photobioreactor using computational fluid dynamics," in *ASME 2012 6th Int. Conf. Energy Sustainability & 10th Fuel Science, Engineering and Technology Conf.*, San Diego, CA, 2012.

[45] G. S. Bari et al., "Hydrodynamic and heat transfer effects of different sparger spacings within a column photobioreactor using computational fluid dynamics," in *ASME 2012 Int. Mechanical Engineering Congr. & Expo.*, Houston, TX, 2012.

[46] S. M. Mortuza et al., "Computational and experimental investigation of bubble circulation patterns within a column photobioreactor," in *ASME 2011 5th Int. Conf. Energy Sustainability & 9th Fuel Cell Science, Engineering and Technology Conf.*, Washington, DC, 2011.

[47] C. R. Gerdes et al., "Investigation of hydrodynamics and heat transfer effects due to light guides in a column photobioreactor," *J. Fuel Cell Sci. and Technol.*, vol. 11, no. 4, pp. 041002-1-041002-7, 2014.

[48] G. A. Anderson et al., "Operation of a porous membrane photobioreactor," in *Proc. ASME 2016 Int. Conf. Energy Sustainability*, Charlotte, NC, 2016.

[49] D. Brooker et al., Drying and Storage of Grains and Oilseeds, New York City, NY: Van Nostrand Rinhold, 1992.

[50] K. VanDevender, "Grain drying concepts and options," n.d.. [Online]. Available: http://www.uaex.edu/publications/pdf/FSA-1072.pdf. [Accessed 27 Apr. 2016].

[51] Alberta Agriculture and Forestry, "Cereal grain drying and storage," 18 Oct. 2010. [Online]. Available: http://www1.agric.gov.ab.ca/$department/deptdocs.nsf/all/crop1204. [Accessed 27 Apr. 2016].

[52] L. M. Mattison et al., "Comparison of theoretical and experimental corn drying profiles within a cross-flow column dryer," in *Proc. ASME 2013 Int. Mechanical Engineering Congr. and Expo.*, San Diego, CA, 2013.

[53] J. Otte, "How much grain do you give away?," 30 Dec. 2008. [Online]. Available: http://farmprogress.com/story-how-much-grain-do-you-give-away-14-21048. [Accessed 25 Oct. 2016].

[54] C. Jia et al., "Mathematical simulation of stresses within a corn kernel during drying," *Drying Technol.*, vol. 18, no. 4-5, pp. 887-906, 2000.

[55] T. N. Suess et al., "Experimental investigation of a lab-scale, cross-flow grain dryer for testing of drying efficiency and characteristic profiles of a packed bed," in *Proc. ASME 2015 Power and Energy Conversion Conf.*, San Diego, CA, 2015.

[56] K. J. Hellevang, "Grain drying," 2016. [Online]. Available: https://www.ag.ndsu.edu/pubs/plantsci/smgrains/ae701.pdf. [Accessed 1 Nov. 2016].

[57] M. Gummert, "Re-circulating batch dryer," 2010. [Online]. Available: http://www.knowledgebank.irri.org/index.php?option=com_zoo&task=item&item_id=1137&Itemid=820. [Accessed 1 Nov. 2016].

[58] K. Karanth and N. Sharma, "CFD analysis on the effect of radial gap on impeller-diffuser flow interaction as well as on the flow characteristics of a centrifugal fan," *Int. J. Rotating Machinery,* vol. 2009, no. 1, pp. 1-8, 2009.

[59] O. P. Singh et al., "Parametric study of centrifugal fan performance: experiments and numerical simulation," *Int. J. Advances in Eng. & Technol.,* vol. 1, no. 2, pp. 33-50, 2011.

[60] J. P. Sitompul et al., "Modelling and simulation of momentum, heat, and mass transfer in a deep-bed grain dryer," *Drying Tech.*, vol. 21, no. 2, pp. 217-229, 2003.

[61] F. Weigler et al., "Investigation of particle and air flows in a mixed-flow dryer," *Drying Technol.*, vol. 30, no. 15, pp. 1730-1741, 2012.

[62] H. Scaar et al., "Experimental and numerical study of the airlfow distribution in mixed-flow grain dryers," *Drying Technology,* vol. 34, no. 5, pp. 595-607, 2015.